

Interstellar extinction, polarization, and grain alignment in the Sh 2-185 (IC 59 and IC 63) region

ARCHANA SOAM,¹ B-G ANDERSSON,¹ V. STRAIŽYS,² MIRANDA CAPUTO,^{3,1} A. KAZLAUSKAS,² R. P. BOYLE,⁴ R. JANUSZ,⁵ J. ZDANAVIČIUS,² AND J.A. ACOSTA-PULIDO^{6,7}

¹*SOFIA Science Center, NASA Ames Research Center, M.S. 232-12, Moffett Field, CA 94035, USA*

²*Institute of Theoretical Physics and Astronomy, Vilnius University, Saulėtekio al. 3, Vilnius, LT-10257, Lithuania*

³*Ritter Astrophysical Research Center, University of Toledo Dept. of Physics and Astronomy, 2801 W. Bancroft St. Toledo, Ohio 43606*

⁴*Vatican Observatory Research Group, Steward Observatory, Tucson, AZ 85721, USA*

⁵*Vatican Observatory, 00120, Vatican City, Italy*

⁶*Instituto de Astrofísica de Canarias (IAC), C/O Via Lactea, s/n E38205- La Laguna, Tenerife, Spain*

⁷*Departamento de Astrofísica, Universidad de La Laguna, E-38205 La Laguna, Tenerife, Spain.*

(Received January 19, 2021; Revised; Accepted)

ABSTRACT

Optical and infrared continuum polarization from the interstellar medium is driven by radiative processes aligning the grains with the magnetic field. While a quantitative, predictive theory of Radiative Alignment Torques (RAT) exists and has been extensively tested, several parameters of the theory remain to be fully constrained. In a recent paper, Medan & Andersson (2019) showed that the polarization efficiency (and therefore grain alignment efficiency) at different locations in the wall of the Local Bubble (LB) could be modeled as proportional to the integrated light intensity from the surrounding stars and OB associations. Here we probe that relationship at high radiation field intensities by studying the extinction and polarization in the two reflection nebulae IC 59 and IC 63 in the Sh 2-185 H II region, illuminated by the B0 IV star γ Cassiopeia. We combine archival visual polarimetry with new 7-band photometry in the Vilnius system, to derive the polarization efficiency from the material. We find that the same linear relationship seen in the Local Bubble wall also applies to the Sh 2-185 region, strengthening the conclusion from the earlier study.

Keywords: interstellar, dust

1. INTRODUCTION

The realization that interstellar polarization of stars is due to asymmetric dust grains, aligned with the magnetic field, has proven to be key for mapping the ISM magnetic fields. Dust-induced interstellar polarization was first detected by Hall (1949) and Hiltner (1949a,b). This effect has been used extensively to derive the magnetic field maps in different environments (e.g. Vrba et al., 1976; Hodapp, 1987; Bhatt & Jain, 1993; Pereyra & Magalhães, 2002; Matthews et al., 2009; Chapman et al., 2011; Sugitani et al., 2011). Polarization of starlight at visible and near-infrared wavelengths is due to dichroic extinction by non-spherical dust grains which are aligned with their short axis parallel to the local

magnetic field (Whittet, 2003). Aligned dust grains can similarly emit polarized thermal radiation in the far infrared and at sub(mm) wavelengths (e.g. Cudlip et al., 1982; Rao et al., 1998; Dotson et al., 2000; Vaillancourt & Matthews, 2012).

The mechanism by which the dust grains align with the magnetic field has long been unclear. A long assumed mechanism to account for the effect, based on paramagnetic relaxation in rapidly rotating grain (Davis & Greenstein, 1951), has now been shown to be unviable in most instances both observationally (Hough et al., 2008) and theoretically (Lazarian & Draine, 1999). However, a radiatively driven mechanism, originally proposed by Dolginov & Mitrofanov (1976) and more fully developed by Draine & Weingartner (1996); Lazarian & Hoang (2007), has now become the generally assumed alignment mechanism. This “Radiative Alignment Torque (RAT) theory” posits that grains are

spun up by the transfer of torques from photons in an anisotropic radiation field to helical dust grains. For paramagnetic grains, the resultant rotation induces a magnetic moment through the Barnett effect (Purcell, 1979). This induced magnetic moment will cause the grain's angular (and magnetic!) momentum vector to Larmor-precess around an external magnetic field. Continued RAT torques during the Larmor-precession finally aligns the grain with the magnetic field. A large number of the predictions of this theory have been confirmed over the last decade (see Andersson et al., 2015, for a review), but details of the mechanism and its components still remain to be probed.

It is important to note that, in most environments, RAT alignment is magnetic alignment; i.e. the grains are aligned with their angular momentum vectors along the magnetic field, and the direction of the observed dichroic extinction polarization traces the plane of the sky projection of the field. Second order effects – such as alignment along the radiation field direction, for very strong radiation fields (e.g. Lazarian & Hoang, 2019; Kataoka et al., 2017), and the impact of non-paramagnetic grain materials (carbon solids, e.g. Andersson et al. 2018; Andersson et al. 2020, in prep.) can be important in, rare, extreme environments.

While the principles of RAT grain alignment are now well established, we still need to understand the quantitative aspects of the grain alignment mechanism in context of the strength of radiation and magnetic fields. Medan & Andersson (2019) presented a detailed study of the interstellar polarization due to dust in the Local Bubble wall (Lallemand et al., 2003), investigating grain alignment and polarization efficiency dependence on radiation from OB and field stars. They used polarization measurements from Berdyugin et al. (2014) combined with spectral classifications and photometry from the literature (Wright et al., 2003; Høg et al., 2000) to investigate the quantitative relationship between the observed polarization efficiency (P/A_V) and the radiation field strength, as well as the strength of magnetic fields. In the present work, we perform a similar investigation of the two nearby (at $d \approx 200$ pc) nebulae IC 59 and IC 63 and compare them with Local Bubble results of Medan & Andersson (2019).

IC 59 and IC 63 are two reflection and emission nebulae in the Sh 2-185 HII region (at $d \approx 200$ pc) illuminated by the B0 IV star, γ Cas (Karr et al., 2005) at a projected distance of ~ 1.3 pc (IC 63) and 1.5 pc (IC 59) from the nebulae (Andersson et al. 2013; Caputo et al. 2020, in press). Sh 2-185 is an HII region with a shell of dust with center at γ Cas. IC 59 and IC 63 are two nebulae in this regions and remain part of this shell.

We have acquired 7-band photometry in the Vilnius system of the region, which yields both the classification and the visual extinction of the stars probed. We analyze these data together with existing polarization data from Soam et al. (2017) and compare the results to those from the study of the Local Bubble (Medan & Andersson, 2019).

This paper is organized as follows: the polarimetric and photometric observations are presented in Section 2. Section 3 includes the results of observation acquired for this work. Our results are analysed and discussed in Section 4 and we summarize our findings in Section 5.

2. DATA ACQUISITION

2.1. Polarimetry

2.1.1. Archival data

Optical imaging (R -band) polarization measurements of nebulae IC 59 and IC 63 were also extracted from Soam et al. (2017). These observations were acquired with the Aries Imaging Polarimeter (AIMPOL) mounted in the Cassegrain focus of the 104-cm optical telescope, India. Details of observations and data reduction can be found in Soam et al. (2017).

2.1.2. Observations

We obtained spectropolarimetric observations from intermediate-dispersion Spectrograph (ISIS) at in the $\sim f/11$ Cassegrain focus of the 4.2 m William Herschel Telescope (WHT) in the Canary Islands, Spain. These observations were carried in 2013 on October 18 and 19, as part of the proposal C9-WHT4/13B. The red and blue, both sides were used for acquiring data. We used EEV12 CCD which provides good quantum efficiency down to the atmospheric cut-off and the R300B grating centered at $0.4\text{ }\mu\text{m}$. Red+ CCD and the R158R grating centered at $0.64\text{ }\mu\text{m}$ were used for the red arm. We are not discussing blue observations here as those were corrupted by scattered light. The red observations have a coverage of $\lambda \approx 0.48 - 0.95\text{ }\mu\text{m}$. We extracted the polarization values at $0.65\text{ }\mu\text{m}$ for comparison with archival data. HD 212311 and HD 204827 were used as zero-polarization and high-polarization standards, respectively. The total integration time was divided into 8 positions of half-wave plate (HWP) settings for minimizing the influence of systematic errors. The standard IRAF routines were used to reduce the data and extract flux. The ordinary (O) and extraordinary (E) spectra were averaged, for each HWP setting observation into $0.05\text{ }\mu\text{m}$ bins and the polarization calculated by fitting $(E-O)/(E+O)$ to a cosine function (Vaillancourt et al., 2020):

$$\frac{E - O}{E + O} = a + P * \cos 4(\alpha - \theta), \quad (1)$$

where P is the amount of polarization, α is the HWP position angle, 2θ is the position angle of measured polarization. The factor a indicates the gain differences between O - and E -beams. We calculated the normalized Stokes parameters $q (= Q/I = P \cos 4(\theta))$ and $u (= U/I = P \sin 4(\theta))$. The value of I is total intensity Stokes parameter. The values of P and θ are calculated as:

$$P = \frac{1}{I} \sqrt{Q^2 + U^2} \quad (2)$$

and

$$\theta = 0.5 \arctan\left(\frac{U}{Q}\right). \quad (3)$$

2.2. Photometry

CCD observations in the Vilnius seven-color photometric system of two $13' \times 13'$ areas, centered on the nebulae IC 59 and IC 63, were obtained with the 1.8 m VATT telescope on Mt. Graham, Arizona using the STA0500A camera and a $4k \times 4k$ CCD chip. Since the areas had no standards of the Vilnius system, tie-in observations to the open cluster IC 1805 were done. This cluster has Vilnius photometry published by [Straižys et al. \(2013\)](#). The angular distance between the IC 59 and IC 63 nebulae and the cluster is about 12 degrees. Processing of CCD frames has been done with the IRAF program package in the aperture mode. The results of photometry of stars down to $V \approx 19$ mag are given in Table 1 (IC 59, 124 stars; online) and Table 2 (IC 63, 185 stars; online). In these tables the last column gives the spectral and luminosity classes in the MK system determined from the photometric data with the QCMPAR code as described in [Straižys et al. \(2019\)](#). The uncertainties of V magnitudes, and color indices $U-V$, $P-V$, $X-V$, $Y-V$, $Z-V$, and $V-S$ given in Tables 1 and 2 take into account the measurement errors and the errors of transformation to the standard system.

To cover all the stars with the available polarization data, another set of CCD exposures with a $35' \times 35'$ field of view, were obtained with the Maksutov-type 35/50 cm telescope of the Molėtai Observatory in Lithuania, using an Apogee Alta U-47 CCD camera. A field center was selected in between the IC 59 and IC 63 nebulae at RA(2000) = $00:58:30$, Dec(2000) = $+61:01:30$. As in the case of the VATT observations, a tie-in to the IC 1805 cluster standards was applied. The processing of CCD frames and the classification of stars has been done with the same methods as in the case of the VATT observations, but the limiting magnitude of Molėtai observations is close to $V = 17$ mag. The catalog of 487 stars, measured and classified from the Molėtai exposures, is given in Table 3 (online).

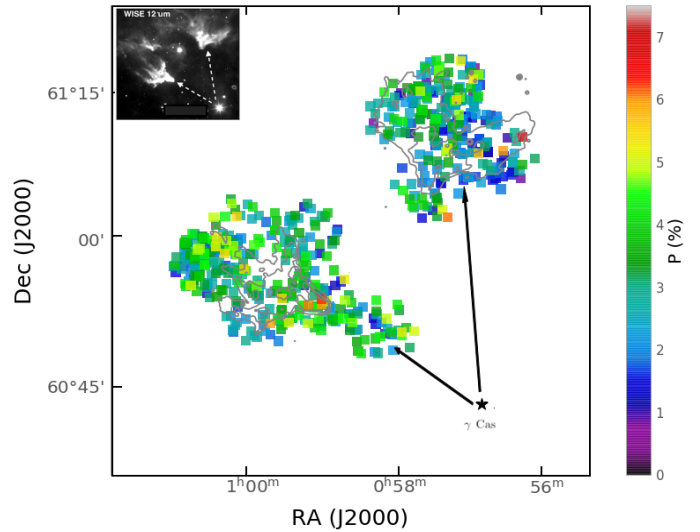


Figure 1. Maps of the amount of polarization observed towards the nebulae IC 59 and IC 63. The inset on left upper corner shows the WISE $12 \mu\text{m}$ dust continuum maps of these nebulae. The location of ionizing star γ Cas and the directions of radiation hitting the nebulae are shown with star symbol and dashed arrows, respectively.

The values A_V of the measured stars were determined from their color excesses E_{Y-V} , which are differences between the observed and the intrinsic color indices $(Y-V)_0$ taken from [Straižys \(1992\)](#):

$$E_{Y-V} = (Y-V)_{\text{obs}} - (Y-V)_0, \quad (4)$$

$$A_V = 4.16 E_{Y-V}, \quad (5)$$

where the coefficient 4.16 corresponds to the normal extinction law. Typical uncertainties of A_V due to the observational errors of $Y-V$ and the errors of the intrinsic $(Y-V)_0$ are ~ 0.1 mag for the stars with $V < 17$ mag and ~ 0.2 mag for V between 17 and 19 mag.

3. RESULTS

Table 4 presents the stars common in polarization measurements of [Soam et al. \(2017\)](#) and photometry observations towards IC 59 and IC 63. This table shows columns with the coordinates of stars, polarization values, visual magnitude, extinction, and polarization efficiency values (note that we will use the expression polarization efficiency to denote the observed line-of-sight averaged ratio of polarization and extinction (P/A_V)).

Figure 1 shows the map of the degree of polarization measured towards the IC 59 and IC 63 nebulae in a color scale. The structure of the clouds are shown with gray solid curves based on the dust continuum emission of these clouds seen in WISE $12 \mu\text{m}$ (inset in upper left corner). The location of the ionizing star and the projected directions of the radiation from γ Cas are also

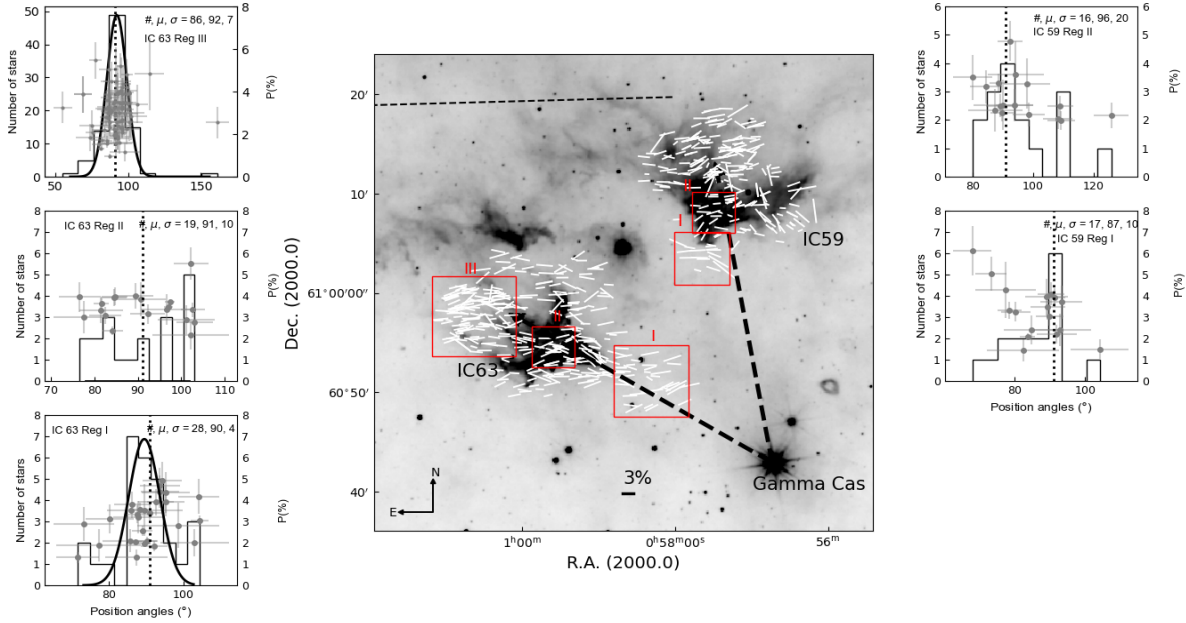


Figure 2. The orientation of the polarization position angles measured for the stars projected towards IC 59 and IC 63 clouds are drawn on the $48' \times 48'$ WISE $12\mu\text{m}$ image. The nebulae, IC 59 and IC 63, and the ionizing star, γ Cas, are identified and labelled. The lengths of the line segments correspond to the measured P . A 3% line segment is drawn for scaling. The arrows with thick broken-line show the direction of the ionizing radiation. The arrows pass through the densest part of the nebulae identified from the $12\mu\text{m}$ intensity. The broken-line shown on the top left corner represents the inclination of the Galactic plane. The Gaussian fitted histograms with the distribution of P and θ_P corresponding to the regions marked in IC 63 and IC 59 are also shown. This figure is adopted from Soam et al. (2017).

shown. A study by Caputo et al. (2020, in press) based on [CII] kinematics found that γ Cas lies behind IC 63 nebula. Therefore, the stars lying outside of the IC 63 in the plane-of-the sky towards γ Cas are not necessarily be significantly close to the γ Cas.

Figure 2, adopted from Soam et al. (2017) shows the distribution of the amounts of polarization and the position angles in different regions (marked) towards IC 59 and IC 63 clouds. This figure will be discussed in further sections.

The two plots in Figure 3 show the A_V (top) and P/A_V (bottom) maps towards the IC 59 and IC 63 nebulae. These A_V and P/A_V values are taken from Table 4 for 78 stars in IC 59 and 126 stars in IC 63, respectively. Interstellar extinctions A_V determined from photometry in the Vilnius system are taken from Tables 4. These data are plotted in sky coordinates with their color indicating the magnitude and %/magnitude values, as seen in the color bars, for A_V and P/A_V , respectively. The WISE $12\mu\text{m}$ contours in gray color with levels from $\sim 45\%$ to $\sim 60\%$ of the maximum value are plotted to show the dust structure of the nebulae. The location of γ Cas is shown as a black star, and the black arrows mark the direction of radiation from this star to the two nebulae.

The upper panel of Figure 4 shows the distribution of extinction values versus their distances from *Gaia* DR2 (Bailer-Jones et al., 2018). The figure shows an increases in A_V with distances and this distribution becomes more dispersed beyond 1.2 kpc. The distributions of degree of polarization and position angles with distances of the targets are shown in the middle and bottom panels of this figure. We limited our analysis to stars with distances of less than 1.5 kpc. The explanation for this choice is given in section 4.1.

Figure 5 shows a toy-model/cartoon illustrating the relationship between A_V and distance in the nebulae. This figure is discussed more in Section 4.1 for understanding the variations of extinction values with distances of the projected targets on nebulae IC 59 and IC 63.

Figure 6 is reproduced from the original figure adopted from Lallement et al. (2014). More about this figure is given in section 4.1.

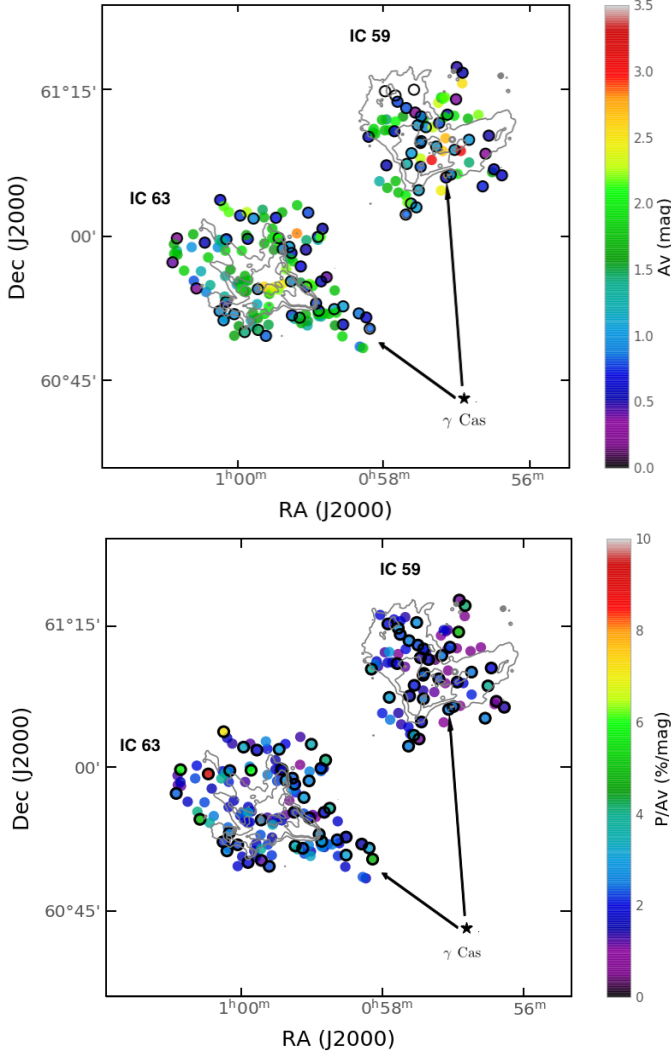


Figure 3. Upper panel shows a map of A_V measurements in IC 59 and IC 63. Gray contours are WISE 12 μ m dust emission. Lower panel is the same as upper panel but for P/A_V values. Symbols with thick boundaries are up to 1.5 kpc and are used in making Figures 4 and 8.

Figure 7 shows the average results of CO($J=1-0$) on-the-fly (OTF)¹ observations towards IC 63 (Soam et al., in prep.). The most prominent emission lines are seen at radial velocities of -20 and 0 km/s.

Figure 8 shows the polarization efficiency (i.e. P/A_V) values for background stars with measured extinctions in the directions of the IC 59 and IC 63 nebulae. The best fitting lines to the distributions are also plotted

¹ In this mode of observations, data is acquired with telescope pointing moves between two points on the sky. The telescope slews in the given stripe duration at a constant speed linearly in RA and linearly in Dec. The OTF mode is typically used to cover large sky areas in short time.

along with equations containing the best-fit parameters in each plot. For plotting these distributions, we have considered only those targets which are at or less than 1.5 kpc away.

The polarization efficiency (P_V/A_V) variation with extinctions for LDN 204- Cloud 3 is shown in Figure 9 by using archival data from Cashman & Clemens (2014).

Figure 10 shows the distribution of polarization efficiencies as a function of radiation flux from the illuminating sources. This plot presents a comparison of the Local Bubble, with UV flux from OB associations (Medan & Andersson, 2019) with our findings towards IC 59 and IC 63 nebulae affected by the UV flux from γ Cas. We also plotted values for LDN 204 adopted from Cashman & Clemens (2014).

A cartoon shown in Figure 11 is adopted from Medan & Andersson (2019) to illustrate the inclination angle (ψ) between the line-of-sight vector and the cloud region.

4. ANALYSIS AND DISCUSSION

4.1. Polarization efficiency and extinction at different distances

To understand the effect of illumination on the grain alignment, we must isolate the dust in, and therefore polarization from, the IC 59 and IC 63 nebula from possible background polarization. We can do this based on the extinction versus distance plots. There are two, likely complementary, origins of steps in these plots (Figure 4). If the surface density (i.e. localized A_V) of each individual extinction layer is uniform, then each step in A_V versus d represents a new layer of dust extinction at the distance of the step. However, multiple steps in A_V versus d can also occur with a single physical, but non-uniform, layer.

We can see this by considering a uniform, but relatively sparse, space distribution of background stars above a given apparent magnitude (i.e. such that they are included in a magnitude limited photometric survey). The surface density on the sky of observed stars will be the product of their space density and the distance to which the observations extend. The surface density of measured stars will then rise linearly with distance probed, or equivalently, the on-the-sky distance between observed stars will shrink with increasing line of sight distance sampled.

If an extinction layer has density enhancements that are small on the scale of the total area surveyed (and, again, the stellar surface density is limited), the probability that such a dense sub-region (Figure 5) intercepts the line of sight to a background star will then be significantly less than one. If the extinction density enhancements have a characteristic scale size, then an

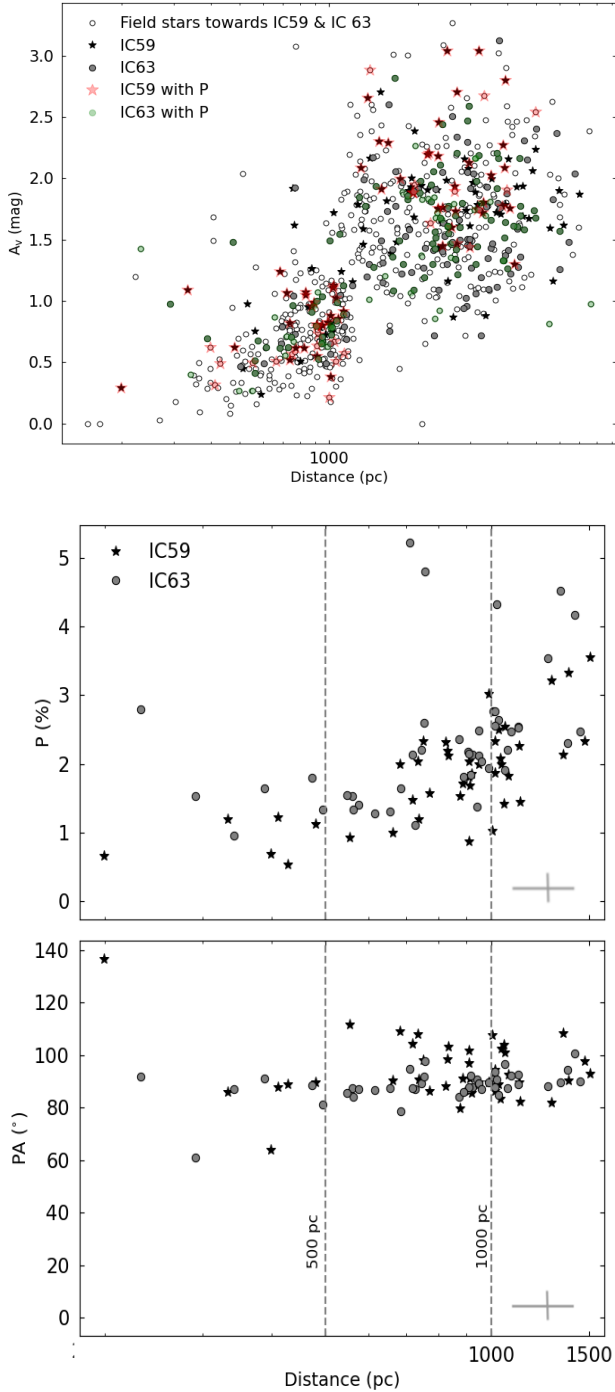


Figure 4. The upper panel shows the distribution of A_V values with *Gaia* DR2 distances from Bailer-Jones et al. (2018) of all the targets where have photometric information only and colored symbols are those where we have both photometric and polarimetric data. The two samples of IC 59 and IC 63 are shown with different symbols. The middle and lower panels show the distributions of the degree of polarization and the position angle with distances. Two vertical dashed lines are drawn at distances of 500 and 1000 pc.

“extinction step” will occur at the distance where that scale size is first effectively sampled by the stellar surface density. For a spectrum of extinction enhancement scales, we would expect a more distributed increase in A_V versus d , yielding increased dispersion in extinction for a given stellar distance.

In this scenario of an extended low-extinction layer with embedded localized higher extinction regions, we would expect the upper envelope of the extinction to rise either abruptly – for a single scale size of denser regions – or gradually for a distribution of high- A_V “clumps”. The lower envelope, corresponding to the large scale low-extinction part of the layer should, however, stay close to constant. For an additional distinct extinction layer, the lower envelope of the A_V distribution should also rise.

It is, of course, also possible to consider an interstellar density distribution where the dense (higher A_V) regions of a physical extinction layer are more broadly distributed with smaller, low A_V , “hole” areas interspersed (see Figure 5). This would, however, still raise both the upper and lower envelopes of the A_V distribution at the characteristic distance, with a small number of lower A_V points remaining, and should still be differentiable from a uniform physical layer or a single inhomogeneous one. This is illustrated in the distributions of A_V vs. d panels of Figure 4.

Therefore, the better diagnostic of a true additional extinction layer with distance will be the minimum extinction as a function of the distance, rather than the maximum extinction as a function of the distance. The upper panel of Figure 4 illustrates this for the direction of Sh 2-185. As is clear from the figure, while there are enhancements of the maximum extinction towards IC 59 and IC 63 between 700 pc–1.2 kpc, the lower envelope of the extinction remains approximately constant all the way from \sim 200 pc to \sim 1.2 kpc. At about 1.2–1.5 kpc a significant increase occurs in both the upper and lower envelopes of the extinction distribution, with a small number of low extinction points remaining at $A_V \lesssim 1$ mag.

This interpretation is consistent with the trigonometric parallax distances to γ Cas, on the one hand, and the Perseus arm, on the other. The *Hipparcos* distance for γ Cas ($l,b=124, -2$) is 188 ± 20 pc. The distance to the Perseus arm can be estimated from the *Gaia* distance to the OB stars in the star forming complex W3 ($l,b=134, +1$) of ≈ 2.2 kpc (Navarete et al., 2019). Since the OB stars are expected to be concentrated towards the center of the spiral arm, we could expect the dust in the arm to be detectable somewhat closer than the OB stars. We therefore assume that our subsequent analysis

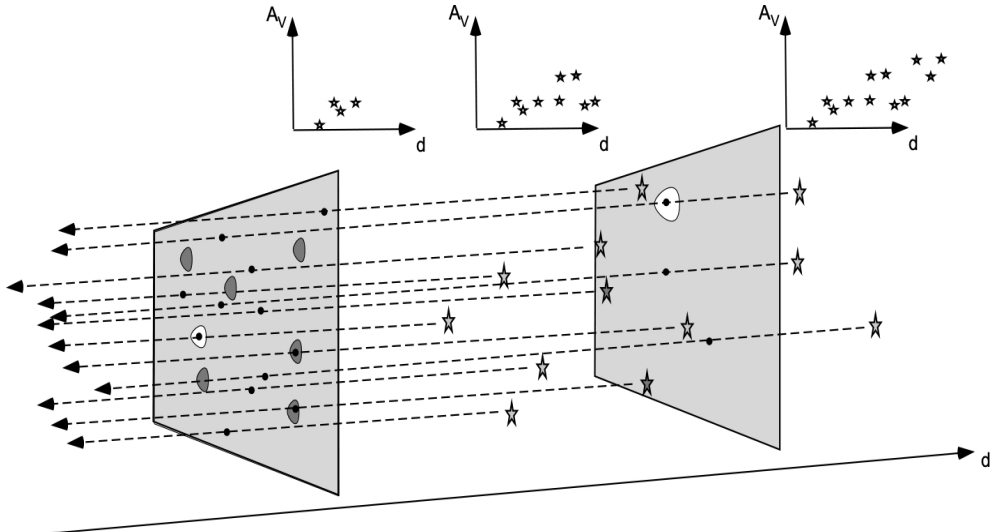


Figure 5. The two causes of extinction steps in an extinction vs. distance plot are illustrated in a toy-model/cartoon. For a cloud with a density structure – especially where the surface area of the high extinction regions is significantly smaller than the average extinction of the cloud/layer – an extinction jump may be detected at a distance corresponding to where the chance of a line of sight encountering a “clump” becomes significant. The lower envelope of the distribution will, however stay fixed. When a second extinction layer is encountered both the upper and lower envelopes of the distribution will change. For extinction layers with low density sub-regions (“holes” shown as white regions in the screens), a small number of low A_V outliers may be expected. These different behaviors can all be seen in the top panel of Figure 4.

that stars out to 1.5 kpc probe only the extinction from dust in Sh 2-185.

Figure 6, adopted from Lallement et al. (2014) shows the differential opacity in the Galactic plane out to ~ 1 kpc. The two over-laid arrows are scaled to represent 1 kpc distance and span the Galactic longitude range of 123.45° to 124.05° (i.e. from just west of IC 59 to just east of IC 63). As the figure shows, the differential opacity in this direction is low out to ~ 200 pc where a high-opacity ridge intercepts our lines of sight (as Figure 3 in Lallement et al. shows, the sampling density of their data indicates that the depth of this ridge is likely, at best, marginally resolved). Beyond this ridge no further high-opacity material is seen to the extent of the mapping (although beyond ~ 700 pc the spatial resolution in the Lallement et al. data decreases, and therefore small-scale structure may not be detected close to the Perseus arm). Thus, our interpretation of our A_V vs. distance plots is consistent with the extinction mapping of Lallement et al. (2014).

In addition, we investigated CO ($J=1-0$) data from Dame et al. (2001) at multiple positions in the near vicinity of IC 59 and IC 63. All positions show a strong CO band with radial velocity close to -20 km/s. According to the “Kinematic Distance Calculator” (Reid et al., 2009), this velocity gives a distance of the cloud close to 1.5 kpc. This is in agreement with our A_V vs. distance plots for the VATT photometric data (upper panel in Figure 4) which at about 1.5 kpc show a steep

rise of the extinction up to A_V close to 3 magnitudes. It is interesting that the Dame et al. radio data do not show any significant intensity maximum at radial velocity close to zero which would correspond to the IC 59 and IC 63 clouds at 200 pc. We note that the Dame et al. (2001) surveys are sampled only on a $7.5'$ grid and hence the small molecular cores of IC 59 and IC 63 would be significantly beam-diluted in their data. However, we found some significant CO($J=1-0$) emission at radial velocity close to zero towards IC 59 and IC 63 in our 13-m single dish observations (Soam et al., in prep.)² from Taeduk Radio Astronomy Observatory (TRAO) with much better resolution ($44''$) than that of observations of Dame et al. (2001). Figure 7 shows the emission at 0 km/s and close to -20 km/s radial velocities. Jansen et al. (1994) also reported a detection of CO ($J=2-1$) in IC 63 nebula at radial velocity 0.6 km/s. Heyer et al. (1998) found a CO ($J=1-0$) emission at velocity close to zero km/s located behind the curved surface of IC 59 facing radiation from γ Cas. Our recent observations of CO ($J=1-0$) and these previous studies show that there is a prominent CO emission towards IC 59 and IC 63 nebulae. As we discussed above on emission from six positions around these nebulae from Dame et al., the emission seen at -20 km/s might correspond to Perseus arm. From these arguments, we conclude that no strong

² A detailed analysis of line observations is beyond the purpose of this paper and will be presented in a work under progress.

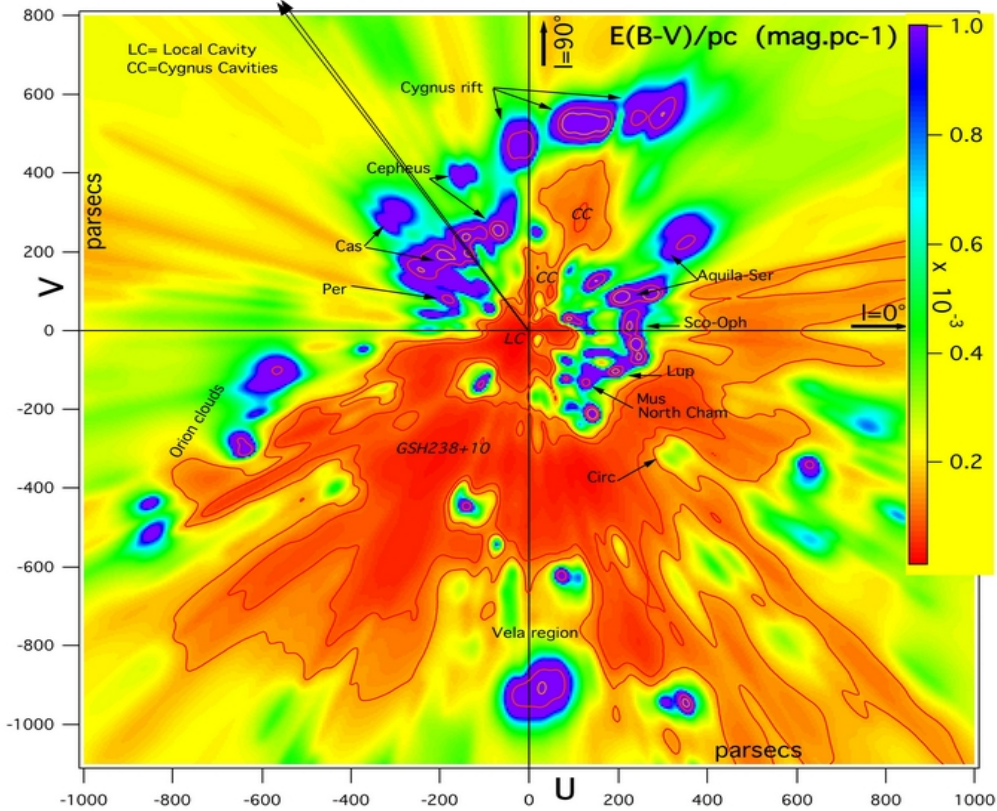


Figure 6. This figure adopted from Lallemand et al. (2014) and reproduced with permission ©ESO. The inverted differential opacity distribution in the Galactic plane in the Solar neighborhood is shown. The sun is located at (0,0) coordinates with the Galactic center toward the right. The color scale from red to violet shows increasing differential opacities. The two arrows are scaled to be 1 kpc in length, and drawn to bracket the extent of the Sh 2–185 region (i.e. from just west of IC 59 to just east of IC 63). The extinction distribution in this map supports our conclusion of very little foreground extinction, or background extinction to at least 1 kpc, in the direction of Sh 2–185.

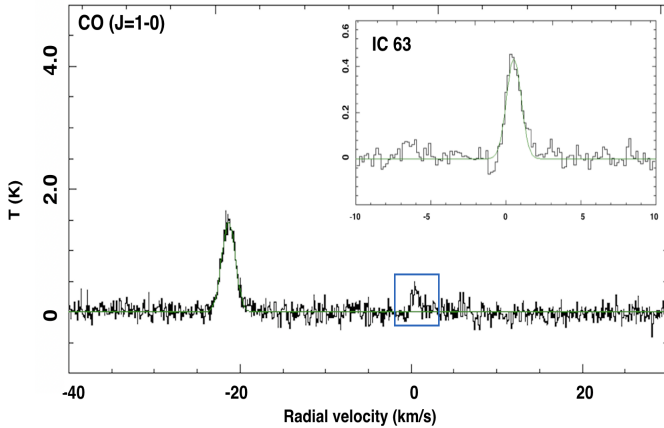


Figure 7. Emission towards IC 63 in CO($J=1-0$) line (Soam et al., in prep.) The dominant peaks are seen at radial velocities close to -20 and 0 km/s. The line feature at 0 km/s framed with blue box is zoomed-in at the upper right corner of the figure.

widespread absorbing and polarizing clouds are present behind γ Cas up to 1 or 1.5 kpc.

4.2. Grain alignment due to external radiation and comparison with Local Bubble

Cashman & Clemens (2014) studied the variations of H-band polarization efficiency (P_H/A_V) in the LDN 204- Cloud 3 with distance from ζ Oph (spectral class O9.5 V). They found that the polarization efficiency steadily decreases with the distance from ζ Oph. Also the power law fit to the distribution of polarization efficiency and extinctions shows a steep index of -0.74 ± 0.07 which suggests less grain alignment at high extinctions compared to other studies performed on different molecular clouds. They noticed (beyond the uncertainties) that the weighted mean polarization efficiencies (P_H/A_V) do vary systematically with distance to ζ Oph.

Medan & Andersson (2019) performed a more general study of the grain alignment variation in the Local Bubble wall, using a large polarization survey of the North Galactic cap from Berdyugin et al. (2014). They found that the polarization efficiency is linearly dependent on the intensity of the illumination of the grains, and is

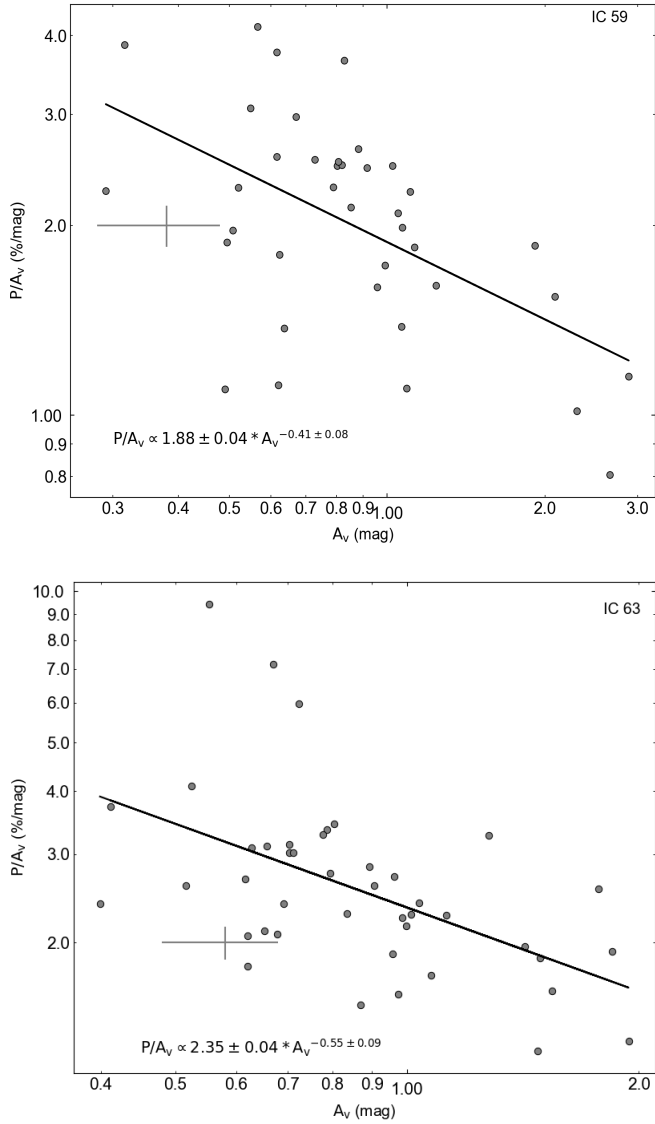


Figure 8. The variation of polarization efficiencies with extinction values measured towards the targets projected on the IC 59 (upper) and IC 63 (lower) nebulae. The best fitted parameters and typical error bars are also indicated.

dominated by the light from the OB association within 150 pc. Adding in contributions from field stars also allowed them to investigate the wavelength dependence of RAT alignment, and to show that the alignment is most sensitive to the blue light from O and B type stars.

In the present study, we add a well defined system with two nebulae radiated upon by higher radiation flux from γ Cas, a B0 IV star, in the Sh 2-185 H II region.

For some regions in Figure 1 no projected star was bright enough to yield significant polarization detections. The spatial distribution of polarization efficiencies shown in lower panel of Figure 3 indicates relatively

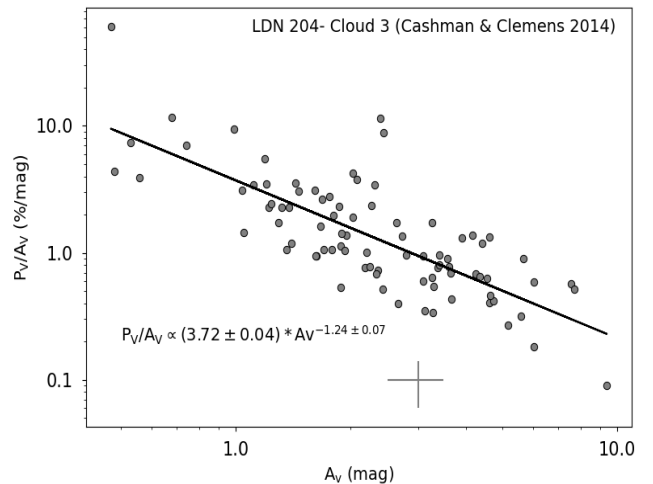


Figure 9. Polarization efficiency (P_V/A_V) vs. extinction distribution of stars observed towards LDN 204-Cloud 3. The data is adopted from Cashman & Clemens (2014). From their archival data, we used only those detections where $P/\sigma P > 3$ is satisfied. The H-band polarization values are transformed to V-band using the relation from Andersson & Potter (2007).

higher polarization efficiencies on the cloud boundaries in low density regimes. Figure 2, adopted from Soam et al. (2017), shows a similar trend, where the polarization measurements in regions I, II, and III in IC 63 and regions I and II in IC 59 [labelled in red color], show a polarization fraction which is relatively higher in regions closer to γ Cas, especially in IC 59. The polarization efficiency as a function of visual extinction can be interpreted in the framework of Jones et al. (1992):

$$\frac{P}{A_V} = \beta A_V^\alpha, \quad (6)$$

where α depends primarily on the turbulence of the medium and – for large extinctions – grain alignment variation (Alves et al., 2014; Jones et al., 2015). For a fully turbulent medium, α is expected to take a value of -0.5, indicating a random walk through a large number of turbulent cells with differently oriented magnetic fields (Jones et al., 1992). The value at $A_V = 1$ can be used as a comparison of the polarization efficiency between samples. Under the assumption that the inherent dust characteristics (roundness, size distribution, mineralogy etc.) are similar for the different regions, P/A_V at $A_V = 1$ can be used as a tracer of grain alignment efficiency.

We used Eq. 6 to fit the polarization and extinction measurements towards IC 59 and IC 63 shown in Figure 8. We considered data upto 1.5 kpc only for plotting and

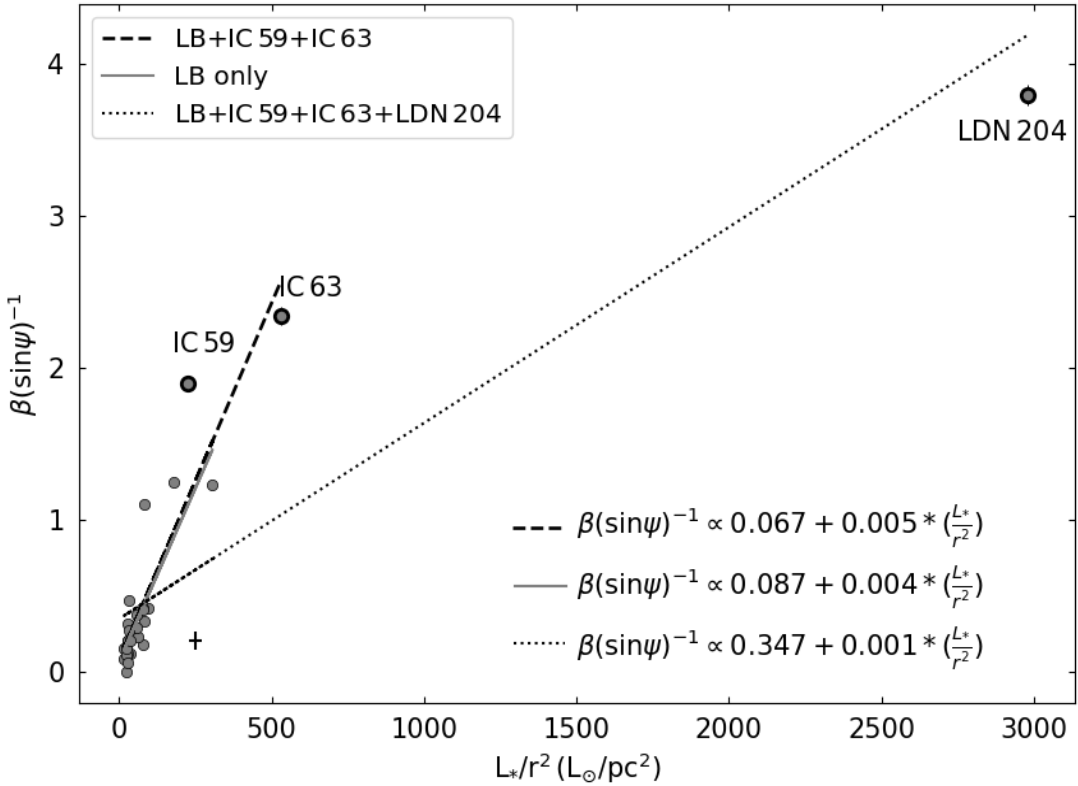


Figure 10. The variation of the polarization efficiency indicated by $\beta(\sin \psi)^{-1}$ (see Medan & Andersson, 2019) with UV photon flux. The values measured toward the Local Bubble (Medan & Andersson, 2019) are shown with gray filled circles and those of IC 59, IC 63 [this work] and LDN 204 (Cashman & Clemens, 2014) with errors are shown as gray filled circles with thick black boundaries. Typical error bar on Local Bubble measurements is also shown. The source of UV fluxes towards IC 59 and IC 63 nebulae is γ Cas and for LDN 204, it is ζ Oph. The walls of local bubble receives UV flux from OB associations.

fitting in this figure. The reason for choosing this distance is given in section 4.1. We find values of α and β of -0.55 ± 0.09 and 2.35 ± 0.04 for IC 63 and -0.41 ± 0.08 and 1.88 ± 0.04 for IC 59, respectively. As we stated above in section 2, we used a typical error of 0.1 mag in A_V for calculating uncertainties in fitted values. To evaluate the sensitivity of the results to systematic errors (such as the incorrect assignment of any polarization or extinction to the two clouds, we systematically removed one line of sight from the sample for each cloud and re-calculated the power-law fits. The resulting sample of fit parameters are consistent with the fit to the full sample for each cloud, indicating that the fit results are dominated by random errors and that the results are robust. For IC 63 the α parameter distribution has a mean of -0.55 with an error on the mean of 0.03, while the β parameter has a mean of 2.34 with an error on the mean of 0.02. For IC 59 the two distributions have means and error on the means of $\alpha:(-0.45, 0.03)$ and $\beta:(1.89, 0.07)$, respectively.

Cashman & Clemens (2014), in their study of Cloud 3 of LDN 204 near ζ Oph, found a slope in P_H/A_V of $\alpha = -0.74 \pm 0.07$. Because of the shape of the Serkowski curve (Serkowski, 1973), the NIR polarization is significantly less than that for optical bands, for almost any extinction. We therefore need to convert the H-band data from Cashman & Clemens (2014) to estimated V-band polarization, in order to compare their results to the Local Bubble wall results. In addition, as suggested by Whittet et al. (2001) and confirmed and expanded on by Andersson & Potter (2007) a universal relationship exists between λ_{\max} and A_V , with a secondary dependence on the average total-to-selective extinction (R_V) in each region. Because the peak of the polarization curve shifts to longer wavelength with increasing extinction, the transformation from P_H to P_V will depend on the extinction of the line of sight, and will result in a steeper P_V/A_V vs. A_V relation than for P_H/A_V vs. A_V . We used the λ_{\max} vs. A_V relationship from Andersson & Potter (2007) together with extinction estimates

from [Cashman & Clemens \(2014\)](#) to convert the H-band measurements to estimates of the V-band polarization, and thence derive P_V/A_V values. Performing this conversion from P_H/A_V to P_V/A_V yields an equivalent, V-band, α value for LDN 204 of $\alpha = -1.24 \pm 0.07$.

Figure 10 shows the variation of polarization efficiency represented by $\beta(\sin\psi)^{-1}$ (assuming $\sin(\psi)=1$ i.e. $\psi = 90^\circ$, β is equivalent to a lower limit of the alignment efficiency ($P/A_V(A_V=1)$, Eq. 6) with flux (L_*/r^2 , where L_* is the luminosity of γ Cas). These expressions are explained later in this section.

As is shown in Figure 10, the values of polarization efficiencies ($P/A_V (A_V = 1)$) are significantly higher in Sh 2-185 than those found in the Local Bubble wall with $\beta = 1.95 \pm 0.05$ for IC 59 and $\beta = 2.24 \pm 0.04$ for IC 63. This indicates a higher grain alignment efficiency in the Sh 2-185 region. Similarly to the results by [Cashman & Clemens \(2014\)](#) in the LDN 204 cloud, we also derived a decrease in polarization efficiency for IC 63 and IC 59 with increasing distance from γ Cas. The polarization efficiency in this context refer to $\beta(\sin\psi)^{-1}$ which is inversely proportional to the square of the distance (r) of the cloud from γ Cas. As seen in Figure 10, $\beta(\sin\psi)^{-1}$ value of IC 59 is less than that of IC 63. This is because IC 63 is a relatively closer ($r=1.3$ pc) to γ Cas than IC 59 ($r=1.5$ pc). For LDN 204 using the P_V/A_V plot we derive $\beta = 3.72 \pm 0.04$.

To test the variation of radiatively driven grain alignment with distance of the cloud from the radiation sources, [Medan & Andersson \(2019\)](#) constructed a model to predict values of $\beta(\sin\psi)^{-1}$ for the Local bubble. The model was defined as:

$$\beta(\sin\psi)^{-1}(\ell, b) \propto \frac{L_*}{(x_* - x_i)^2 + (y_* - y_i)^2 + (z_* - z_i)^2} \quad (7)$$

where $L_*^{(i)}$ is luminosity of the source i , x_* (etc.) are the locations of the source, and x_i (etc.) refer to the position at the nebula [wall of LB]. Combining the all sources in LB, the model of [Medan & Andersson \(2019\)](#) takes the form:

$$\beta(\sin\psi)^{-1} = A + B \cdot \Sigma \frac{L_*^{(i)}}{r_i^2} \quad (8)$$

where $L_*^{(i)}$ is the luminosity of the source i at a distance r_i from the cloud. The function $\sin\psi$ accounts for the fact that dust-induced polarization only probes the magnetic field component in the plane of the sky. Since the grains are spinning around the field lines, no polarization is generated along the magnetic field direction (see [Medan & Andersson, 2019](#), for details). Figure 11 illustrates the concept.

Under the assumption of RAT alignment the alignment efficiency will depend on the intensity of the radiation field at the location of the grain. This will, in turn, depend on the extinction between the illumination source and the grain, and, if the radiation field is dominated by a point source, the distance from the source to the grain (through the r^{-2} dependence). For regions with rapidly varying radiation fields (i.e. close to a point source) or with significant extinction, the measured polarization efficiency (P/A_V) may sample regions with different alignment efficiency, especially at higher observational line-of-light visual extinction. However, because of the RAT condition, $\lambda < 2a$, and because the extinction curve falls to the red, RAT alignment is relatively insensitive to the extinction between the source and the grain for moderate column densities, which will somewhat lessen the variability relative to the visual ($\lambda=0.55 \mu\text{m}$) extinction. In addition, along an observed line of sight the polarization efficiency will probe dust and gas at varying levels of source-to-grain extinction in a poorly constrained way that depends on the density and location of the cloud relative to the illuminating source. Because the power-law fits in [Medan & Andersson \(2019\)](#) and Figure 8 (this work) are dominated by line-of-sight extinction with $A_V < 1$ mag., internal radiation damping in these clouds should not have a significant impact on the fitted α or β values. In Figure 9, which shows the data from [Cashman & Clemens \(2014\)](#) after transformation from P_H/A_V to P_V/A_V (from their archival data, we used only those detections where $P/\sigma P > 3$ is satisfied. The H-band polarization values are transformed to V-band using the relation from [Andersson & Potter \(2007\)](#)), the larger best-fit α value may indicate a significant contribution of cloud-internal extinction vis-à-vis ζ Oph (suppressing the alignment efficiency, and therefore P/A_V , at the higher extinctions). However, as the points at $A_V < 1$ are continuous with the ones at $A_V > 1$, the β value is unlikely to be severely affected, certainly not to the level of $\beta \approx 13$ that the straight line of the Local Bubble wall and Sh 2-185 results would imply³.

For the region between Galactic latitude $30\text{--}42^\circ$, [Medan & Andersson \(2019\)](#) found $A = 0.0055 \pm 0.0103$ and $B = 0.0047 \pm 0.0002$ from the best fit of model predicted radiative driven grain alignment based on luminosities of local OB association versus the measured grain alignment (see Figure 12 of [Medan & Andersson 2019](#)).

³ if we calculate $\beta(\sin\psi)^{-1}$ using best fitted A and B values of Local bubble and IC 59 and IC 63 nebulae and $L/r^2 \approx 3000$ of LDN 204, we get a value close to 13.

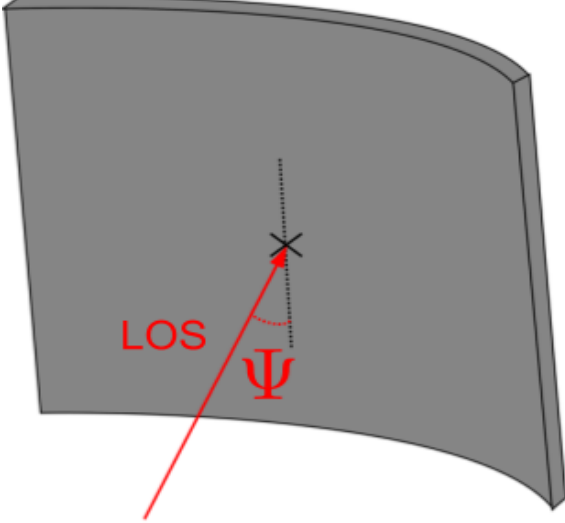


Figure 11. Adapted from Medan & Andersson (2019). The diagram represents one of the regions of LB wall. The center of the region is intersected by line-of-sight vector in red color. The inclination angle between the line-of-sight vector and the shaded cloud region is represented by ψ .

For IC 63 and IC 59 we assume that the magnetic field is oriented close to the plane of the sky and, therefore $\sin(\psi)$ is unity. Crutcher et al. (2003) showed that the average Galactic magnetic field in the Solar neighborhood is directed towards $l, b \approx 80.6, 0$. Since Sh 2-185 is located at $l \approx 124^\circ$ this means that the Galactic magnetic field, nominally, makes an angle of $\psi \approx 46^\circ$ with the clouds in the region. However, because of the dynamics of a magnetized H II region (Stil et al., 2009; Gendelev & Krumholz, 2012), it is not clear that the magnetic field threading IC 59 and IC 63 agree with the direction of the Galactic average. As shown by the polarization mapping by Soam et al. (2017) a significant plane-of-the-sky component of the magnetic field is present in the nebulae. As noted above, an assumption of $\sin(\psi)=1$ (i.e. $\psi = 90^\circ$) makes β equivalent to a lower limit of the alignment efficiency ($P/A_V(A_V=1)$, Eq. 6). Given the distance of the nebulae from γ Cas of 1.3 and 1.5 pc (Hoang et al., 2015), we can put the results for Sh 2-185 on the same plot as those for the Local Bubble wall.

Figure 10 shows the values of polarization efficiency modified by $\beta(\sin \psi)^{-1}$ in the Local Bubble (Medan & Andersson, 2019) with luminosities from of the blue source(s) modified by their distances from the clouds. Overlaid are the resultant values for IC 59 and IC 63 corrected for the Sh 2-185 geometry (Caputo et al. 2020, in press). As is evident from Figure 2 some of the dust in Sh 2-185 extends beyond the immediate confines of the two clouds. The exact location of this dust is not clear,

but given the dynamics of H II regions it is likely to either be associated with the dense clouds, or swept up in an irregular shell around the star. While this means that the exact level of the radiation field strength at the location of this dust is also unclear, we assign each of these line of sight to the nearest of the two clouds and, treat the unknown difference in radiation field strength as systematic errors. As discussed above, systematically excluding individual data points from the analysis does not change our results, indicating that these uncertainties do not dominate the behaviour of the grain alignment in Sh 2-185. Finally, the alignment efficiency and estimated illumination flux based on the data for LDN 204 from Cashman & Clemens (2014) are also plotted.

As seen in Figure 10, for the Local Bubble wall data alone (Medan & Andersson, 2019) found a best linear fit of $A = 0.067 \pm 0.012$ and $B = 0.0047 \pm 0.0002$. Including the results for IC 59 and IC 63 yields parameter values of $A = 0.087 \pm 0.011$ and $B = 0.00444 \pm 0.0002$, within the 2σ mutual errors of the fits for the Local Bubble wall alone. If we include the results for LDN 204- Cloud 3 (Cashman & Clemens, 2014), a significantly shallower slope results, but with a poorer fit to the low luminosity end, with parameters $A = 0.347 \pm 0.023$ and $B = 0.0013 \pm 0.0001$.

Because not all grains can cause polarization (due to sphericity, grain mineralogy, etc.), we would, under RAT alignment, expect that there will exist a radiative illumination intensity where the observed linear relationship between polarization efficiency and radiation intensity breaks down, since at that intensity all grains that *can* be aligned *will* be aligned. It is possible that the change in slope seen when including the LDN 204-Cloud 3 (Cashman & Clemens, 2014) results is an indication of such a saturation effect. We are in the process of exploring the polarization efficiency in even more extreme environment where this possibility can be further tested.

4.3. Comparison with modeled values

Hoang et al. (2015) analytically modeled the grain alignment by radiative torque in the IC 63 nebula. The presence of external high energy radiation provides extra torque to the dust grains providing opportunity to quantify the RAT and effects of additional torque. Hoang et al. (2015) noticed the shallower slope, i.e. $\alpha \sim -0.1$ for $A_V < 3$ and a very steep slope of $\alpha \sim -2$ for $A_V > 4$. They attributed the enhancement in P_λ/A_V due to combined effects of extra radiative torque and H_2 formation torque. The high grain alignment and polarization efficiency in IC 63 also implies the lowest values of rotational of anisotropic radiation field compared to the values in Local Bubble. The observed polarization values in IC 59 and IC 63 probe the regions of $A_V < 3.5$,

and we obtained the slopes of -0.55 and -0.41 in IC 63 and IC 59, respectively. This value is in good agreement with the modeled values of Hoang et al. (2015).

5. SUMMARY

We used the optical polarization and multiband photometric observations towards nebulae IC 59 and IC 63 to probe the grain alignment and polarization efficiency. Using the distances to the nebulae and known flux of their illuminating star γ Cas we have interpreted the results in the context of radiative grain alignment. We compared our results to polarization efficiencies measured in the Local Bubble walls (Medan & Andersson, 2019). Polarization efficiencies are found to be higher in the IC 59 and IC 63 nebulae than those estimated for the Local Bubble. This suggests an enhanced grain alignment due to RAT in these nebulae “because of the close” vicinity of γ Cas compared to the large distances of the walls of Local Bubble from OB associations. Because not all grains can cause polarization (due to sphericity, grain mineralogy, etc.), we would expect that there will

exist a radiative intensity where the observed linear relationship between polarization efficiency and radiation intensity breaks down. We are currently exploring such extreme environments.

We thank anonymous referee for very constructive reports which helped significantly in improvement in the content of this paper. The WHT is operated on the island of La Palma by the Isaac Newton Group of Telescopes in the Spanish Observatorio del Roque de Los Muchachos of the Instituto de Astrofísica de Canarias. B-G.A. and A.S. acknowledge the financial support from the NSF through grant AST-1715876. V.S., A.K. and J.Z. acknowledge the financial support from the Research Council of Lithuania, grant No. S-MIP-17-74.

Facility: WHT, AIMPOL, VATT, Molétei

Software: Astropy (Astropy Collaboration et al., 2013), Matplotlib (Hunter, 2007), SciPy (Virtanen et al., 2020), NumPy (Harris et al., 2020)

REFERENCES

- Alves, F. O., Frau, P., Girart, J. M., et al. 2014, A&A, 569, L1, doi: [10.1051/0004-6361/201424678](https://doi.org/10.1051/0004-6361/201424678)
- Andersson, B. G., Hoang, T., Lopez-Rodriguez, E., et al. 2018, in American Astronomical Society Meeting Abstracts, Vol. 231, American Astronomical Society Meeting Abstracts #231, 414.04
- Andersson, B.-G., Lazarian, A., & Vaillancourt, J. E. 2015, ARA&A, 53, 501, doi: [10.1146/annurev-astro-082214-122414](https://doi.org/10.1146/annurev-astro-082214-122414)
- Andersson, B.-G., & Potter, S. B. 2007, ApJ, 665, 369, doi: [10.1086/519755](https://doi.org/10.1086/519755)
- Andersson, B.-G., Piironen, V., De Buizer, J., et al. 2013, ApJ, 775, 84, doi: [10.1088/0004-637X/775/2/84](https://doi.org/10.1088/0004-637X/775/2/84)
- Astropy Collaboration, Robitaille, T. P., Tollerud, E. J., et al. 2013, A&A, 558, A33, doi: [10.1051/0004-6361/201322068](https://doi.org/10.1051/0004-6361/201322068)
- Bailer-Jones, C. A. L., Rybizki, J., Fouesneau, M., Mantelet, G., & Andrae, R. 2018, AJ, 156, 58, doi: [10.3847/1538-3881/aacb21](https://doi.org/10.3847/1538-3881/aacb21)
- Berdyugin, A., Piironen, V., & Teerikorpi, P. 2014, A&A, 561, A24, doi: [10.1051/0004-6361/201322604](https://doi.org/10.1051/0004-6361/201322604)
- Bhatt, H. C., & Jain, S. K. 1993, A&A, 276, 507
- Cashman, L. R., & Clemens, D. P. 2014, ApJ, 793, 126, doi: [10.1088/0004-637X/793/2/126](https://doi.org/10.1088/0004-637X/793/2/126)
- Chapman, N. L., Goldsmith, P. F., Pineda, J. L., et al. 2011, ApJ, 741, 21, doi: [10.1088/0004-637X/741/1/21](https://doi.org/10.1088/0004-637X/741/1/21)
- Crutcher, R., Heiles, C., & Troland, T. 2003, in Lecture Notes in Physics, Berlin Springer Verlag, Vol. 614, Turbulence and Magnetic Fields in Astrophysics, ed. E. Falgarone & T. Passot, 155–181
- Cudlipp, W., Furniss, I., King, K. J., & Jennings, R. E. 1982, MNRAS, 200, 1169, doi: [10.1093/mnras/200.4.1169](https://doi.org/10.1093/mnras/200.4.1169)
- Dame, T. M., Hartmann, D., & Thaddeus, P. 2001, ApJ, 547, 792, doi: [10.1086/318388](https://doi.org/10.1086/318388)
- Davis, L. J., & Greenstein, J. L. 1951, ApJ, 114, 206
- Dolginov, A. Z., & Mitrofanov, I. G. 1976, Ap&SS, 43, 291
- Dotson, J. L., Davidson, J., Dowell, C. D., Schleuning, D. A., & Hildebrand, R. H. 2000, ApJS, 128, 335, doi: [10.1086/313384](https://doi.org/10.1086/313384)
- Draine, B. T., & Weingartner, J. C. 1996, ApJ, 470, 551, doi: [10.1086/177887](https://doi.org/10.1086/177887)
- Gendelev, L., & Krumholz, M. R. 2012, ApJ, 745, 158, doi: [10.1088/0004-637X/745/2/158](https://doi.org/10.1088/0004-637X/745/2/158)
- Hall, J. S. 1949, Science, 109, 166
- Harris, C. R., Millman, K. J., van der Walt, S. J., et al. 2020, Nature, 585, 357–362, doi: [10.1038/s41586-020-2649-2](https://doi.org/10.1038/s41586-020-2649-2)
- Heyer, M. H., Brunt, C., Snell, R. L., et al. 1998, ApJS, 115, 241, doi: [10.1086/313086](https://doi.org/10.1086/313086)
- Hiltner, W. A. 1949a, Science, 109, 165
- . 1949b, ApJ, 109, 471

- Hoang, T., Lazarian, A., & Andersson, B.-G. 2015, MNRAS, 448, 1178, doi: [10.1093/mnras/stu2758](https://doi.org/10.1093/mnras/stu2758)
- Hodapp, K.-W. 1987, ApJ, 319, 842, doi: [10.1086/165502](https://doi.org/10.1086/165502)
- Høg, E., Fabricius, C., Makarov, V. V., et al. 2000, A&A, 355, L27.
[http://cdsads.u-strasbg.fr/cgi-bin/nph-bib_query?
bibcode=2000A...355L..27H&db_key=AST](http://cdsads.u-strasbg.fr/cgi-bin/nph-bib_query?bibcode=2000A...355L..27H&db_key=AST)
- Hough, J. H., Aitken, D. K., Whittet, D. C. B., Adamson, A. J., & Chrysostomou, A. 2008, MNRAS, 387, 797, doi: [10.1111/j.1365-2966.2008.13274.x](https://doi.org/10.1111/j.1365-2966.2008.13274.x)
- Hunter, J. D. 2007, Computing in Science & Engineering, 9, 90, doi: [10.1109/MCSE.2007.55](https://doi.org/10.1109/MCSE.2007.55)
- Jansen, D. J., van Dishoeck, E. F., & Black, J. H. 1994, A&A, 282, 605
- Jones, T. J., Bagley, M., Krejny, M., Andersson, B.-G., & Bastien, P. 2015, AJ, 149, 31, doi: [10.1088/0004-6256/149/1/31](https://doi.org/10.1088/0004-6256/149/1/31)
- Jones, T. J., Klebe, D., & Dickey, J. M. 1992, ApJ, 389, 602, doi: [10.1086/171233](https://doi.org/10.1086/171233)
- Karr, J. L., Noriega-Crespo, A., & Martin, P. G. 2005, AJ, 129, 954, doi: [10.1086/426912](https://doi.org/10.1086/426912)
- Kataoka, A., Tsukagoshi, T., Pohl, A., et al. 2017, ApJL, 844, L5, doi: [10.3847/2041-8213/aa7e33](https://doi.org/10.3847/2041-8213/aa7e33)
- Lallement, R., Vergely, J.-L., Valette, B., et al. 2014, A&A, 561, A91, doi: [10.1051/0004-6361/201322032](https://doi.org/10.1051/0004-6361/201322032)
- Lallement, R., Welsh, B. Y., Vergely, J. L., Crifo, F., & Sfeir, D. 2003, A&A, 411, 447
- Lazarian, A., & Draine, B. T. 1999, ApJL, 516, L37, doi: [10.1086/311986](https://doi.org/10.1086/311986)
- Lazarian, A., & Hoang, T. 2007, MNRAS, 378, 910, doi: [10.1111/j.1365-2966.2007.11817.x](https://doi.org/10.1111/j.1365-2966.2007.11817.x)
- . 2019, ApJ, 883, 122, doi: [10.3847/1538-4357/ab3d39](https://doi.org/10.3847/1538-4357/ab3d39)
- Matthews, B. C., McPhee, C. A., Fissel, L. M., & Curran, R. L. 2009, ApJS, 182, 143, doi: [10.1088/0067-0049/182/1/143](https://doi.org/10.1088/0067-0049/182/1/143)
- Medan, I., & Andersson, B.-G. 2019, ApJ, 873, 87, doi: [10.3847/1538-4357/ab063c](https://doi.org/10.3847/1538-4357/ab063c)
- Navarete, F., Galli, P. A. B., & Damineli, A. 2019, MNRAS, 487, 2771, doi: [10.1093/mnras/stz1442](https://doi.org/10.1093/mnras/stz1442)
- Pereyra, A., & Magalhães, A. M. 2002, ApJS, 141, 469, doi: [10.1086/340933](https://doi.org/10.1086/340933)
- Purcell, E. M. 1979, ApJ, 231, 404, doi: [10.1086/157204](https://doi.org/10.1086/157204)
- Rao, R., Crutcher, R. M., Plambeck, R. L., & Wright, M. C. H. 1998, ApJL, 502, L75, doi: [10.1086/311485](https://doi.org/10.1086/311485)
- Reid, M. J., Menten, K. M., Zheng, X. W., et al. 2009, ApJ, 700, 137, doi: [10.1088/0004-637X/700/1/137](https://doi.org/10.1088/0004-637X/700/1/137)
- Serkowski, K. 1973, in IAU Symp. 52: Interstellar Dust and Related Topics, Vol. 52, 145.
[http://adsabs.harvard.edu/cgi-bin/nph-bib_query?
bibcode=1973IAUS...52..145S&db_key=AST](http://adsabs.harvard.edu/cgi-bin/nph-bib_query?bibcode=1973IAUS...52..145S&db_key=AST)
- Soam, A., Maheswar, G., Lee, C. W., Neha, S., & Andersson, B. G. 2017, MNRAS, 465, 559, doi: [10.1093/mnras/stw2649](https://doi.org/10.1093/mnras/stw2649)
- Stil, J., Wityk, N., Ouyed, R., & Taylor, A. R. 2009, ApJ, 701, 330, doi: [10.1088/0004-637X/701/1/330](https://doi.org/10.1088/0004-637X/701/1/330)
- Straižys, V. 1992, Multicolor stellar photometry (Tucson, Arizona, Pachart Publishing House), available in pdf format from
<http://www.itpa.lt/MulticolorStellarPhotometry/>
- Straižys, V., Boyle, R. P., Janusz, R., Laugalys, V., & Kazlauskas, A. 2013, A&A, 554, A3, doi: [10.1051/0004-6361/201321029](https://doi.org/10.1051/0004-6361/201321029)
- Straižys, V., Boyle, R. P., Milašius, K., et al. 2019, A&A, 623, A22, doi: [10.1051/0004-6361/201833987](https://doi.org/10.1051/0004-6361/201833987)
- Sugitani, K., Nakamura, F., Watanabe, M., et al. 2011, ApJ, 734, 63, doi: [10.1088/0004-637X/734/1/63](https://doi.org/10.1088/0004-637X/734/1/63)
- Vaillancourt, J. E., Andersson, B.-G., Clemens, D. P., et al. 2020, arXiv e-prints, arXiv:2011.00114.
<https://arxiv.org/abs/2011.00114>
- Vaillancourt, J. E., & Matthews, B. C. 2012, ApJS, 201, 13, doi: [10.1088/0067-0049/201/2/13](https://doi.org/10.1088/0067-0049/201/2/13)
- Virtanen, P., Gommers, R., Oliphant, T. E., et al. 2020, Nature Methods, 17, 261, doi: [10.1038/s41592-019-0686-2](https://doi.org/10.1038/s41592-019-0686-2)
- Vrba, F. J., Strom, S. E., & Strom, K. M. 1976, AJ, 81, 958, doi: [10.1086/111976](https://doi.org/10.1086/111976)
- Whittet, D. C. B. 2003, Dust in the galactic environment - 2:nd ed. (Dust in the galactic environment Institute of Physics Publishing, 390 p.).
[http://adsabs.harvard.edu/cgi-bin/nph-bib_query?
bibcode=2003QB791.W45.....&db_key=AST](http://adsabs.harvard.edu/cgi-bin/nph-bib_query?bibcode=2003QB791.W45.....&db_key=AST)
- Whittet, D. C. B., Gerakines, P. A., Hough, J. H., & Shenoy, S. S. 2001, ApJ, 547, 872, doi: [10.1086/318421](https://doi.org/10.1086/318421)
- Wright, C. O., Egan, M. P., Kraemer, K. E., & Price, S. D. 2003, AJ, 125, 359, doi: [10.1086/345511](https://doi.org/10.1086/345511)

Table 1. Results of photometry and classification of stars in the Vilnius system for the IC 59 stars with the VATT telescope.

No.	RA (J2000) (hh:mm:ss)	DEC (J2000) (dd:mm:ss)	V (mag)	$U - V$ (mag)	$P - V$ (mag)	$X - V$ (mag)	$Y - V$ (mag)	$Z - V$ (mag)	$V - S$ (mag)	$e(V)$ (mag)	$e(U - V)$ (mag)	$e(P - V)$ (mag)	$e(X - V)$ (mag)	$e(Y - V)$ (mag)	$e(Z - V)$ (mag)	$e(V - S)$ (mag)	Sp type	A _v (mag)	d (pc)
1	00:56:37.79	+61:07:49.5	16.341	—	2.867	1.963	0.896	0.313	0.859	0.012	—	0.033	0.017	0.013	0.016	f5 III	1.868	7008.0	
2	00:56:38.76	+61:12:48.3	15.831	3.636	2.694	1.748	0.788	0.290	0.674	0.032	0.062	0.026	0.033	0.012	0.039	0.012	a6 IV	2.205	2170.0
3	00:56:43.71	+61:03:28.5	13.669	2.777	2.071	1.296	0.544	0.198	0.539	0.013	0.020	0.025	0.016	0.014	0.017	0.012	a5 V	1.24	1102.0
4	00:56:46.94	+61:10:13.2	13.316	2.974	2.245	1.543	0.693	0.270	0.635	0.012	0.020	0.025	0.015	0.013	0.016	0.012	f5 III	1.023	1056.0
5	00:56:47.02	+61:07:52.1	14.418	3.063	2.268	1.535	0.757	0.260	0.637	0.013	0.021	0.026	0.016	0.016	0.018	0.013	f3 V	1.439	2988.0
6	00:56:47.65	+61:12:25.0	14.963	3.237	2.407	1.661	0.831	0.292	0.685	0.014	0.022	0.026	0.017	0.019	0.021	0.014	f3 V	1.747	3160.0
7	00:56:49.29	+61:03:27.8	13.958	2.780	2.238	1.560	0.649	0.256	0.645	0.013	0.021	0.026	0.016	0.015	0.017	0.013	g1 V	0.445	512.0
8	00:56:51.92	+61:04:50.5	13.377	2.715	2.030	1.309	0.560	0.216	0.506	0.012	0.020	0.025	0.015	0.013	0.016	0.012	f0 V	0.953	849.0
9	00:56:52.75	+61:06:28.4	16.065	3.483	2.919	2.021	0.811	0.357	0.766	0.022	0.036	0.035	0.024	0.012	0.024	0.022	k0 V	0.724	970.0
10	00:56:54.04	+61:09:04.2	17.671	—	3.215	2.039	0.963	0.358	0.740	0.013	—	0.083	0.019	0.014	0.017	0.014	a4 V	3.041	3203.0
11	00:56:55.10	+61:03:56.9	16.926	3.729	3.106	2.120	0.816	0.357	0.832	0.012	0.055	0.035	0.017	0.013	0.016	0.013	k0 V	0.745	1025.0
12	00:56:55.85	+61:06:41.4	16.817	—	3.030	2.162	1.007	0.374	0.941	0.012	—	0.031	0.017	0.012	0.016	0.012	f9 IV	2.026	3523.0
13	00:56:57.76	+61:14:25.7	15.955	3.612	3.079	2.117	0.798	0.390	0.829	0.020	0.030	0.034	0.022	0.038	0.033	0.020	k3 V	0.379	1012.0
14	00:56:59.22	+61:12:33.4	12.599	2.778	2.034	1.346	0.674	0.230	0.557	0.012	0.020	0.025	0.015	0.012	0.015	0.012	b7 III	2.384	1940.0
15	00:56:59.27	+61:09:10.9	13.558	2.981	2.282	1.577	0.712	0.287	0.647	0.012	0.020	0.025	0.015	0.013	0.016	0.012	f5 IV	1.069	834.0
16	00:57:00.37	+61:07:24.5	17.710	—	2.668	2.023	0.947	0.358	0.995	0.013	—	0.063	0.026	0.015	0.017	0.022	f7 V	1.905	2315.0
17	00:57:02.71	+61:06:37.1	12.692	3.828	3.130	2.184	0.899	0.350	0.835	0.012	0.020	0.025	0.015	0.013	0.015	0.012	g7 III	0.882	1013.0
18	00:57:04.70	+61:06:35.9	14.182	5.017	4.064	2.990	1.316	0.483	1.203	0.013	0.025	0.025	0.016	0.016	0.016	0.013	g4 II	2.8	3944.0
19	00:57:04.81	+61:03:57.9	11.445	2.705	1.976	1.209	0.492	0.194	0.447	0.012	0.020	0.025	0.015	0.012	0.015	0.012	a6 IV	0.973	531.0
20	00:57:05.20	+61:12:50.7	14.063	2.771	2.163	1.508	0.642	0.235	0.603	0.013	0.020	0.025	0.016	0.014	0.015	0.013	f9 V	0.52	738.0
21	00:57:06.74	+61:06:19.5	12.733	4.606	3.870	2.631	1.007	0.461	0.929	0.012	0.020	0.025	0.015	0.013	0.015	0.012	k2 III	0.616	771.0
22	00:57:07.01	+61:10:24.1	15.242	5.210	4.213	3.099	1.362	0.506	1.206	0.015	0.056	0.039	0.019	0.030	0.022	0.015	g8 III	2.704	2693.0
23	00:57:07.11	+61:14:39.6	14.122	2.777	1.974	1.288	0.665	0.245	0.568	0.013	0.021	0.025	0.015	0.018	0.015	0.016	b8 V	2.184	2338.0
24	00:57:07.71	+61:12:34.9	16.820	—	2.873	2.177	0.999	0.381	0.870	0.012	—	0.030	0.016	0.013	0.016	0.013	g0 IV	1.939	2648.0
25	00:57:08.89	+61:14:29.9	16.169	3.611	2.647	1.656	0.754	0.282	0.642	0.025	0.022	0.036	0.027	0.052	0.046	0.025	a5 IV	2.126	2974.0
26	00:57:09.45	+61:09:04.3	17.060	4.171	3.367	2.528	1.192	0.441	1.104	0.012	0.091	0.061	0.019	0.013	0.016	0.013	g2 V	2.658	1348.0
27	00:57:09.92	+61:06:26.7	16.457	—	3.343	2.427	1.075	0.399	0.977	0.012	—	0.031	0.016	0.012	0.015	0.012	g6 IV	1.93	1882.0
28	00:57:10.54	+61:14:38.2	15.127	3.682	2.851	2.009	0.915	0.370	0.833	0.017	0.020	0.025	0.015	0.034	0.020	0.017	f5 IV	1.914	1503.0
29	00:57:11.03	+61:04:58.5	16.972	4.411	—	2.708	1.189	0.436	1.094	0.012	0.062	—	0.019	0.013	0.016	0.013	g5 IV	2.459	2345.0
30	00:57:12.35	+61:11:58.8	16.254	3.369	2.744	1.970	0.795	0.343	0.742	0.024	0.032	0.042	0.026	0.012	0.046	0.024	g7 V	0.803	949.0
31	00:57:12.93	+61:14:04.5	15.730	3.620	2.696	1.765	0.799	0.340	0.659	0.019	0.027	0.025	0.021	0.033	0.028	0.019	a5 V	2.3	1471.0
32	00:57:14.96	+61:09:32.2	15.323	3.243	2.550	1.797	0.783	0.322	0.691	0.016	0.023	0.028	0.018	0.022	0.018	0.016	f9 V	1.107	1028.0
33	00:57:17.81	+61:05:07.0	17.750	3.826	—	2.146	0.963	0.333	0.873	0.013	0.102	—	0.020	0.014	0.017	0.014	f8 IV	1.901	5974.0
34	00:57:17.96	+61:11:31.9	14.460	3.737	2.748	1.771	0.808	0.316	0.689	0.013	0.021	0.026	0.016	0.016	0.013	0.013	a6 III	2.292	1580.0
35	00:57:18.88	+61:08:08.9	16.440	—	2.931	1.956	0.932	0.337	0.709	0.012	—	0.034	0.016	0.012	0.015	0.012	a2 IV	3.041	2500.0
36	00:57:19.80	+61:06:34.7	17.627	—	2.825	2.040	0.968	0.361	0.957	0.013	—	0.083	0.026	0.016	0.017	0.017	g1 III	1.672	4717.0
37	00:57:20.02	+61:06:22.8	16.788	—	2.641	1.618	0.748	0.261	0.680	0.012	—	0.031	0.017	0.013	0.016	0.013	a4 IV	2.159	4037.0
38	00:57:23.69	+61:11:33.5	14.751	3.188	2.575	1.815	0.783	0.322	0.714	0.013	0.021	0.026	0.016	0.018	0.016	0.013	g2 V	0.957	876.0
39	00:57:25.66	+61:12:23.8	15.110	5.749	4.713	3.373	1.373	0.571	1.188	0.014	0.061	0.058	0.019	0.026	0.023	0.015	k4 III	1.731	2675.0
40	00:57:27.73	+61:10:06.6	15.259	3.193	2.554	1.831	0.791	0.337	0.712	0.015	0.023	0.028	0.018	0.022	0.018	0.016	g2 V	0.99	887.0
41	00:57:27.82	+61:12:40.5	15.473	2.953	2.343	1.682	0.747	0.324	0.665	0.016	0.023	0.028	0.019	0.027	0.027	0.016	g1 V	0.853	1072.0
42	00:57:28.33	+61:07:26.5	15.431	3.263	2.663	1.906	0.799	0.354	0.759	0.016	0.024	0.028	0.019	0.026	0.019	0.016	g7 V	0.82	735.0
43	00:57:28.37	+61:09:55.1	15.715	3.021	2.385	1.696	0.750	0.310	0.682	0.019	0.026	0.031	0.021	0.030	0.021	0.019	g0 V	0.915	1121.0
44	00:57:28.42	+61:08:19.1	17.133	3.963	3.134	2.371	1.092	0.409	0.940	0.012	0.078	0.057	0.019	0.013	0.016	0.013	g1 IV	2.271	3862.0
45	00:57:29.40	+61:09:44.8	14.423	3.119	2.524	1.766	0.746	0.312	0.696	0.013	0.021	0.026	0.016	0.016	0.013	0.013	g3 V	0.753	562.0
46	00:57:30.04	+61:05:01.2	13.264	2.880	2.112	1.301	0.560	0.222	0.494	0.012	0.020	0.025	0.015	0.013	0.015	0.012	a8 IV	1.127	1037.0
47	00:57:30.66	+61:11:45.5	16.059	3.302	2.755	1.998	0.847	0.337	0.781	0.012	0.029	0.034	0.024	0.043	0.035	0.022	g6 V	1.065	718.0
48	00:57:31.72	+61:06:28.9	13.607	3.381	2.414	1.368	0.654	0.243	0.550	0.012	0.020	0.025	0.015	0.013	0.015	0.012	a2 III	1.905	2144.0
49	00:57:32.10	+61:03:14.5	16.737	4.798	—	2.918	1.069	0.578	1.189	0.012	0.104	—	0.018	0.012	0.016	0.012	k5 V	1.09	333.0
50	00:57:32.40	+61:06:52.1	16.152	3.075	2.264	1.431	0.688	0.268	0.546	0.023	0.030	0.033	0.024	0.043	0.024	0.024	a6 V	1.785	3942.

No.	RA (J2000) (hh:mm:ss)	DEC (J2000) (dd:mm:ss)	<i>V</i> (mag)	<i>U</i> − <i>V</i> (mag)	<i>P</i> − <i>V</i> (mag)	<i>X</i> − <i>V</i> (mag)	<i>Y</i> − <i>V</i> (mag)	<i>Z</i> − <i>V</i> (mag)	<i>V</i> − <i>S</i> (mag)	<i>e</i> (<i>V</i>) (mag)	<i>e</i> (<i>U</i> − <i>V</i>) (mag)	<i>e</i> (<i>P</i> − <i>V</i>) (mag)	<i>e</i> (<i>X</i> − <i>V</i>) (mag)	<i>e</i> (<i>Y</i> − <i>V</i>) (mag)	<i>e</i> (<i>Z</i> − <i>V</i>) (mag)	<i>e</i> (<i>V</i> − <i>S</i>) (mag)	Sp type	<i>A</i> _{<i>V</i>} (mag)	d (pc)
66	00:57:45.81	+61:09:18.2	15.456	3.705	2.790	1.852	0.865	0.326	0.750	0.016	0.025	0.029	0.019	0.025	0.019	0.016	a3 IV	2.704	1492.0
67	00:57:47.15	+61:08:26.5	16.691	–	2.736	2.038	0.973	0.363	0.824	0.012	–	0.030	0.016	0.012	0.016	0.012	f3 IV	1.943	2049.0
68	00:57:47.29	+61:04:46.9	16.388	3.414	2.476	1.509	0.680	0.249	0.547	0.012	0.022	0.026	0.015	0.012	0.015	0.012	a6 IV	1.756	4087.0
69	00:57:47.60	+61:12:31.8	17.431	–	2.589	1.839	0.860	0.352	0.698	0.013	–	0.035	0.017	0.013	0.017	0.014	f9 V	1.427	2362.0
70	00:57:47.86	+61:14:12.4	14.050	3.016	2.349	1.607	0.694	0.264	0.667	0.013	0.020	0.025	0.016	0.014	0.015	0.014	f8 V	0.79	910.0
71	00:57:48.96	+61:12:44.8	16.822	4.321	–	2.585	0.986	0.537	1.008	0.012	0.056	–	0.017	0.013	0.016	0.013	k3 V	1.161	5691.0
72	00:57:49.60	+61:12:09.3	14.927	3.476	2.459	1.434	0.698	0.267	0.577	0.014	0.022	0.025	0.017	0.018	0.021	0.014	a2 III	2.088	3916.0
73	00:57:49.65	+61:05:58.2	17.149	3.619	2.691	1.957	0.897	0.318	0.821	0.012	0.033	0.030	0.017	0.013	0.016	0.013	f6 V	1.764	2417.0
74	00:57:50.56	+61:11:08.9	14.468	3.099	2.504	1.788	0.726	0.297	0.719	0.013	0.021	0.025	0.016	0.016	0.016	0.013	g4 V	0.624	481.0
75	00:57:52.03	+61:05:28.6	17.463	3.647	–	2.073	0.943	0.339	0.852	0.013	0.048	–	0.019	0.013	0.017	0.013	g0 V	1.718	1038.0
76	00:57:53.64	+61:09:36.0	13.802	3.119	2.324	1.411	0.610	0.274	0.577	0.028	0.073	0.048	0.038	0.035	0.035	0.035	a6 IV	1.464	1306.0
77	00:57:54.82	+61:11:16.3	15.168	3.736	2.915	2.082	0.957	0.349	0.866	0.015	0.023	0.028	0.018	0.022	0.015	0.015	f5 V	2.088	1280.0
78	00:57:55.02	+61:05:36.1	17.956	–	2.616	1.747	0.775	0.272	0.677	0.014	–	0.060	0.020	0.015	0.018	0.016	a9 V	1.939	4509.0
79	00:57:55.29	+61:08:06.7	15.267	3.107	2.236	1.308	0.607	0.218	0.487	0.016	0.022	0.027	0.018	0.021	0.018	0.016	a3 V	1.614	2753.0
80	00:57:55.41	+61:06:21.5	17.194	4.404	–	2.592	1.067	0.446	1.000	0.012	0.102	–	0.019	0.013	0.016	0.013	k0 V	1.789	1249.0
81	00:57:56.72	+61:05:16.4	17.414	3.478	2.621	1.853	0.848	0.297	0.790	0.013	0.042	0.032	0.017	0.013	0.016	0.013	f4 V	1.718	3290.0
82	00:57:57.34	+61:12:22.2	17.059	3.798	–	2.321	1.001	0.380	0.991	0.012	0.044	–	0.017	0.013	0.016	0.013	g8 IV	1.468	2698.0
83	00:57:57.43	+61:07:36.7	15.876	3.336	2.771	1.917	0.743	0.314	0.738	0.019	0.026	0.032	0.021	0.031	0.021	0.019	g8 V	0.549	913.0
84	00:57:58.23	+61:10:31.7	17.804	–	2.971	1.991	0.909	0.349	0.862	0.013	–	0.072	0.021	0.014	0.017	0.015	f8 V	1.685	1933.0
85	00:57:58.62	+61:03:22.4	17.485	–	2.716	1.856	0.857	0.267	0.825	0.013	–	0.038	0.017	0.013	0.016	0.013	f6 IV	1.593	5575.0
86	00:57:58.76	+61:11:14.8	12.325	2.078	1.515	1.018	0.509	0.194	0.420	0.012	0.020	0.025	0.015	0.012	0.015	0.012	b6 III	1.756	2331.0
87	00:58:00.28	+61:03:24.8	15.935	3.282	2.632	1.876	0.831	0.267	0.794	0.012	0.021	0.026	0.015	0.012	0.015	0.012	g2 V	1.156	1199.0
88	00:58:01.00	+61:07:59.2	14.056	3.001	2.159	1.312	0.593	0.226	0.545	0.013	0.020	0.025	0.016	0.014	0.016	0.013	a6 V	1.389	1623.0
89	00:58:01.12	+61:12:20.0	15.704	3.717	2.651	1.732	0.780	0.316	0.688	0.018	0.027	0.025	0.020	0.029	0.030	0.018	f1 III	1.772	3848.0
90	00:58:01.78	+61:11:54.9	16.779	3.268	2.361	1.456	0.672	0.262	0.556	0.012	0.026	0.027	0.016	0.012	0.016	0.013	a3 III	1.585	–
91	00:58:02.54	+61:12:18.3	16.601	3.736	2.865	2.007	0.896	0.355	0.813	0.012	0.029	0.028	0.016	0.012	0.015	0.012	f2 IV	2.159	2861.0
92	00:58:02.94	+61:12:27.4	16.860	–	3.545	2.373	0.902	0.445	0.917	0.012	–	0.052	0.017	0.013	0.016	0.013	k3 V	0.811	1004.0
93	00:58:03.18	+61:08:06.8	16.284	3.415	2.511	1.517	0.704	0.254	0.601	0.028	0.035	0.037	0.028	0.056	0.029	0.028	a4 V	1.964	3063.0
94	00:58:03.45	+61:05:57.6	17.582	3.996	–	2.454	0.994	0.383	1.042	0.013	0.098	–	0.023	0.014	0.017	0.013	g9 IV	1.302	4231.0
95	00:58:04.52	+61:07:27.5	14.930	4.812	3.917	2.853	1.201	0.454	1.144	0.014	0.027	0.031	0.017	0.022	0.017	0.014	k0 III	1.789	3157.0
96	00:58:04.93	+61:12:13.0	16.501	3.692	2.901	2.108	0.954	0.374	0.841	0.012	0.028	0.028	0.016	0.012	0.015	0.012	g0 IV	1.751	2336.0
97	00:58:05.34	+61:08:49.9	16.789	3.581	2.577	1.559	0.696	0.254	0.574	0.012	0.030	0.027	0.016	0.012	0.013	0.013	a4 V	1.93	4309.0
98	00:58:05.81	+61:04:33.3	16.360	–	3.770	2.740	1.162	0.441	1.139	0.012	–	0.038	0.017	0.012	0.015	0.012	g9 IV	2.001	1903.0
99	00:58:06.62	+61:10:24.3	16.855	3.341	2.572	1.753	0.840	0.316	0.851	0.012	0.027	0.028	0.016	0.013	0.016	0.013	f2 V	1.901	1855.0
100	00:58:06.96	+61:10:52.7	15.030	2.777	1.997	1.249	0.610	0.254	0.518	0.014	0.022	0.026	0.017	0.019	0.022	0.015	a0 V	1.805	3326.0
101	00:58:07.99	+61:09:50.4	17.233	–	2.716	1.743	0.766	0.283	0.610	0.013	–	0.032	0.017	0.013	0.016	0.014	a4 IV	2.234	4965.0
102	00:58:08.00	+61:06:27.9	16.934	3.427	2.683	1.940	0.872	0.302	0.874	0.012	0.026	0.029	0.016	0.013	0.016	0.013	f9 V	1.477	1692.0
103	00:58:08.18	+61:11:23.6	13.724	4.601	3.737	2.671	1.139	0.431	1.046	0.012	0.021	0.026	0.016	0.014	0.017	0.012	g7 III	1.88	1918.0
104	00:58:08.41	+61:08:06.3	15.704	3.497	3.047	2.030	0.743	0.365	0.771	0.018	0.025	0.026	0.021	0.029	0.021	0.018	k2 V	0.237	591.0
105	00:58:08.47	+61:03:58.2	17.484	–	2.511	1.794	0.809	0.264	0.774	0.013	–	0.035	0.017	0.013	0.016	0.013	g0 V	1.161	2513.0
106	00:58:09.16	+61:11:02.9	14.009	5.703	4.739	3.320	1.305	0.551	1.198	0.013	0.039	0.025	0.016	0.016	0.018	0.013	k4 III	1.448	2419.0
107	00:58:09.45	+61:06:22.2	18.046	3.391	–	1.953	0.911	0.294	0.851	0.014	0.088	–	0.022	0.016	0.019	0.020	f3 V	2.08	2953.0
108	00:58:09.49	+61:05:39.6	18.009	3.565	2.718	1.963	0.899	0.283	0.881	0.014	0.098	0.068	0.021	0.015	0.018	0.015	f6 V	1.772	3388.0
109	00:58:10.07	+61:09:43.1	15.306	3.373	2.452	1.478	0.635	0.245	0.562	0.016	0.023	0.027	0.018	0.022	0.018	0.016	a5 V	1.618	765.0
110	00:58:10.58	+61:11:37.7	16.544	3.501	2.491	1.530	0.699	0.278	0.586	0.012	0.026	0.027	0.016	0.012	0.015	0.012	a3 V	1.997	3531.0
111	00:58:11.06	+61:03:37.7	13.678	5.634	4.681	3.321	1.339	0.535	1.257	0.013	0.020	0.025	0.068	0.016	0.015	0.013	k4 II	1.618	6200.0
112	00:58:11.40	+61:10:01.6	15.877	3.429	2.659	1.891	0.871	0.331	0.780	0.022	0.030	0.033	0.024	0.041	0.024	0.022	f7 V	1.589	1301.0
113	00:58:12.66	+61:10:34.6	14.514	3.422	2.760	1.877	0.750	0.311	0.749	0.013	0.021	0.026	0.016	0.016	0.016	0.013	g7 V	0.616	825.0
114	00:58:13.07	+61:06:53.1	17.373	3.477	2.547	1.595	0.701	0.257	0.658	0.013	0.037	0.033	0.017	0.013	0.016	0.014	a2 V	2.063	4854.0
115	00:58:13.31	+61:																	

Table 2. Results of photometry and classification of stars in the Vilnius system for the IC 63 stars with the VATT telescope.

No.	RA (J2000) (hh:mm:ss)	DEC (J2000) (dd:mm:ss)	<i>V</i>	<i>U</i> – <i>V</i>	<i>P</i> – <i>V</i>	<i>X</i> – <i>V</i>	<i>Y</i> – <i>V</i>	<i>Z</i> – <i>V</i>	<i>V</i> – <i>S</i>	<i>e</i> (<i>V</i>)	<i>e</i> (<i>U</i> – <i>V</i>)	<i>e</i> (<i>P</i> – <i>V</i>)	<i>e</i> (<i>X</i> – <i>V</i>)	<i>e</i> (<i>Y</i> – <i>V</i>)	<i>e</i> (<i>Z</i> – <i>V</i>)	<i>e</i> (<i>V</i> – <i>S</i>)	Sp type	<i>A_V</i>	d (pc)	
1	00:58:39.02	+00:55:56.4	17.717	3.672	–	2.093	0.979	0.375	0.884	0.014	0.063	–	0.020	0.015	0.018	0.016	g1 IV	1.801	3705.0	
2	00:58:40.22	+00:52:19.8	14.451	3.211	2.390	1.438	0.649	0.233	0.572	0.013	0.022	0.025	0.016	0.016	0.018	0.012	a2 V	1.847	1265.0	
3	00:58:40.73	+00:58:59.0	15.417	3.402	2.561	1.675	0.766	0.284	0.675	0.016	0.027	0.025	0.019	0.024	0.026	0.016	a7 IV	2.051	2416.0	
4	00:58:40.94	+00:56:56.2	14.642	6.149	5.142	3.623	1.515	0.584	1.357	0.013	0.030	0.033	0.021	0.022	0.021	0.013	k3 III	2.508	2060.6	
5	00:58:41.21	+00:57:08.2	14.825	2.795	2.190	1.551	0.667	0.260	0.631	0.014	0.022	0.025	0.017	0.018	0.020	0.014	f8 V	0.678	948.0	
6	00:58:41.25	+00:51:00.1	15.884	4.997	–	2.996	1.236	0.472	1.187	0.012	0.050	–	0.016	0.012	0.015	0.012	k2 III	1.568	5994.0	
7	00:58:41.50	+00:54:37.9	16.802	3.730	–	2.114	0.972	0.366	0.901	0.012	0.026	–	0.016	0.013	0.016	0.013	g1 IV	1.772	2533.0	
8	00:58:41.88	+00:52:41.7	13.558	2.919	2.127	1.184	0.502	0.188	0.436	0.012	0.020	0.025	0.015	0.013	0.015	0.012	a4 V	1.123	1118.0	
9	00:58:42.46	+01:00:33.8	17.253	3.584	–	2.145	0.949	0.345	0.901	0.013	0.038	–	0.017	0.013	0.016	0.013	g6 V	1.489	1499.0	
10	00:58:43.51	+00:57:06.2	17.187	3.866	–	1.775	0.813	0.320	0.650	0.014	0.036	–	0.017	0.014	0.017	0.018	a6 IV	2.309	4564.0	
11	00:58:44.05	+00:52:22.7	17.135	3.647	–	1.837	0.836	0.329	0.740	0.013	0.035	–	0.017	0.013	0.016	0.013	a6 IV	2.404	5013.0	
12	00:58:45.00	+01:00:39.0	15.876	2.775	–	1.629	0.707	0.271	0.674	0.012	0.020	–	0.015	0.012	0.015	0.012	g1 V	0.686	1146.0	
13	00:58:46.39	+00:52:12.0	14.143	3.272	2.399	1.394	0.645	0.235	0.520	0.013	0.021	0.025	0.016	0.014	0.017	0.013	a3 V	1.772	1329.0	
14	00:58:46.96	+00:50:01.2	17.657	3.040	–	1.694	0.760	0.273	0.734	0.013	0.035	–	0.017	0.014	0.017	0.014	g0 V	0.957	2910.0	
15	00:58:47.70	+01:00:12.6	17.356	3.833	–	2.144	0.984	0.363	0.883	0.013	0.050	–	0.017	0.013	0.016	0.013	f7 IV	2.051	2925.0	
16	00:58:47.83	+00:54:15.6	16.708	3.949	–	1.916	0.851	0.346	0.703	0.012	0.027	–	0.016	0.012	0.016	0.012	g1 IV	1.269	3020.0	
17	00:58:47.80	+00:53:22.1	13.040	2.974	2.371	1.652	0.677	0.266	0.652	0.012	0.020	0.025	0.015	0.013	0.015	0.012	g3 V	0.466	503.0	
18	00:58:48.35	+00:56:00.2	13.458	2.679	2.111	1.458	0.616	0.253	0.571	0.012	0.020	0.025	0.015	0.013	0.015	0.012	f9 V	0.412	561.0	
19	00:58:50.08	+00:50:16.0	15.610	4.162	–	2.459	1.043	0.398	1.025	0.012	0.022	–	0.015	0.012	0.015	0.012	g9 III	1.26	6008.0	
20	00:58:50.13	+00:52:14.2	15.093	3.338	2.447	1.499	0.671	0.267	0.546	0.014	0.024	0.027	0.018	0.020	0.022	0.014	a4 V	1.826	1840.0	
21	00:58:50.71	+00:52:55.1	16.195	4.060	3.480	2.372	0.897	0.480	0.857	0.026	0.024	0.038	0.035	0.012	0.051	0.027	k3 V	0.79	693.0	
22	00:58:51.06	+00:50:55.1	15.780	3.042	2.303	1.325	0.593	0.238	0.418	0.019	0.029	0.025	0.021	0.028	0.031	0.019	a4 V	1.502	2928.0	
23	00:58:51.81	+01:01:02.6	11.541	2.530	1.773	0.842	0.331	0.113	0.293	0.012	0.020	0.025	0.015	0.012	0.015	0.012	a2 V	0.524	922.0	
24	00:58:52.86	+00:51:55.8	16.546	4.165	–	2.655	1.130	0.450	1.017	0.012	0.042	–	0.016	0.012	0.016	0.012	k1 III	1.327	3899.0	
25	00:58:52.87	+00:58:53.3	15.091	4.947	4.086	2.949	1.265	0.493	1.154	0.014	0.022	0.034	0.021	0.024	0.023	0.014	k0 III	2.055	1674.0	
26	00:58:52.96	+00:55:34.4	15.050	3.163	2.597	1.802	0.740	0.297	0.698	0.014	0.023	0.027	0.018	0.020	0.022	0.014	g6 V	0.62	727.0	
27	00:58:53.30	+00:50:20.2	15.326	2.927	2.167	1.221	0.544	0.183	0.439	0.016	0.024	0.027	0.018	0.022	0.023	0.016	a4 V	1.298	2503.0	
28	00:58:53.33	+01:00:12.2	16.488	–	2.789	1.790	0.812	0.294	0.700	0.012	–	0.030	0.016	0.012	0.012	a8 III	2.167	4402.0		
29	00:58:53.57	+00:59:22.9	17.312	3.681	–	1.980	0.894	0.361	0.761	0.013	0.044	–	0.017	0.013	0.017	0.013	f6 IV	1.747	3206.0	
30	00:58:54.40	+00:58:43.9	15.242	3.567	2.970	2.015	0.813	0.345	0.735	0.015	0.026	0.028	0.019	0.022	0.024	0.015	k0 V	0.732	770.0	
31	00:58:54.96	+00:51:58.0	16.107	3.285	2.545	1.845	0.830	0.350	0.724	0.013	0.025	0.034	0.027	0.012	0.065	0.023	f9 V	1.302	1777.0	
32	00:58:55.05	+00:52:31.9	13.046	2.893	2.225	1.554	0.675	0.251	0.628	0.012	0.020	0.025	0.015	0.013	0.015	0.012	f8 IV	0.703	747.0	
33	00:58:55.66	+00:52:11.2	14.183	4.276	3.478	2.494	1.075	0.409	0.933	0.013	0.023	0.026	0.016	0.016	0.018	0.014	g5 III	1.797	2818.0	
34	00:58:55.67	+00:59:53.3	16.302	4.466	–	2.588	1.075	0.411	1.030	0.012	0.040	–	0.067	0.012	0.015	0.012	k0 III	1.265	4006.0	
35	00:58:55.75	+01:00:11.4	11.311	2.652	1.925	1.226	0.514	0.190	0.502	0.012	0.020	0.025	0.015	0.012	0.015	0.012	f1 IV	0.678	574.0	
36	00:58:56.44	+00:50:17.8	16.324	3.073	2.334	1.654	0.752	0.299	0.665	0.012	0.021	0.026	0.015	0.012	0.015	0.012	f5 V	1.236	1898.0	
37	00:58:56.95	+00:51:40.7	17.272	3.505	–	1.955	0.890	0.349	0.782	0.013	0.028	–	0.017	0.013	0.016	0.013	g1 IV	1.431	3525.0	
38	00:58:57.22	+00:53:16.8	15.518	3.261	2.711	1.869	0.782	0.303	0.718	0.017	0.041	0.062	0.024	0.026	0.028	0.023	g6 V	0.795	905.0	
39	00:58:57.61	+00:50:55.0	16.353	4.309	–	2.593	1.111	0.434	1.012	0.012	0.028	–	0.016	0.012	0.015	0.012	k0 III	1.414	4029.0	
40	00:59:00.19	+00:55:04.9	16.261	3.483	2.625	1.848	0.900	0.385	0.780	0.027	0.022	0.039	0.031	0.012	0.078	0.037	f4 III	1.98	3147.0	
41	00:59:00.79	+00:49:49.0	15.339	2.983	2.087	1.164	0.545	0.238	0.441	0.016	0.025	0.027	0.018	0.022	0.024	0.016	a1 V	1.468	3563.0	
42	00:59:01.56	+00:50:40.7	16.610	3.466	–	1.969	0.868	0.349	0.776	0.012	0.023	–	0.016	0.012	0.016	0.012	g6 V	1.152	1522.0	
43	00:59:02.80	+00:55:18.1	15.433	3.540	2.578	1.601	0.762	0.280	0.620	0.016	0.029	0.029	0.019	0.019	0.024	0.026	0.023	a5 III	2.167	3730.0
44	00:59:04.21	+00:51:27.9	15.916	2.978	2.176	1.246	0.597	0.248	0.392	0.022	0.031	0.032	0.024	0.033	0.050	0.043	a4 V	1.518	3915.0	
45	00:59:04.51	+00:50:35.2	16.610	3.319	2.661	1.940	0.865	0.356	0.772	0.012	0.022	0.028	0.016	0.012	0.016	0.012	g2 V	1.298	1363.0	
46	00:59:04.58	+00:50:59.7	16.578	3.208	2.549	1.849	0.837	0.344	0.733	0.012	0.022	0.028	0.016	0.012	0.016	0.012	g0 V	1.277	1413.0	
47	00:59:04.59	+00:59:50.9	15.591	3.074	2.250	1.417	0.655	0.286	0.542	0.017	0.026	0.028	0.019	0.025	0.028	0.024	a9 IV	1.444	3163.0	
48	00:59:05.68	+00:55:00.0	15.635	3.018	2.461	1.707	0.722	0.303	0.686	0.018	0.028	0.026	0.021	0.027	0.029	0.019	g3 V	0.653	941.0	
49	00:59:05.91	+00:58:52.0	13.030	3.407	2.783	1.923	0.772	0.322	0.726	0.012	0.020	0.025	0.015	0.013	0.015	0.012	g8 IV	0.516	563.0	
50	00:59:06.09	+00:52:08.9	16.594	3.069	2.209	1.336	0.623	0.256	0.457	0.012	0.022	0.027	0.015	0.012</td						

No.	RA (J2000) (hh:mm:ss)	DEC (J2000) (dd:mm:ss)	<i>V</i> (mag)	<i>U</i> − <i>V</i> (mag)	<i>P</i> − <i>V</i> (mag)	<i>X</i> − <i>V</i> (mag)	<i>Y</i> − <i>V</i> (mag)	<i>Z</i> − <i>V</i> (mag)	<i>V</i> − <i>S</i> (mag)	<i>e</i> (<i>V</i>) (mag)	<i>e</i> (<i>U</i> − <i>V</i>) (mag)	<i>e</i> (<i>P</i> − <i>V</i>) (mag)	<i>e</i> (<i>X</i> − <i>V</i>) (mag)	<i>e</i> (<i>Y</i> − <i>V</i>) (mag)	<i>e</i> (<i>Z</i> − <i>V</i>) (mag)	<i>e</i> (<i>V</i> − <i>S</i>) (mag)	Sp type	<i>A</i> _{<i>V</i>} (mag)	d (pc)
66	00:59:16.98	+60:57:39.3	17.100	3.599	—	2.082	0.977	0.378	0.811	0.013	0.028	—	0.016	0.013	0.016	0.013	g0 V	1.86	1838.0
67	00:59:17.61	+60:52:02.6	15.254	3.231	2.664	1.812	0.774	0.324	0.700	0.015	0.024	0.025	0.018	0.022	0.024	0.015	g5 V	0.786	1027.0
68	00:59:17.73	+60:51:26.9	17.194	3.245	—	1.796	0.827	0.324	0.766	0.013	0.025	—	0.016	0.013	0.016	0.013	f9 IV	1.277	4350.0
69	00:59:18.12	+60:58:30.6	12.585	2.620	1.978	1.252	0.532	0.206	0.480	0.012	0.020	0.025	0.015	0.012	0.015	0.012	f2 V	0.62	615.0
70	00:59:18.22	+60:50:52.5	14.340	4.260	3.476	2.485	1.037	0.411	0.964	0.013	0.024	0.026	0.016	0.016	0.018	0.013	g7 III	1.456	2932.0
71	00:59:18.52	+60:55:34.4	13.966	3.363	2.771	1.962	0.836	0.366	0.786	0.013	0.021	0.025	0.016	0.014	0.016	0.013	g7 V	0.973	291.0
72	00:59:19.43	+60:50:56.9	16.036	3.211	2.616	1.856	0.728	0.328	0.773	0.029	0.022	0.028	0.017	0.050	0.043	0.029	g8 V	0.487	975.0
73	00:59:19.44	+60:57:37.5	15.394	5.619	—	3.294	1.310	0.583	1.149	0.016	0.048	—	0.016	0.033	0.029	0.016	k4 III	1.468	2241.0
74	00:59:20.03	+60:59:09.1	12.302	2.817	2.051	1.200	0.506	0.180	0.441	0.012	0.020	0.025	0.015	0.012	0.012	0.012	a6 III	1.036	947.0
75	00:59:20.74	+60:50:17.9	15.815	4.946	4.077	2.896	1.202	0.433	1.108	0.019	0.029	0.045	0.030	0.068	0.036	0.027	g8 III	2.038	6769.0
76	00:59:22.61	+60:56:48.2	14.831	5.282	4.348	3.116	1.302	0.509	1.141	0.014	0.028	0.038	0.020	0.021	0.017	0.014	k0 III	2.209	3682.0
77	00:59:22.99	+60:59:58.7	15.918	3.273	2.573	1.873	0.873	0.340	0.803	0.019	0.021	0.032	0.024	0.035	0.021	0.020	f7 IV	1.589	1861.0
78	00:59:23.32	+60:58:41.6	15.581	—	2.379	1.468	0.696	0.282	0.648	0.019	—	0.026	0.021	0.027	0.021	0.028	a7 III	1.756	374.0
79	00:59:23.53	+60:58:55.5	15.340	3.276	2.675	1.946	0.826	0.358	0.821	0.016	0.030	0.028	0.019	0.025	0.018	0.012	g6 IV	0.894	1119.0
80	00:59:25.54	+60:55:18.7	16.844	3.645	—	1.910	0.921	0.360	0.771	0.012	0.050	—	0.016	0.013	0.016	0.013	f0 IV	2.471	2929.0
81	00:59:25.94	+60:51:16.0	16.712	3.194	2.390	1.683	0.805	0.323	0.679	0.012	0.022	0.028	0.016	0.012	0.016	0.013	f3 V	1.639	2430.0
82	00:59:25.99	+60:50:59.8	13.835	3.062	2.502	1.735	0.703	0.295	0.671	0.013	0.021	0.025	0.016	0.014	0.017	0.013	g5 V	0.491	603.0
83	00:59:26.18	+60:49:55.6	13.523	5.794	4.835	3.381	1.331	0.580	1.185	0.012	0.053	0.028	0.016	0.014	0.017	0.013	k5 III	1.414	2248.0
84	00:59:27.24	+60:56:25.8	17.273	3.711	—	2.191	1.023	0.404	0.878	0.013	0.056	—	0.017	0.013	0.016	0.013	g2 IV	1.93	3420.0
85	00:59:27.37	+60:49:30.7	14.116	4.093	3.228	2.353	1.044	0.384	0.960	0.013	0.020	0.026	0.016	0.016	0.018	0.013	g6 III	1.581	1861.0
86	00:59:28.03	+61:00:29.4	17.502	3.482	—	1.974	0.926	0.359	0.804	0.013	0.094	—	0.021	0.016	0.017	0.026	f8 V	1.756	2519.0
87	00:59:28.96	+61:00:03.4	14.779	3.098	2.247	1.401	0.597	0.228	0.540	0.012	0.020	0.025	0.015	0.012	0.015	0.012	a4 III	1.543	1086.0
88	00:59:28.96	+60:54:43.0	15.316	—	4.354	3.122	1.341	0.541	1.185	0.016	—	0.035	0.040	0.029	0.018	0.016	k1 III	2.205	2699.0
89	00:59:29.79	+60:50:13.9	11.638	1.805	1.339	0.880	0.438	0.175	0.334	0.012	0.020	0.025	0.015	0.012	0.015	0.012	b6 III	1.46	2585.0
90	00:59:30.17	+61:01:25.6	16.420	3.036	2.425	1.767	0.745	0.264	0.708	0.049	0.021	0.047	0.048	0.013	0.046	0.012	g1 V	0.844	1055.0
91	00:59:30.70	+61:00:18.1	13.377	4.843	4.008	2.870	1.194	0.449	1.059	0.012	0.023	0.026	0.016	0.013	0.015	0.012	g7 III	2.109	2374.0
92	00:59:31.23	+60:59:50.5	16.674	3.388	2.632	1.753	0.832	0.323	0.668	0.012	0.029	0.029	0.016	0.013	0.016	0.013	f1 V	1.98	2034.0
93	00:59:32.05	+60:51:35.8	17.373	3.488	—	1.960	0.903	0.343	0.751	0.015	0.064	—	0.021	0.016	0.019	0.017	f8 V	1.66	2753.0
94	00:59:32.97	+60:54:56.9	15.422	3.761	2.747	1.747	0.827	0.324	0.677	0.016	0.031	0.029	0.019	0.025	0.019	0.016	a5 III	2.438	2415.0
95	00:59:33.06	+60:58:50.6	16.806	3.447	—	1.989	0.928	0.363	0.796	0.012	0.033	—	0.016	0.013	0.016	0.013	g0 IV	1.643	3936.0
96	00:59:33.61	+60:51:0.5	17.934	3.522	—	1.855	0.943	0.307	0.832	0.014	0.063	—	0.020	0.016	0.019	0.016	a1 V	3.124	3763.0
97	00:59:33.85	+60:59:23.8	15.229	—	3.891	2.812	1.202	0.454	1.086	0.015	—	0.049	0.045	0.028	0.018	0.015	g8 III	2.038	3072.0
98	00:59:34.51	+61:00:03.0	16.016	3.250	2.491	1.621	0.744	0.285	0.593	0.021	0.021	0.033	0.024	0.039	0.023	0.021	a9 V	1.81	2211.0
99	00:59:35.08	+60:56:0.0	16.988	3.715	—	2.132	1.001	0.387	0.836	0.013	0.037	—	0.016	0.013	0.016	0.013	g1 V	1.893	1930.0
100	00:59:35.49	+60:52:03.8	16.774	3.146	2.441	1.441	0.657	0.245	0.542	0.013	0.024	0.038	0.016	0.013	0.016	0.014	a4 V	1.768	3391.0
101	00:59:36.12	+60:54:26.0	16.795	3.799	—	2.027	0.973	0.399	0.812	0.012	0.034	—	0.016	0.013	0.016	0.013	f5 III	2.188	3199.0
102	00:59:36.82	+60:54:16.1	17.227	3.435	—	1.951	0.903	0.355	0.829	0.013	0.035	—	0.017	0.013	0.016	0.012	f9 V	1.606	2514.0
103	00:59:37.24	+60:52:55.4	15.775	3.479	2.667	1.753	0.803	0.304	0.641	0.012	0.022	0.027	0.015	0.012	0.015	0.012	a9 IV	2.059	2251.0
104	00:59:37.43	+60:51:03.5	15.976	3.357	2.601	1.869	0.865	0.327	0.760	0.012	0.021	0.026	0.015	0.012	0.015	0.012	f4 IV	1.493	1730.0
105	00:59:38.81	+60:51:12.8	17.455	3.791	—	2.058	0.972	0.349	0.851	0.038	0.060	—	0.040	0.038	0.039	0.038	f3 III	2.371	5857.0
106	00:59:39.16	+60:56:11.7	15.433	3.159	2.257	1.430	0.707	0.272	0.538	0.012	0.020	0.025	0.015	0.012	0.015	0.012	a5 V	1.918	2999.0
107	00:59:39.38	+60:56:36.4	13.986	4.849	3.958	2.870	1.268	0.469	1.114	0.012	0.020	0.025	0.015	0.012	0.015	0.012	g5 III	2.6	1589.0
108	00:59:39.54	+60:49:54.1	14.191	2.832	2.177	1.467	0.636	0.254	0.581	0.012	0.020	0.025	0.015	0.012	0.015	0.012	f4 V	0.836	1058.0
109	00:59:39.80	+60:55:09.8	16.359	3.643	2.780	1.777	0.837	0.323	0.629	0.012	0.022	0.027	0.015	0.012	0.015	0.012	a7 V	2.338	2705.0
110	00:59:40.78	+60:52:10.7	16.646	3.279	—	1.711	0.769	0.278	0.632	0.012	0.040	—	0.016	0.013	0.016	0.014	a9 IV	1.918	3685.0
111	00:59:41.16	+60:55:06.6	15.677	4.934	—	3.025	1.335	0.307	1.178	0.012	0.030	—	0.016	0.012	0.015	0.012	g8 III	2.592	2963.0
112	00:59:41.23	+60:59:28.8	15.870	5.452	—	3.176	1.320	0.508	1.179	0.012	0.065	—	0.016	0.012	0.015	0.012	k3 III	1.697	4428.0
113	00:59:41.54	+60:49:44.5	15.515	2.974	2.377	1.631	0.689	0.266	0.646	0.012	0.020	0.025	0.015	0.012	0.015	0.012	g2 V	0.566	1015.0
114	00:59:41.73	+60:54:31.1	16.849	3.616	—	2.098	0.995	0.360	0.915	0.012	0.030	—	0.016	0.013	0.016	0.016	f9 V	1.988	1307.0
115	00:59:41.99	+60:56:39.2	17.371	3.797	—</														

No.	RA (J2000) (hh:mm:ss)	DEC (J2000) (dd:mm:ss)	V (mag)	$U - V$ (mag)	$P - V$ (mag)	$X - V$ (mag)	$Y - V$ (mag)	$Z - V$ (mag)	$V - S$ (mag)	$e(V)$ (mag)	$e(U - V)$ (mag)	$e(P - V)$ (mag)	$e(X - V)$ (mag)	$e(Y - V)$ (mag)	$e(Z - V)$ (mag)	$e(V - S)$ (mag)	Sp type	A_V (mag)	d (pc)
131	00:59:51.38	+60:50:09.8	17.486	3.464	—	2.006	0.906	0.325	0.768	0.014	0.042	—	0.018	0.014	0.017	0.014	g1 IV	1.498	2767.0
132	00:59:51.86	+60:50:21.7	17.584	3.256	—	1.920	0.864	0.312	0.800	0.014	0.033	—	0.018	0.014	0.017	0.015	g3 IV	1.219	4094.0
133	00:59:52.05	+60:57:46.5	13.680	4.115	3.464	2.375	0.961	0.389	0.908	0.012	0.020	0.025	0.015	0.012	0.015	0.012	k0 III	0.79	1123.0
134	00:59:52.23	+60:51:30.6	14.544	2.584	1.840	1.024	0.484	0.185	0.427	0.012	0.020	0.025	0.015	0.012	0.015	0.012	a1 V	1.215	2722.0
135	00:59:52.44	+60:57:27.9	14.448	2.452	1.924	1.329	0.646	0.237	0.559	0.012	0.020	0.025	0.015	0.012	0.015	0.012	f6 V	0.72	3259.0
136	00:59:52.66	+60:49:32.8	16.782	—	2.288	1.550	0.701	0.252	0.627	0.012	—	0.030	0.016	0.013	0.016	0.013	f5 V	1.023	2897.0
137	00:59:54.60	+60:50:27.6	15.916	3.121	2.275	1.330	0.587	0.216	0.468	0.012	0.021	0.026	0.015	0.012	0.015	0.013	a4 V	1.477	2603.0
138	00:59:54.68	+60:55:39.2	16.288	3.254	2.355	1.388	0.646	0.239	0.514	0.012	0.022	0.026	0.015	0.012	0.015	0.012	a3 V	1.776	4421.0
139	00:59:55.14	+60:55:30.5	17.443	3.402	—	1.596	0.742	0.283	0.597	0.015	0.054	—	0.019	0.015	0.019	0.069	a3 V	1.876	3986.0
140	00:59:55.20	+60:56:17.4	16.371	3.432	2.759	1.977	0.837	0.333	0.797	0.012	0.022	0.027	0.015	0.012	0.015	0.012	g5 V	1.048	1094.0
141	00:59:55.26	+60:59:57.8	16.475	3.536	3.025	2.030	0.826	0.332	0.791	0.012	0.023	0.029	0.016	0.012	0.015	0.012	k1 V	0.724	1021.0
142	00:59:56.20	+60:54:31.7	15.556	3.724	2.973	2.115	0.959	0.359	0.866	0.012	0.021	0.026	0.015	0.012	0.015	0.012	g3 IV	1.614	2523.0
143	00:59:56.45	+61:00:21.1	16.425	3.110	2.289	1.340	0.612	0.223	0.513	0.012	0.021	0.026	0.015	0.012	0.015	0.012	a4 V	1.581	4570.0
144	00:59:56.55	+60:49:42.1	16.376	2.976	2.131	1.185	0.543	0.187	0.411	0.012	0.021	0.026	0.015	0.012	0.015	0.012	a3 V	1.348	3431.0
145	00:59:56.75	+60:57:23.1	15.267	3.337	2.683	1.915	0.826	0.320	0.756	0.012	0.020	0.025	0.015	0.012	0.015	0.012	g4 V	1.04	757.0
146	00:59:57.51	+60:56:07.0	14.584	4.590	3.838	2.704	1.148	0.424	1.048	0.012	0.021	0.026	0.015	0.012	0.015	0.012	g9 III	1.697	2662.0
147	00:59:57.65	+60:55:32.4	15.857	3.201	2.470	1.730	0.798	0.292	0.697	0.012	0.021	0.026	0.015	0.012	0.015	0.012	f5 IV	1.427	2275.0
148	00:59:58.13	+60:54:28.7	15.192	3.432	2.451	1.491	0.690	0.253	0.612	0.012	0.020	0.025	0.015	0.012	0.015	0.012	a8 III	1.66	3526.0
149	00:59:58.66	+60:59:07.6	17.442	3.363	—	1.893	0.861	0.303	0.775	0.013	0.040	—	0.017	0.013	0.017	0.014	f9 V	1.431	2107.0
150	01:00:00.29	+60:58:44.0	16.244	3.717	2.975	2.192	0.999	0.374	0.910	0.012	0.022	0.028	0.016	0.012	0.015	0.012	g0 IV	1.939	1444.0
151	01:00:00.24	+60:50:59.3	16.556	3.051	2.225	1.483	0.679	0.234	0.564	0.012	0.022	0.027	0.016	0.012	0.016	0.013	f0 V	1.448	2989.0
152	01:00:00.89	+60:54:44.9	15.625	3.257	2.454	1.718	0.795	0.295	0.711	0.012	0.020	0.025	0.015	0.012	0.015	0.012	f0 IV	1.947	2211.0
153	01:00:02.26	+60:50:27.6	17.000	—	2.533	1.757	0.821	0.294	0.731	0.013	—	0.033	0.016	0.013	0.016	0.013	f7 IV	1.373	3926.0
154	01:00:02.44	+60:50:54.1	15.478	3.134	2.279	1.419	0.635	0.223	0.559	0.012	0.020	0.025	0.015	0.012	0.015	0.012	a6 V	1.564	2281.0
155	01:00:02.58	+60:55:28.5	15.334	3.259	2.394	1.439	0.631	0.240	0.517	0.012	0.020	0.025	0.015	0.012	0.015	0.012	a6 IV	1.552	2532.0
156	01:00:02.96	+60:56:24.1	16.181	3.245	2.451	1.782	0.822	0.303	0.760	0.012	0.021	0.026	0.015	0.012	0.015	0.012	f5 V	1.527	1807.0
157	01:00:03.76	+60:59:46.4	16.790	3.317	2.605	1.891	0.845	0.311	0.766	0.012	0.024	0.029	0.016	0.013	0.016	0.013	f8 V	1.419	1637.0
158	01:00:05.63	+60:51:08.4	17.153	3.496	—	1.740	0.771	0.281	0.702	0.013	0.030	—	0.017	0.013	0.016	0.013	a9 V	1.922	766.0
159	01:00:05.77	+60:51:29.6	17.325	3.241	—	1.700	0.798	0.287	0.657	0.013	0.026	—	0.017	0.013	0.017	0.014	a5 V	2.296	2933.0
160	01:00:06.20	+60:49:54.4	16.155	3.079	2.275	1.403	0.631	0.212	0.534	0.012	0.021	0.026	0.015	0.012	0.015	0.012	a5 V	1.602	2773.0
161	01:00:06.35	+60:52:08.5	13.427	2.803	2.129	1.415	0.614	0.219	0.579	0.012	0.020	0.025	0.015	0.012	0.015	0.012	f2 IV	0.986	1070.0
162	01:00:06.80	+60:54:13.4	17.657	3.431	—	1.612	0.722	0.261	0.643	0.013	0.050	—	0.017	0.014	0.017	0.015	a2 V	2.151	4663.0
163	01:00:08.23	+60:51:09.7	17.606	3.313	—	1.649	0.759	0.296	0.636	0.016	0.045	—	0.020	0.016	0.020	0.021	f6 V	1.19	3257.0
164	01:00:08.57	+60:59:55.8	18.198	2.462	—	1.771	0.827	0.279	0.874	0.016	0.060	—	0.022	0.016	0.020	0.020	f8 V	1.344	2665.0
165	01:00:09.81	+60:56:46.0	14.183	2.361	1.709	1.085	0.528	0.194	0.462	0.012	0.020	0.025	0.015	0.012	0.015	0.012	b8 V	1.614	4209.0
166	01:00:10.02	+60:55:36.0	16.007	3.162	2.484	1.778	0.805	0.289	0.766	0.012	0.021	0.026	0.015	0.012	0.015	0.012	f9 V	1.198	1341.0
167	01:00:11.75	+60:54:47.5	17.250	3.311	—	2.004	0.891	0.328	0.914	0.013	0.037	—	0.017	0.013	0.016	0.013	g4 V	1.31	1520.0
168	01:00:12.15	+60:54:37.0	17.835	3.239	—	1.853	0.827	0.315	0.869	0.014	0.050	—	0.019	0.014	0.018	0.015	g3 V	1.09	2339.0
169	01:00:12.77	+60:53:10.1	17.213	3.008	—	1.678	0.758	0.267	0.724	0.013	0.037	—	0.017	0.013	0.017	0.014	f8 V	1.057	3135.0
170	01:00:13.34	+60:53:24.2	14.232	3.086	2.513	1.722	0.724	0.265	0.695	0.012	0.020	0.025	0.015	0.012	0.015	0.012	g4 V	0.616	684.0
171	01:00:13.37	+60:59:55.1	15.906	3.470	3.037	2.069	0.818	0.317	0.855	0.012	0.021	0.027	0.015	0.012	0.015	0.012	k1 V	0.691	389.0
172	01:00:13.98	+60:51:47.3	16.362	3.162	2.454	1.763	0.790	0.273	0.771	0.012	0.022	0.027	0.015	0.012	0.015	0.012	g0 V	1.082	1650.0
173	01:00:14.12	+60:54:11.2	16.080	3.127	2.327	1.510	0.688	0.240	0.628	0.012	0.021	0.026	0.015	0.012	0.015	0.012	f4 III	1.098	3456.0
174	01:00:14.21	+60:56:05.5	15.047	2.413	1.736	1.014	0.478	0.172	0.421	0.012	0.020	0.025	0.015	0.012	0.015	0.012	b9 V	1.331	3868.0
175	01:00:14.22	+60:59:43.0	16.368	3.095	2.419	1.680	0.751	0.254	0.736	0.012	0.021	0.026	0.015	0.012	0.015	0.012	f7 V	1.09	1935.0
176	01:00:14.26	+60:58:43.7	16.713	3.267	2.496	1.723	0.784	0.268	0.744	0.012	0.026	0.028	0.016	0.013	0.016	0.013	f0 V	1.884	2022.0
177	01:00:14.60	+60:53:58.0	14.348	3.107	2.247	1.295	0.559	0.200	0.463	0.012	0.020	0.025	0.015	0.012	0.015	0.012	a4 V	1.36	1637.0
178	01:00:15.37	+60:51:29.9	16.781	4.163	—	2.479	0.938	0.468	1.007	0.012	0.058	—	0.017	0.013	0.016	0.013	k3 V	0.961	755.0
179	01:00:17.32	+60:59:36.0	14.786	4.496	3.825	2.658	1.084	0.371	1.057	0.012	0.021	0.029	0.015	0.012	0.015	0.012	k0 III	1.302	3137.0
180	01:00:18.75	+60:52:27.1	13.013	2.691	2.019	1.182	0.499	0.159	0.445	0.012	0.020	0.025	0.015	0.012	0.015	0.012	a6 V	0.998	908.0
181</td																			

Table 3. Results of photometry and classification of stars in the Vilnius system for the IC 59 and IC 63 stars with the Maksutov-type telescope

No.	RA (J2000) (hh:mm:ss)	DEC (J2000) (dd:mm:ss)	V (mag)	U – V (mag)	P – V (mag)	X – V (mag)	Y – V (mag)	Z – V (mag)	V – S (mag)	e(V) (mag)	e(U – V) (mag)	e(P – V) (mag)	e(X – V) (mag)	e(Y – V) (mag)	e(Z – V), e(V – S) (mag)	Sp type	Av (mag)	d (pc)	
1	00:56:15.50	+61:20:35.5	14.864	–	2.899	2.103	1.063	0.407	0.849	0.071	–	0.118	0.100	0.113	0.110	0.118	f5 III	2.563	1405.0
2	00:56:19.17	+61:06:30.2	13.715	2.885	2.292	1.604	0.686	0.291	0.630	0.028	0.060	0.052	0.044	0.035	0.034	0.036	g0 IV	0.636	908.0
3	00:56:19.37	+61:16:50.7	12.919	2.701	2.077	1.396	0.605	0.249	0.591	0.026	0.048	0.041	0.033	0.031	0.029	0.031	f6 IV	0.545	767.0
4	00:56:20.86	+61:11:13.6	14.953	–	2.503	1.751	0.769	0.315	0.700	0.035	–	0.079	0.052	0.044	0.048	0.045	g5 V	0.765	811.0
5	00:56:22.21	+61:04:37.2	14.292	–	3.096	1.973	0.953	0.348	0.875	0.033	–	0.065	0.047	0.042	0.042	0.040	a3 III	3.087	2434.0
6	00:56:22.45	+61:20:29.4	11.068	–	–	1.867	0.910	0.379	0.852	0.068	–	–	0.086	0.088	0.082	0.091	a1 III	0.562	1048.0
7	00:56:22.61	+61:00:17.1	15.062	–	2.406	1.663	0.705	0.303	0.663	0.045	–	0.093	0.058	0.056	0.059	0.069	g6 V	0.474	971.0
8	00:56:25.92	+61:07:08.3	11.934	2.725	2.207	1.515	0.695	0.299	0.510	0.054	0.070	0.068	0.067	0.067	0.078	0.071	g1 IV	0.62	398.0
9	00:56:26.03	+60:51:37.0	14.234	3.219	2.341	1.443	0.724	0.258	0.612	0.030	0.082	0.053	0.041	0.038	0.040	0.040	a0 V	2.28	2056.0
10	00:56:26.69	+61:12:14.2	12.438	2.963	2.153	1.326	0.564	0.239	0.519	0.024	0.047	0.036	0.030	0.029	0.027	0.031	a8 III	1.136	1026.0
11	00:56:27.43	+61:06:50.4	14.702	2.893	2.179	1.365	0.668	0.260	0.571	0.043	0.101	0.077	0.055	0.053	0.057	0.068	a7 V	1.635	2198.0
12	00:56:28.23	+61:00:35.2	14.878	–	2.552	1.742	0.723	0.314	0.662	0.036	–	0.073	0.052	0.046	0.047	0.047	g8 V	0.466	985.0
13	00:56:28.38	+61:18:20.8	15.260	–	3.150	2.197	1.035	0.397	0.842	0.044	–	0.103	0.071	0.057	0.061	0.061	a9 III	3.012	1645.0
14	00:56:29.58	+61:11:29.8	15.143	–	2.491	1.751	0.725	0.300	0.730	0.037	–	0.082	0.054	0.049	0.059	0.048	g7 V	0.512	782.0
15	00:56:29.62	+60:58:27.7	14.312	–	2.803	1.839	0.743	0.334	0.684	0.033	–	0.074	0.046	0.041	0.042	0.041	k0 V	0.441	635.0
16	00:56:30.02	+61:10:38.0	14.272	2.849	2.301	1.618	0.698	0.302	0.656	0.032	0.077	0.054	0.045	0.040	0.042	0.040	g4 V	0.508	662.0
17	00:56:30.40	+61:22:04.2	14.837	2.664	2.260	1.595	0.660	0.278	0.655	0.036	0.103	0.066	0.048	0.046	0.049	0.051	g6 V	0.287	629.0
18	00:56:30.68	+61:14:07.0	14.121	2.683	2.047	1.393	0.606	0.257	0.555	0.029	0.068	0.051	0.039	0.036	0.037	0.039	f3 V	0.811	1063.0
19	00:56:30.98	+60:53:16.9	11.752	4.160	3.474	2.395	0.940	0.378	0.882	0.024	0.044	0.038	0.030	0.028	0.025	0.031	a2 V	0.553	877.0
20	00:56:31.07	+61:23:08.6	10.768	2.472	1.719	0.814	0.338	0.156	0.265	0.025	0.040	0.034	0.032	0.029	0.027	0.029	k0 III	0.703	715.0
21	00:56:32.96	+61:08:45.7	12.740	–	–	1.830	0.791	0.320	0.738	0.047	–	–	0.069	0.069	0.061	0.064	g2 V	0.316	411.0
22	00:56:34.03	+61:00:54.6	15.058	–	2.431	1.668	0.678	0.299	0.673	0.040	–	0.090	0.058	0.052	0.056	0.050	g9 V	0.225	845.0
23	00:56:35.59	+61:05:22.5	15.195	–	2.388	1.659	0.728	0.270	0.635	0.040	–	0.092	0.056	0.052	0.054	0.050	g2 V	0.728	919.0
24	00:56:36.88	+60:54:53.2	15.180	–	2.596	1.545	0.782	0.253	0.667	0.046	–	0.097	0.063	0.062	0.068	0.066	a1 IV	2.479	3385.0
25	00:56:41.03	+61:22:04.7	15.379	–	2.817	1.930	0.914	0.340	0.822	0.044	–	0.108	0.065	0.059	0.060	0.058	a8 IV	2.6	1394.0
26	00:56:42.71	+60:53:20.0	14.223	2.685	2.072	1.399	0.666	0.256	0.598	0.031	0.070	0.058	0.041	0.039	0.040	0.040	f3 V	1.061	1022.0
27	00:56:43.57	+61:15:01.1	15.144	–	2.709	1.875	0.724	0.318	0.731	0.038	–	0.095	0.057	0.050	0.051	0.048	k0 V	0.362	629.0
28	00:56:43.76	+60:50:06.4	14.916	–	2.868	1.972	1.012	0.404	0.788	0.066	–	0.106	0.082	0.078	0.080	0.080	a4 III	3.27	2604.0
29	00:56:48.11	+61:16:55.0	13.116	3.222	2.711	1.853	0.731	0.343	0.760	0.026	0.058	0.041	0.034	0.031	0.030	0.032	k0 V	0.391	350.0
30	00:56:48.88	+60:58:30.5	11.080	1.769	1.353	0.906	0.464	0.180	0.376	0.023	0.038	0.033	0.029	0.028	0.025	0.027	b5 III	1.639	4370.0
31	00:56:49.69	+60:54:15.3	13.608	2.801	2.220	1.536	0.671	0.262	0.620	0.027	0.059	0.047	0.036	0.035	0.034	0.034	f9 IV	0.628	970.0
32	00:56:50.84	+60:54:49.3	14.930	–	2.487	1.768	0.704	0.298	0.680	0.035	–	0.077	0.055	0.045	0.048	0.047	g9 V	0.333	657.0
33	00:56:51.64	+60:52:04.9	13.430	–	–	1.895	0.771	0.362	0.703	0.048	–	–	0.078	0.061	0.067	0.063	f6 V	0.524	641.0
34	00:56:52.05	+61:17:11.1	15.507	–	2.825	1.919	0.773	0.322	0.789	0.044	–	0.103	0.063	0.061	0.056	0.056	k0 V	0.566	752.0
35	00:56:52.27	+60:59:10.8	15.000	–	2.211	1.378	0.675	0.253	0.555	0.039	–	0.070	0.050	0.056	0.050	0.055	a6 V	1.731	1330.0
36	00:56:52.43	+61:16:05.1	15.007	–	–	2.403	0.853	0.563	0.873	0.054	–	–	0.092	0.072	0.073	0.075	b7 V	2.542	4963.0
37	00:56:52.66	+61:00:16.4	14.240	2.566	1.866	1.210	0.606	0.224	0.520	0.032	0.074	0.053	0.041	0.040	0.042	0.042	b8 III	2.034	5581.0
38	00:56:54.37	+61:19:13.0	13.511	2.627	2.014	1.359	0.591	0.233	0.563	0.027	0.055	0.044	0.034	0.032	0.031	0.034	f2 V	0.865	700.0
39	00:56:54.70	+61:22:25.1	14.477	2.981	2.413	1.684	0.711	0.287	0.693	0.031	0.090	0.060	0.045	0.039	0.043	0.042	g0 IV	0.74	950.0
40	00:56:55.12	+60:55:49.3	13.588	2.807	2.303	1.569	0.645	0.278	0.617	0.027	0.056	0.048	0.037	0.034	0.034	0.034	g3 V	0.333	475.0
41	00:56:55.71	+60:56:10.5	14.823	–	2.784	1.822	0.854	0.290	0.721	0.035	–	0.082	0.080	0.046	0.046	0.044	a8 III	2.342	4945.0
42	00:56:56.39	+61:16:32.1	10.600	2.543	2.088	1.376	0.524	0.238	0.537	0.023	0.037	0.032	0.029	0.027	0.027	0.027	g6 V	0.0	153.0
43	00:56:56.95	+61:17:46.6	13.851	3.175	2.734	1.855	0.742	0.334	0.739	0.028	0.076	0.054	0.038	0.034	0.034	0.034	g9 V	0.491	428.0
44	00:56:58.93	+60:52:59.2	14.232	2.765	2.173	1.493	0.680	0.278	0.585	0.031	0.077	0.054	0.041	0.039	0.042	0.040	f5 V	0.936	773.0
45	00:56:59.11	+60:57:32.1	15.091	–	2.074	1.232	0.591	0.239	0.496	0.050	–	0.085	0.062	0.067	0.069	0.086	a3 V	1.548	2573.0
46	00:56:59.40	+61:12:43.4	15.218	–	2.649	1.565	0.701	0.263	0.630	0.038	–	0.084	0.055	0.050	0.053	0.053	a4 V	1.951	1949.0
47	00:57:00.73	+60:50:31.1	15.964	–	2.451	1.630	0.867	0.334	0.662	0.064	–	0.118	0.090	0.080	0.087	0.080	g8 V	3.024	3738.0
48	00:57:01.53	+61:22:28.2	14.999	–	2.577	1.793	0.710	0.292	0.736	0.035	–	0.070	0.050	0.043	0.048	0.049	g8 V	0.412	589.0
49	00:57:03.14	+60:50:17.8	10.459	2.634	2.029	1.338	0.562	0.229	0.538	0.023	0.037	0.033	0.029	0.028	0.026	0.026	f5 III	0.478	509.0
50	00:57:04.47	+60:55:29.3	13.101	2.691	1.948	1.087	0.440	0.188	0.363	0.026	0.049	0.039	0.033	0.031	0.030	0.034	a4 V	0.865	1009.0
51	00:57:07.70	+60:58:43.6	11.967	2.767	2.124	1.419	0.622	0.250	0.569	0.026	0.042	0.036	0.032	0.031	0.029	0.031	f4 III	0.824	716.0
52	00:57:10.77	+60:52:10.6	15.016	–	3.125														

No.	RA (J2000) (hh:mm:ss)	DEC (J2000) (dd:mm:ss)	V (mag)	$U - V$ (mag)	$P - V$ (mag)	$X - V$ (mag)	$Y - V$ (mag)	$Z - V$ (mag)	$V - S$ (mag)	$e(V)$ (mag)	$e(U - V)$ (mag)	$e(P - V)$ (mag)	$e(X - V)$ (mag)	$e(Y - V)$ (mag)	$e(Z - V)$, (mag)	$e(V - S)$, (mag)	Sp type	A_V (mag)	d (pc)
66	00:57:21.68	+60:59:20.1	14.696	-	2.408	1.402	0.658	0.239	0.552	0.034	-	0.064	0.047	0.043	0.045	0.044	a3 III	1.86	3198.0
67	00:57:22.41	+61:02:11.8	14.905	-	2.271	1.620	0.680	0.275	0.615	0.035	-	0.070	0.050	0.043	0.048	0.047	g1 V	0.574	878.0
68	00:57:23.45	+60:50:40.2	15.337	-	2.521	1.781	0.693	0.286	0.704	0.041	-	0.087	0.058	0.054	0.057	0.057	g9 V	0.287	875.0
69	00:57:23.81	+61:22:46.8	13.928	3.427	2.448	1.490	0.689	0.254	0.635	0.029	0.081	0.056	0.043	0.037	0.038	0.036	a8 III	1.656	1957.0
70	00:57:24.98	+61:01:08.6	14.042	2.773	2.272	1.548	0.659	0.264	0.625	0.030	0.068	0.051	0.039	0.037	0.038	0.038	g3 V	0.391	627.0
71	00:57:26.45	+60:58:07.5	14.746	2.879	2.468	1.706	0.743	0.301	0.646	0.033	0.098	0.064	0.048	0.045	0.046	0.044	g4 V	0.695	933.0
72	00:57:27.96	+60:57:12.7	15.095	-	2.103	0.937	0.335	0.879	0.879	0.063	-	-	0.101	0.084	0.088	0.076	a6 V	2.08	1319.0
73	00:57:30.05	+61:01:42.2	12.411	2.745	2.218	1.487	0.613	0.248	0.595	0.025	0.046	0.037	0.031	0.030	0.027	0.030	g3 V	0.2	449.0
74	00:57:32.80	+60:58:17.8	15.835	-	2.636	2.004	0.991	0.376	0.811	0.048	-	0.108	0.091	0.066	0.069	0.064	f4 III	2.359	4139.0
75	00:57:33.53	+60:57:23.1	15.239	-	1.412	0.664	0.219	0.659	0.659	0.062	-	-	0.088	0.086	0.079	0.097	f6 III	1.751	2803.0
76	00:57:33.68	+60:47:25.1	13.357	2.840	2.363	1.628	0.713	0.296	0.665	0.034	0.108	0.067	0.049	0.044	0.046	0.047	g1 V	0.279	680.0
77	00:57:33.71	+61:15:27.0	14.927	2.625	2.141	1.408	0.609	0.241	0.564	0.034	0.088	0.068	0.049	0.042	0.047	0.044	g6 V	0.508	1054.0
78	00:57:36.32	+60:55:13.9	15.054	-	3.037	2.098	1.028	0.337	0.895	0.040	-	0.093	0.108	0.052	0.055	0.049	a8 IV	3.074	773.0
79	00:57:36.65	+60:48:53.5	15.116	3.016	2.220	1.234	0.578	0.216	0.423	0.037	0.093	0.075	0.053	0.046	0.050	0.047	g3 V	0.541	1097.0
80	00:57:36.71	+61:01:36.2	14.280	-	2.325	1.577	0.695	0.293	0.594	0.039	-	0.085	0.057	0.050	0.053	0.056	a2 V	1.552	1695.0
81	00:57:38.51	+61:20:18.1	12.763	3.881	3.266	2.271	0.913	0.386	0.811	0.030	0.097	0.058	0.042	0.036	0.036	0.048	g6 IV	1.256	865.0
82	00:57:38.69	+61:20:11.3	10.990	4.028	3.402	2.326	0.921	0.373	0.888	0.024	0.048	0.036	0.044	0.035	0.026	0.065	k0 III	0.624	734.0
83	00:57:39.25	+60:51:17.3	15.545	2.621	1.883	0.958	0.387	0.167	0.301	0.043	0.106	0.092	0.064	0.055	0.057	0.056	a7 V	2.6	1179.0
84	00:57:39.30	+61:02:17.0	11.881	-	2.848	1.931	0.900	0.319	0.780	0.049	-	0.108	0.073	0.068	0.070	0.065	a4 III	0.67	953.0
85	00:57:40.73	+61:22:21.9	14.209	-	3.210	1.296	0.536	1.146	0.399	0.039	-	-	0.086	0.055	0.052	0.046	g7 IV	0.541	867.0
86	00:57:41.12	+61:02:29.6	15.628	-	2.189	1.636	0.703	0.293	0.665	0.046	-	0.097	0.067	0.061	0.068	0.059	g3 V	0.574	1125.0
87	00:57:41.95	+60:58:03.8	14.363	3.063	2.687	1.826	0.731	0.337	0.686	0.034	0.094	0.075	0.047	0.041	0.045	0.043	g9 V	0.445	397.0
88	00:57:42.83	+60:49:07.1	14.819	-	2.529	1.612	0.807	0.271	0.661	0.034	-	0.080	0.049	0.045	0.058	0.044	a5 V	2.334	2477.0
89	00:57:43.50	+61:16:01.2	15.966	-	2.567	1.642	0.848	0.322	0.644	0.071	-	0.118	0.091	0.088	0.101	0.095	a2 V	2.675	3342.0
90	00:57:43.81	+61:22:09.6	14.329	2.893	2.134	1.253	0.603	0.242	0.504	0.031	0.103	0.058	0.042	0.039	0.041	0.043	a1 V	1.71	2787.0
91	00:57:43.90	+61:10:48.6	12.828	-	2.777	1.198	0.470	1.094	0.404	0.042	-	-	0.073	0.059	0.060	0.053	k0 III	2.887	1377.0
92	00:57:44.05	+61:20:17.2	14.083	2.790	2.118	1.364	0.575	0.237	0.539	0.029	0.076	0.050	0.039	0.036	0.038	0.040	f0 V	1.015	1063.0
93	00:57:45.92	+60:56:03.9	12.996	2.782	2.264	1.541	0.633	0.273	0.619	0.026	0.050	0.042	0.033	0.032	0.030	0.032	g3 V	0.283	389.0
94	00:57:46.41	+61:21:45.7	13.087	3.175	2.221	1.298	0.626	0.244	0.538	0.026	0.056	0.043	0.033	0.031	0.030	0.035	a5 III	1.602	1697.0
95	00:57:46.96	+60:52:54.9	12.612	2.695	2.060	1.338	0.574	0.236	0.529	0.025	0.046	0.039	0.032	0.031	0.029	0.030	f3 III	0.716	2878.0
96	00:57:47.79	+61:15:35.6	13.583	2.134	1.667	1.156	0.596	0.258	0.492	0.028	0.051	0.042	0.035	0.034	0.034	0.036	b8 V	1.897	2649.0
97	00:57:48.36	+60:55:04.6	15.159	-	1.646	0.715	0.266	0.775	0.771	0.071	-	-	0.096	0.091	0.097	0.089	b8 IV	2.9	3967.0
98	00:57:49.60	+61:14:51.5	15.213	-	2.405	1.468	0.734	0.307	0.557	0.038	-	0.079	0.055	0.048	0.052	0.051	g4 V	0.67	1042.0
99	00:57:49.72	+61:01:10.0	15.632	-	2.510	1.534	0.718	0.220	0.610	0.044	-	0.109	0.066	0.058	0.061	0.062	a5 V	1.964	2002.0
100	00:57:49.83	+61:21:24.5	15.652	-	3.064	1.363	0.514	1.219	0.245	0.045	-	-	0.068	0.057	0.059	0.058	g6 V	0.691	913.0
101	00:57:50.46	+61:17:02.6	15.457	-	2.965	1.930	0.821	0.345	0.762	0.042	-	0.096	0.062	0.053	0.058	0.065	g9 V	0.82	1013.0
102	00:57:50.65	+60:58:00.1	15.221	-	2.732	1.694	0.737	0.294	0.594	0.038	-	0.102	0.056	0.053	0.052	0.049	a5 IV	2.055	2806.0
103	00:57:51.31	+61:00:38.1	14.151	2.973	2.069	1.191	0.591	0.224	0.435	0.039	0.088	0.061	0.049	0.049	0.052	0.054	a0 III	1.772	2479.0
104	00:57:52.21	+61:23:09.3	14.698	3.228	2.633	1.839	0.775	0.333	0.733	0.034	0.101	0.070	0.047	0.046	0.047	0.044	g5 V	0.79	729.0
105	00:57:53.16	+61:15:46.7	15.500	-	2.466	1.477	0.699	0.273	0.622	0.044	-	0.158	0.063	0.056	0.059	0.059	a5 III	1.905	3981.0
106	00:57:55.06	+61:21:47.2	14.916	2.677	2.260	1.576	0.682	0.280	0.668	0.038	0.098	0.068	0.052	0.050	0.052	0.054	g6 V	0.379	910.0
107	00:57:55.57	+60:53:37.3	13.542	3.612	2.604	1.579	0.745	0.275	0.598	0.028	0.084	0.055	0.040	0.035	0.033	0.034	f3 III	2.03	1230.0
108	00:57:56.18	+60:58:57.5	15.421	-	2.340	1.307	0.596	0.234	0.420	0.041	-	0.087	0.061	0.054	0.055	0.056	a3 V	1.568	2293.0
109	00:57:58.39	+61:23:25.3	14.196	-	2.889	1.932	0.729	0.356	0.770	0.032	-	0.070	0.045	0.039	0.042	0.040	k2 V	0.179	304.0
110	00:57:58.44	+61:15:18.3	14.323	-	2.031	0.935	0.343	0.843	0.843	0.070	-	-	0.112	0.104	0.096	0.093	g2 V	0.495	553.0
111	00:57:59.81	+61:20:49.4	14.720	-	2.310	1.575	0.696	0.264	0.668	0.036	-	0.064	0.048	0.047	0.046	0.045	f9 V	0.745	1109.0
112	00:58:01.91	+61:02:18.0	15.125	-	2.564	1.727	0.727	0.297	0.707	0.038	-	0.076	0.055	0.050	0.051	0.052	g7 V	0.52	786.0
113	00:58:03.93	+60:57:34.3	15.331	-	2.447	1.676	0.713	0.318	0.652	0.040	-	0.085	0.060	0.054	0.057	0.055	g5 V	0.532	968.0
114	00:58:04.27	+61:23:39.6	15.242	-	2.709	1.895	0.853	0.351	0.790	0.040	-	0.090	0.061	0.052	0.053	0.053	g5 IV	1.061	1627.0
115	00:58:05.05	+61:16:15.3	14.542	-	3.032	2.003	0.921	0.350	0.842	0.033	-	0.086	0.048	0.043	0.044	0.042	f6 III	1.88	1919.0
116	00:58:07.77	+60:47:22.9	15.338	3.408	2.856	1.933	0.732	0.359	0.736	0.040	0.105	0.084	0.058	0.050	0.052	0.052	f8 IV	1.543	1439.0
117	00:58:07.83	+61:01:50.3																	

No.	RA (J2000) (hh:mm:ss)	DEC (J2000) (dd:mm:ss)	<i>V</i> (mag)	<i>U</i> − <i>V</i> (mag)	<i>P</i> − <i>V</i> (mag)	<i>X</i> − <i>V</i> (mag)	<i>Y</i> − <i>V</i> (mag)	<i>Z</i> − <i>V</i> (mag)	<i>V</i> − <i>S</i> (mag)	<i>e</i> (<i>V</i>) (mag)	<i>e</i> (<i>U</i> − <i>V</i>) (mag)	<i>e</i> (<i>P</i> − <i>V</i>) (mag)	<i>e</i> (<i>X</i> − <i>V</i>) (mag)	<i>e</i> (<i>Y</i> − <i>V</i>) (mag)	<i>e</i> (<i>Z</i> − <i>V</i>) (mag)	<i>e</i> (<i>V</i> − <i>S</i>) (mag)	Sp type	<i>A</i> _{<i>V</i>} (mag)	d (pc)
131	00:58:19.57	+60:48:13.4	15.803	−	2.010	1.134	0.626	0.204	0.505	0.049	−	0.112	0.070	0.066	0.070	0.064	b9 V	1.947	3224.0
132	00:58:20.28	+60:48:47.9	15.819	−	2.389	1.653	0.738	0.269	0.661	0.049	−	0.103	0.073	0.096	0.074	0.064	g0 IV	0.853	2279.0
133	00:58:20.78	+61:00:12.7	14.177	2.722	2.098	1.479	0.654	0.251	0.575	0.031	0.071	0.053	0.041	0.038	0.040	0.039	f5 V	0.828	778.0
134	00:58:21.13	+60:52:14.8	14.923	−	2.782	1.867	0.820	0.362	0.735	0.037	−	0.075	0.054	0.052	0.052	0.047	g8 V	0.869	656.0
135	00:58:21.25	+60:47:15.5	13.619	−	2.844	1.004	0.601	1.065	0.040	−	−	0.091	0.055	0.061	0.050	0.050	f6 V	0.774	738.0
136	00:58:21.62	+61:09:39.1	13.311	2.755	2.160	1.483	0.637	0.264	0.600	0.026	0.058	0.041	0.035	0.033	0.031	0.032	f7 V	0.616	612.0
137	00:58:21.94	+60:58:25.2	14.094	3.664	2.680	1.767	0.830	0.279	0.729	0.029	0.087	0.060	0.042	0.036	0.036	0.039	a4 III	2.513	1241.0
138	00:58:22.28	+61:15:51.1	15.159	2.757	2.204	1.513	0.790	0.281	0.695	0.056	0.113	0.083	0.150	0.109	0.095	0.064	b9 V	2.629	5667.0
139	00:58:22.48	+61:22:06.6	14.405	3.273	2.679	1.776	0.742	0.311	0.692	0.033	0.098	0.079	0.046	0.041	0.042	0.042	g6 IV	0.545	864.0
140	00:58:23.16	+61:16:52.4	14.349	3.179	2.240	1.339	0.671	0.238	0.574	0.030	0.087	0.057	0.042	0.039	0.040	0.040	a0 III	2.105	3083.0
141	00:58:23.38	+61:16:23.7	15.418	−	2.845	1.973	0.938	0.356	0.860	0.044	−	0.104	0.062	0.056	0.056	0.056	f7 IV	1.86	1337.0
142	00:58:23.64	+60:57:17.7	15.649	−	2.697	1.707	0.773	0.296	0.627	0.045	−	0.102	0.088	0.057	0.063	0.058	a4 IV	2.263	2133.0
143	00:58:23.66	+61:02:19.6	14.195	3.172	2.399	1.634	0.757	0.280	0.684	0.030	0.085	0.052	0.048	0.038	0.038	0.039	f2 IV	1.581	1214.0
144	00:58:23.29	+61:06:24.4	14.866	−	2.196	1.366	0.659	0.270	0.539	0.034	−	0.067	0.048	0.045	0.049	0.046	a7 III	1.602	3194.0
145	00:58:25.39	+61:09:32.6	14.783	−	2.644	1.652	0.734	0.288	0.603	0.035	−	0.074	0.050	0.046	0.047	0.046	a3 V	2.142	1271.0
146	00:58:26.59	+60:56:43.6	13.062	−	4.857	3.418	1.426	0.552	1.294	0.026	−	0.143	0.042	0.035	0.032	0.031	k2 III	2.359	1276.0
147	00:58:26.66	+61:07:29.9	12.359	2.648	1.922	1.050	0.446	0.186	0.384	0.024	0.044	0.035	0.030	0.029	0.027	0.029	a4 V	0.89	710.0
148	00:58:26.82	+61:09:42.5	15.136	−	2.313	1.627	0.695	0.289	0.663	0.037	−	0.075	0.053	0.047	0.052	0.050	g5 V	0.458	863.0
149	00:58:27.58	+61:05:06.3	14.432	3.081	2.611	1.808	0.761	0.317	0.758	0.032	0.088	0.058	0.046	0.042	0.044	0.046	g9 V	0.57	544.0
150	00:58:27.94	+61:07:01.5	12.857	2.978	2.121	1.258	0.616	0.236	0.522	0.029	0.049	0.043	0.039	0.034	0.032	0.033	a0 V	1.83	1100.0
151	00:58:28.09	+60:48:13.3	12.729	1.819	1.392	1.001	0.541	0.211	0.511	0.027	0.046	0.037	0.033	0.032	0.031	0.032	b3 V	2.043	4247.0
152	00:58:29.25	+61:20:01.9	15.724	−	2.505	1.546	0.702	0.261	0.661	0.047	−	0.099	0.068	0.061	0.064	0.068	a6 III	1.851	3610.0
153	00:58:29.32	+60:48:27.0	14.310	−	2.802	1.803	0.766	0.306	0.710	0.041	−	0.100	0.062	0.054	0.066	0.055	a4 IV	2.018	1325.0
154	00:58:29.42	+61:01:06.5	15.594	3.224	2.418	1.588	0.714	0.292	0.576	0.044	0.108	0.094	0.065	0.056	0.058	0.057	g8 V	0.645	775.0
155	00:58:29.51	+60:54:48.0	13.070	2.657	2.038	1.308	0.559	0.228	0.515	0.027	0.050	0.055	0.034	0.033	0.031	0.033	f4 V	0.516	690.0
156	00:58:29.68	+61:16:22.1	14.771	−	2.604	1.868	0.818	0.345	0.740	0.041	−	0.075	0.057	0.054	0.057	0.055	g5 V	0.969	798.0
157	00:58:29.83	+61:08:55.6	14.804	−	4.002	3.039	1.288	0.459	1.202	0.034	−	0.094	0.062	0.047	0.049	0.044	k2 III	1.785	3778.0
158	00:58:30.33	+60:53:24.4	15.436	−	1.382	0.750	0.143	0.640	0.098	−	−	0.138	0.136	0.120	0.124	0.124	a3 V	1.955	3071.0
159	00:58:30.98	+61:21:07.6	15.193	−	2.264	1.604	0.692	0.276	0.670	0.038	−	0.082	0.056	0.049	0.051	0.050	g3 V	0.528	957.0
160	00:58:32.16	+61:03:07.6	14.892	2.902	2.080	1.152	0.525	0.217	0.414	0.036	0.094	0.068	0.049	0.044	0.048	0.048	a2 V	1.331	2683.0
161	00:58:34.23	+61:05:23.9	14.801	2.919	2.353	1.644	0.731	0.308	0.656	0.036	0.093	0.070	0.048	0.047	0.061	0.049	g2 V	0.74	865.0
162	00:58:34.36	+60:52:58.8	13.815	2.786	2.122	1.451	0.641	0.240	0.609	0.028	0.055	0.044	0.038	0.037	0.035	0.036	f2 V	1.073	916.0
163	00:58:34.40	+60:51:05.5	12.278	4.004	3.351	2.288	0.922	0.376	0.860	0.025	0.053	0.038	0.032	0.030	0.028	0.029	k0 III	0.628	988.0
164	00:58:34.59	+61:19:36.8	13.911	2.757	2.152	1.468	0.639	0.254	0.600	0.029	0.070	0.053	0.037	0.035	0.037	0.038	f6 V	0.691	820.0
165	00:58:35.05	+60:49:51.9	15.146	−	2.515	1.524	0.686	0.262	0.564	0.041	−	0.082	0.056	0.055	0.055	0.054	a4 V	1.889	1765.0
166	00:58:35.35	+61:06:44.2	11.369	2.755	1.943	1.003	0.419	0.187	0.320	0.028	0.044	0.037	0.035	0.032	0.031	0.032	a4 V	0.778	662.0
167	00:58:35.88	+61:10:12.0	15.242	−	2.841	1.763	0.802	0.305	0.705	0.040	−	0.080	0.059	0.053	0.056	0.054	a6 III	2.267	2491.0
168	00:58:36.04	+61:09:08.4	15.430	−	2.917	2.031	0.793	0.411	0.767	0.041	−	0.099	0.063	0.055	0.064	0.054	k1 V	0.587	705.0
169	00:58:36.48	+61:12:28.7	13.514	−	1.575	0.589	0.301	0.598	0.603	−	−	0.126	0.097	0.101	0.100	0.100	f0 V	1.231	2180.0
170	00:58:38.07	+61:17:13.7	12.090	4.875	4.142	2.822	1.082	0.469	1.003	0.027	0.074	0.046	0.036	0.032	0.030	0.033	k3 III	0.707	1054.0
171	00:58:38.54	+60:48:13.0	14.595	3.054	2.427	1.627	0.771	0.287	0.704	0.034	0.096	0.065	0.049	0.045	0.045	0.045	f4 IV	1.406	1539.0
172	00:58:39.30	+60:47:12.4	15.267	4.115	3.422	2.338	0.952	0.381	0.868	0.025	0.057	0.046	0.032	0.031	0.028	0.029	g9 III	0.882	1140.0
173	00:58:39.41	+61:18:43.0	14.477	−	2.583	1.571	0.722	0.277	0.633	0.031	−	0.058	0.044	0.041	0.043	0.043	a4 V	2.038	511.0
174	00:58:39.69	+61:15:11.6	15.551	−	2.333	1.701	0.751	0.300	0.743	0.044	−	0.092	0.064	0.057	0.059	0.059	g3 V	0.774	1105.0
175	00:58:40.65	+61:05:55.4	14.492	−	2.678	1.798	0.836	0.294	0.749	0.032	−	0.059	0.044	0.043	0.042	0.041	f5 I	1.606	3374.0
176	00:58:40.77	+61:06:45.9	13.847	2.783	2.176	1.442	0.631	0.250	0.591	0.028	0.065	0.048	0.036	0.034	0.035	0.037	f3 V	0.915	857.0
177	00:58:41.81	+61:11:48.1	14.690	−	2.462	1.641	0.747	0.283	0.694	0.033	−	0.071	0.046	0.044	0.046	0.044	a8 V	1.897	1150.0
178	00:58:43.97	+61:02:43.5	15.796	−	2.502	1.763	0.735	0.328	0.747	0.047	−	0.108	0.076	0.063	0.069	0.061	g9 V	0.462	1007.0
179	00:58:46.59	+61:23:06.0	15.390	−	2.708	1.934	0.867	0.306	0.850	0.043	−	0.096	0.064	0.058	0.057	0.059	g2 IV	1.281	1987.0
180	00:58:46.70	+61:13:50.8	12.328	2.825	2.011	1.054	0.450	0.195	0										

No.	RA (J2000) (hh:mm:ss)	DEC (J2000) (dd:mm:ss)	V (mag)	$U - V$ (mag)	$P - V$ (mag)	$X - V$ (mag)	$Y - V$ (mag)	$Z - V$ (mag)	$V - S$ (mag)	$e(V)$ (mag)	$e(U - V)$ (mag)	$e(P - V)$ (mag)	$e(X - V)$ (mag)	$e(Y - V)$ (mag)	$e(Z - V)$, (mag)	$e(V - S)$, (mag)	Sp type	A_V (mag)	d (pc)
196	00:58:57.80	+61:07:43.3	11.447	2.370	1.627	0.818	0.339	0.163	0.283	0.024	0.038	0.033	0.030	0.028	0.026	0.029	a3 V	0.499	781.0
197	00:58:58.13	+61:08:28.4	13.625	3.150	2.430	1.641	0.721	0.279	0.663	0.028	0.067	0.048	0.037	0.035	0.033	0.034	f0 IV	1.639	977.0
198	00:58:58.28	+61:09:43.3	10.643	2.738	1.991	1.177	0.485	0.212	0.436	0.023	0.038	0.033	0.030	0.028	0.025	0.029	a6 III	0.948	470.0
199	00:58:58.36	+61:23:42.5	14.757	-	2.641	1.609	0.803	0.308	0.645	0.033	-	0.065	0.047	0.043	0.046	0.047	a3 III	2.463	4007.0
200	00:58:58.64	+61:19:36.9	14.146	2.880	2.311	1.623	0.693	0.275	0.661	0.031	0.092	0.053	0.041	0.042	0.039	0.040	g3 V	0.532	681.0
201	00:58:58.72	+61:08:37.8	15.134	-	2.390	1.646	0.726	0.275	0.687	0.047	-	0.075	0.059	0.056	0.060	0.057	g1 V	0.765	997.0
202	00:59:00.68	+60:47:19.7	15.668	-	2.476	1.574	0.740	0.300	0.632	0.046	-	0.099	0.067	0.061	0.061	0.058	a9 III	1.785	6012.0
203	00:59:02.13	+60:48:42.6	14.779	2.867	2.290	1.500	0.700	0.256	0.633	0.034	0.097	0.068	0.047	0.046	0.047	0.045	f0 III	1.531	3104.0
204	00:59:03.10	+61:12:45.7	15.740	2.319	1.700	1.095	0.552	0.220	0.466	0.046	0.112	0.100	0.069	0.059	0.061	0.060	a0 V	2.658	2921.0
205	00:59:03.14	+61:04:48.0	12.732	-	2.600	1.561	0.815	0.260	0.591	0.068	-	0.102	0.088	0.093	0.098	0.101	b7 III	1.876	1823.0
206	00:59:04.01	+61:02:42.3	13.030	4.240	3.427	2.333	0.933	0.370	0.862	0.026	0.079	0.051	0.034	0.031	0.031	0.031	g9 III	0.803	1012.0
207	00:59:04.64	+61:08:54.3	12.970	2.880	2.070	1.223	0.585	0.227	0.489	0.027	0.051	0.040	0.034	0.032	0.031	0.031	a0 V	1.701	1189.0
208	00:59:06.09	+60:48:21.8	15.369	-	1.270	0.727	0.295	0.496	0.078	-	-	0.120	0.110	0.109	0.110	0.110	a3 V	1.731	3705.0
209	00:59:06.49	+61:09:04.8	13.116	2.777	2.103	1.372	0.610	0.248	0.557	0.026	0.049	0.040	0.033	0.031	0.030	0.033	f1 V	1.057	657.0
210	00:59:06.51	+61:11:16.2	15.598	-	2.601	1.775	0.837	0.299	0.788	0.045	-	0.099	0.066	0.059	0.062	0.061	a9 V	2.196	1171.0
211	00:59:06.83	+60:47:19.0	16.062	-	2.483	1.828	0.862	0.323	0.738	0.057	-	0.113	0.082	0.076	0.072	0.075	f9 V	1.435	1486.0
212	00:59:09.68	+61:24:05.3	14.675	-	2.624	1.687	0.768	0.285	0.727	0.036	-	0.065	0.048	0.046	0.048	0.047	a5 IV	2.184	1452.0
213	00:59:09.92	+61:09:13.5	14.377	3.272	2.297	1.356	0.669	0.250	0.569	0.033	0.082	0.056	0.045	0.041	0.042	0.041	a1 V	1.984	2589.0
214	00:59:10.13	+61:20:08.7	14.074	3.169	2.620	1.783	0.739	0.309	0.688	0.030	0.078	0.057	0.042	0.038	0.039	0.039	g6 V	0.616	683.0
215	00:59:10.93	+61:13:31.2	13.339	3.229	2.324	1.346	0.640	0.243	0.511	0.026	0.066	0.045	0.034	0.033	0.031	0.033	a2 IV	1.826	1377.0
216	00:59:11.48	+61:07:02.1	15.778	-	2.693	1.879	0.862	0.299	0.804	0.047	-	0.101	0.069	0.061	0.066	0.061	g1 V	1.331	1299.0
217	00:59:13.40	+61:03:28.4	14.605	3.266	2.353	1.319	0.644	0.256	0.509	0.034	0.087	0.061	0.045	0.041	0.043	0.045	a2 V	1.826	2065.0
218	00:59:14.44	+61:11:35.6	15.413	-	2.304	1.651	0.708	0.277	0.727	0.041	-	0.088	0.060	0.052	0.055	0.053	g5 V	0.512	831.0
219	00:59:15.45	+61:17:48.2	13.415	2.796	2.054	1.331	0.652	0.250	0.578	0.027	0.057	0.042	0.034	0.033	0.032	0.035	a7 III	1.572	2344.0
220	00:59:16.77	+61:16:21.1	15.791	-	2.307	1.536	0.760	0.278	0.641	0.047	-	0.104	0.070	0.063	0.064	0.061	f0 V	1.785	1235.0
221	00:59:17.70	+60:48:27.7	14.779	-	2.026	0.936	0.366	0.811	0.053	-	-	0.086	0.075	0.072	0.073	0.073	g0 IV	1.419	1269.0
222	00:59:18.14	+61:14:42.1	13.663	-	1.735	0.850	0.362	0.686	0.081	-	-	0.114	0.100	0.121	0.103	0.103	b9 V	2.126	2100.0
223	00:59:18.32	+61:04:26.7	13.490	2.384	1.803	1.245	0.627	0.223	0.557	0.027	0.053	0.042	0.034	0.032	0.032	0.032	b5 IV	2.205	294.0
224	00:59:19.34	+61:03:44.8	10.227	-	2.488	1.109	0.417	1.048	0.037	-	-	0.065	0.049	0.055	0.050	0.050	k3 III	0.15	466.0
225	00:59:19.46	+61:05:39.4	14.205	2.959	2.357	1.636	0.712	0.284	0.667	0.030	0.073	0.053	0.041	0.038	0.038	0.039	f9 V	0.811	740.0
226	00:59:19.61	+61:22:21.8	12.478	3.937	3.322	2.253	0.902	0.368	0.836	0.027	0.060	0.044	0.036	0.034	0.031	0.036	g9 IV	0.919	767.0
227	00:59:20.06	+61:06:44.3	14.107	2.883	2.193	1.475	0.661	0.257	0.603	0.030	0.079	0.059	0.039	0.038	0.039	0.039	f2 V	1.156	895.0
228	00:59:20.17	+61:21:24.3	13.426	2.774	2.065	1.235	0.528	0.223	0.456	0.027	0.056	0.043	0.035	0.034	0.032	0.038	a6 V	1.119	948.0
229	00:59:21.28	+61:09:53.0	12.487	2.918	2.160	1.353	0.589	0.240	0.546	0.025	0.048	0.039	0.031	0.030	0.028	0.030	a7 IV	1.315	770.0
230	00:59:22.11	+60:48:20.3	14.364	-	3.284	2.288	0.964	0.361	0.910	0.032	-	0.076	0.053	0.044	0.042	0.041	g9 III	0.932	2703.0
231	00:59:23.49	+60:48:43.1	15.996	-	2.282	1.661	0.722	0.262	0.723	0.052	-	0.110	0.076	0.068	0.076	0.070	g0 V	0.799	1605.0
232	00:59:24.52	+61:22:34.1	15.977	-	2.441	1.588	0.738	0.293	0.588	0.055	-	0.109	0.074	0.072	0.074	0.068	a9 III	1.776	3433.0
233	00:59:26.12	+61:02:43.8	15.398	-	2.509	1.478	0.659	0.273	0.513	0.042	-	0.090	0.060	0.053	0.060	0.057	a5 V	1.718	2317.0
234	00:59:28.16	+61:17:10.3	15.367	-	2.449	1.780	0.777	0.301	0.714	0.041	-	0.091	0.059	0.054	0.056	0.054	g1 V	0.978	1102.0
235	00:59:28.85	+61:20:57.7	14.981	-	2.452	1.753	0.753	0.304	0.711	0.037	-	0.078	0.053	0.049	0.050	0.049	g4 V	0.736	1110.0
236	00:59:31.44	+61:02:10.0	15.629	-	2.723	1.982	0.795	0.352	0.758	0.044	-	0.102	0.072	0.057	0.061	0.058	g9 V	0.711	720.0
237	00:59:31.71	+61:15:58.4	13.592	2.880	2.088	1.192	0.494	0.204	0.417	0.027	0.063	0.045	0.034	0.033	0.032	0.036	a4 V	1.09	1112.0
238	00:59:32.55	+61:14:28.0	13.947	2.951	2.130	1.273	0.631	0.264	0.511	0.033	0.068	0.053	0.041	0.040	0.043	0.047	a0 V	1.893	1905.0
239	00:59:33.28	+60:49:15.2	15.300	-	2.263	1.344	0.605	0.207	0.582	0.043	-	0.082	0.058	0.054	0.057	0.062	a6 IV	1.444	2778.0
240	00:59:33.46	+60:47:22.2	14.272	2.707	2.086	1.421	0.637	0.248	0.596	0.032	0.085	0.054	0.042	0.042	0.041	0.042	f4 V	0.84	928.0
241	00:59:34.26	+61:22:14.3	14.132	3.457	2.547	1.518	0.702	0.279	0.570	0.029	0.090	0.053	0.040	0.036	0.038	0.039	a5 V	1.897	1271.0
242	00:59:34.31	+61:20:47.1	13.315	2.774	2.114	1.414	0.610	0.245	0.576	0.027	0.053	0.045	0.034	0.034	0.032	0.037	f2 V	0.944	802.0
243	00:59:34.51	+61:01:02.2	15.726	-	2.381	1.703	0.745	0.277	0.713	0.046	-	0.099	0.068	0.059	0.060	0.060	a6 IV	1.797	3268.0
244	00:59:34.52	+61:09:46.2	15.311	-	2.803	0.973	0.607	1.133	0.130	0.040	-	-	0.065	0.050	0.053	0.051	g1 V	0.844	1096.0
245	00:59:35.78	+61:20:12.3	13.343	-	5.289	3.627	1.439	0.608	1.281	0.027	-	0.087	0.048	0.035	0.034	0.036	k5 III	1.864	2071.0
246	00:59:37.14	+61:20:10.6	14.354	-	2.732	1.879	0.881	0.342	0.819	0.035	-	0.067	0.047	0.043	0.046				

No.	RA (J2000) (hh:mm:ss)	DEC (J2000) (dd:mm:ss)	<i>V</i> (mag)	<i>U</i> − <i>V</i> (mag)	<i>P</i> − <i>V</i> (mag)	<i>X</i> − <i>V</i> (mag)	<i>Y</i> − <i>V</i> (mag)	<i>Z</i> − <i>V</i> (mag)	<i>V</i> − <i>S</i> (mag)	<i>e</i> (<i>V</i>) (mag)	<i>e</i> (<i>U</i> − <i>V</i>) (mag)	<i>e</i> (<i>P</i> − <i>V</i>) (mag)	<i>e</i> (<i>X</i> − <i>V</i>) (mag)	<i>e</i> (<i>Y</i> − <i>V</i>) (mag)	<i>e</i> (<i>Z</i> − <i>V</i>) (mag)	<i>e</i> (<i>V</i> − <i>S</i>) (mag)	Sp type	<i>A</i> _{<i>V</i>} (mag)	d (pc)
261	00:59:43.05	+61:19:28.1	14.278	2.938	2.346	1.598	0.703	0.273	0.673	0.031	0.099	0.058	0.041	0.041	0.042	f9 IV	0.761	1024.0	
262	00:59:43.39	+61:21:35.3	14.142	2.720	2.191	1.547	0.664	0.285	0.639	0.030	0.074	0.051	0.040	0.039	0.038	0.039	g1 V	0.508	521.0
263	00:59:44.30	+61:15:52.6	12.084	4.484	3.757	2.577	1.015	0.407	0.945	0.025	0.055	0.047	0.033	0.030	0.028	0.030	k0 III	1.015	1134.0
264	00:59:44.71	+60:47:39.2	14.988	2.797	—	1.621	0.709	0.275	0.694	0.037	0.098	—	0.054	0.049	0.052	0.048	g2 V	0.649	802.0
265	00:59:45.19	+61:13:23.9	14.728	—	2.451	1.555	0.712	0.294	0.612	0.034	—	0.081	0.048	0.044	0.046	0.043	a6 V	1.884	1126.0
266	00:59:45.23	+60:48:00.7	15.105	—	2.304	1.277	0.562	0.208	0.528	0.040	—	0.076	0.053	0.049	0.051	0.051	a4 III	1.398	3921.0
267	00:59:45.47	+61:15:07.6	15.097	—	—	2.754	1.213	0.454	1.061	0.040	—	—	0.068	0.054	0.061	0.052	a2 V	1.86	1902.0
268	00:59:45.85	+61:21:12.3	14.500	—	3.468	2.451	1.129	0.429	1.029	0.034	—	0.096	0.051	0.045	0.046	0.043	g2 II	2.263	3165.0
269	00:59:45.97	+61:13:55.7	14.679	—	2.603	1.696	0.779	0.315	0.664	0.037	—	0.070	0.049	0.047	0.048	0.048	a5 IV	2.23	1551.0
270	00:59:46.23	+61:04:27.8	13.583	2.848	2.261	1.565	0.671	0.267	0.647	0.028	0.060	0.045	0.037	0.034	0.033	0.034	f8 V	0.695	494.0
271	00:59:49.34	+61:19:32.4	13.782	—	—	1.660	0.794	0.256	0.934	0.073	—	—	0.093	0.101	0.098	0.101	a6 V	1.082	1075.0
272	00:59:50.41	+61:02:04.6	14.575	3.195	2.525	1.768	0.772	0.303	0.709	0.033	0.103	0.061	0.048	0.042	0.043	0.042	g1 V	0.957	891.0
273	00:59:50.48	+61:14:06.8	14.810	—	2.991	2.183	0.990	0.382	0.888	0.035	—	0.080	0.052	0.046	0.048	0.044	g2 IV	1.793	1287.0
274	00:59:50.71	+61:10:30.2	15.179	—	3.168	2.109	0.819	0.387	0.819	0.039	—	0.108	0.057	0.052	0.052	0.050	k2 V	0.553	487.0
275	00:59:50.89	+60:17:35.0	15.402	—	2.683	1.739	0.831	0.309	0.639	0.044	—	0.100	0.061	0.058	0.064	0.057	a5 V	2.434	1499.0
276	00:59:51.19	+60:48:06.1	14.894	3.179	2.496	1.643	0.753	0.300	0.706	0.036	0.109	0.086	0.049	0.048	0.051	0.047	f1 IV	1.672	1489.0
277	00:59:51.24	+61:24:00.9	13.308	3.208	2.693	1.791	0.720	0.306	0.696	0.027	0.065	0.041	0.036	0.033	0.040	0.040	g9 IV	0.162	569.0
278	00:59:54.52	+60:57:43.0	12.495	—	—	1.539	0.699	0.273	0.609	0.066	—	—	0.090	0.079	0.096	0.088	a1 V	1.09	992.0
279	00:59:55.08	+61:08:30.6	14.237	—	2.421	1.538	0.743	0.262	0.652	0.031	—	0.053	0.041	0.040	0.040	0.041	a6 III	2.022	2137.0
280	00:59:55.15	+61:07:12.1	14.823	3.076	2.372	1.660	0.749	0.270	0.692	0.036	0.086	0.066	0.048	0.045	0.047	0.047	f3 V	1.406	761.0
281	00:59:55.69	+61:20:41.8	15.317	—	2.567	1.811	0.845	0.324	0.768	0.040	—	0.086	0.059	0.054	0.058	0.055	f9 IV	1.352	1259.0
282	00:59:56.07	+61:02:44.6	14.106	3.781	2.803	1.818	0.836	0.314	0.780	0.034	0.107	0.067	0.046	0.047	0.047	0.050	a8 III	2.267	1956.0
283	00:59:57.40	+61:11:36.1	14.919	—	3.823	2.665	1.112	0.408	1.044	0.034	—	0.096	0.058	0.046	0.047	0.044	a8 III	1.419	3598.0
284	00:59:57.48	+60:50:17.7	12.993	3.043	2.129	1.164	0.534	0.212	0.426	0.026	0.051	0.043	0.032	0.030	0.033	0.033	a1 V	1.423	232.0
285	00:59:58.27	+61:02:21.2	15.119	—	2.183	1.260	0.625	0.238	0.493	0.044	—	0.075	0.057	0.055	0.059	0.066	a0 V	1.868	3227.0
286	00:59:59.01	+61:02:09.6	15.333	—	—	1.942	0.876	0.234	0.937	0.057	—	—	0.087	0.087	0.072	0.071	a8 III	1.602	6978.0
287	00:59:59.95	+61:21:36.3	15.610	—	2.799	1.763	0.784	0.303	0.681	0.044	—	0.100	0.065	0.056	0.062	0.061	a6 IV	2.188	2686.0
288	01:00:06.62	+61:09:29.1	13.617	3.036	2.297	1.530	0.678	0.267	0.610	0.028	0.067	0.048	0.036	0.034	0.035	0.035	f2 V	1.227	801.0
289	01:00:01:21	+61:21:16.4	13.866	2.760	2.111	1.428	0.610	0.257	0.570	0.033	0.073	0.053	0.041	0.040	0.052	0.052	f3 V	0.828	921.0
290	01:00:01:19.7	+61:02:22.7	14.653	2.964	2.122	1.266	0.538	0.220	0.490	0.033	0.080	0.062	0.046	0.040	0.043	0.043	f7 V	0.778	1014.0
291	01:00:02:09	+61:01:06.8	15.683	—	2.001	1.181	0.565	0.213	0.491	0.045	—	0.097	0.067	0.058	0.060	0.064	a5 V	1.327	3888.0
292	01:00:02:23	+61:19:55.6	14.563	—	—	1.638	0.806	0.283	0.623	0.065	—	—	0.088	0.091	0.082	0.085	a6 V	1.394	1390.0
293	01:00:03:22	+60:47:34.9	13.956	2.622	2.001	1.304	0.572	0.230	0.543	0.030	0.064	0.051	0.038	0.038	0.038	0.039	f2 V	0.786	948.0
294	01:00:04:32	+61:21:09.7	13.998	—	—	1.904	0.851	0.354	0.863	0.071	—	—	0.101	0.090	0.089	0.091	a6 IV	1.577	1365.0
295	01:00:04:33	+60:55:13.8	12.021	—	2.374	1.431	0.637	0.251	0.545	0.030	—	0.055	0.039	0.038	0.037	0.041	a8 III	1.065	1884.0
296	01:00:05:45	+61:10:42.1	14.919	—	2.558	1.754	0.731	0.320	0.721	0.035	—	0.083	0.049	0.045	0.048	0.047	k0 V	0.391	587.0
297	01:00:05:77	+61:15:39.2	15.001	—	2.842	1.923	0.877	0.323	0.822	0.040	—	0.087	0.058	0.054	0.054	0.052	g1 IV	1.377	1837.0
298	01:00:05:95	+60:48:33.6	14.939	—	2.399	1.503	0.661	0.238	0.612	0.036	—	0.069	0.050	0.047	0.051	0.048	a7 IV	1.614	1841.0
299	01:00:07:32	+60:47:28.5	15.797	—	2.678	1.756	0.765	0.290	0.741	0.049	—	0.110	0.070	0.065	0.069	0.065	f4 IV	1.381	1612.0
300	01:00:07:37	+60:48:37.8	15.638	—	2.351	1.469	0.676	0.245	0.563	0.045	—	0.096	0.066	0.059	0.061	0.061	a4 III	1.872	3575.0
301	01:00:08:16	+61:19:28.1	14.597	2.690	2.180	1.497	0.672	0.253	0.589	0.033	0.102	0.065	0.045	0.042	0.044	0.043	g1 V	0.541	1115.0
302	01:00:09:29	+61:20:54.4	15.064	—	2.667	1.825	0.696	0.314	0.753	0.037	—	0.081	0.057	0.047	0.051	0.050	k0 V	0.245	522.0
303	01:00:09:44	+61:19:18.5	12.585	2.762	1.961	1.040	0.414	0.181	0.336	0.027	0.048	0.040	0.033	0.032	0.037	0.035	a5 V	0.699	863.0
304	01:00:10:54	+61:06:20.7	12.220	2.566	1.928	1.383	0.721	0.263	0.606	0.025	0.044	0.037	0.032	0.030	0.028	0.029	b7 III	2.579	2577.0
305	01:00:11:44	+61:02:44.4	13.566	—	—	1.943	0.874	0.336	0.775	0.048	—	—	0.076	0.066	0.075	0.070	b7 III	2.163	3135.0
306	01:00:12:14	+61:23:38.9	14.451	—	2.395	1.389	0.651	0.242	0.546	0.033	—	0.059	0.044	0.044	0.048	0.048	a5 III	1.706	2510.0
307	01:00:12:39	+60:53:43.7	15.509	—	—	1.969	0.840	0.308	0.758	0.048	—	—	0.071	0.064	0.067	0.063	g5 V	0.424	856.0
308	01:00:13:16	+61:15:35.4	15.359	—	2.215	1.236	0.564	0.243	0.493	0.041	—	0.084	0.059	0.054	0.056	0.054	a2 V	1.493	3032.0
309	01:00:14:18	+61:15:16.7	13.521	—	—	1.737	0.730	0.280	0.782	0.073	—	—	0.107	0.103	0.092	0.095	f5 V	0.836	691.0
310	01:00:14:53	+61:12:29.4	14.938	—	—	1.771	0.825	0.366	0.739	0.062	—	—	0.116	0.082	0.090	0.080	f7 V	0.973	853.0
311	01:00:14:92</td																		

No.	RA (J2000) (hh:mm:ss)	DEC (J2000) (dd:mm:ss)	V (mag)	$U - V$ (mag)	$P - V$ (mag)	$X - V$ (mag)	$Y - V$ (mag)	$Z - V$ (mag)	$V - S$ (mag)	$e(V)$ (mag)	$e(U - V)$ (mag)	$e(P - V)$ (mag)	$e(X - V)$ (mag)	$e(Y - V)$ (mag)	$e(Z - V)$ (mag)	$e(V - S)$ (mag)	Sp type	A_V (mag)	d (pc)
326	01:00:25.42	+60:49:10.4	15.302	–	2.349	1.598	0.683	0.261	0.714	0.040	–	0.082	0.058	0.051	0.055	0.052	g3 V	0.491	1115.0
327	01:00:25.64	+61:04:16.8	15.535	–	2.517	1.698	0.728	0.294	0.701	0.045	–	0.091	0.066	0.059	0.060	0.059	g5 V	0.595	1030.0
328	01:00:25.90	+61:21:38.4	14.516	–	–	1.596	0.688	0.251	0.625	0.047	–	–	0.069	0.063	0.069	0.063	k1 V	0.524	427.0
329	01:00:26.62	+60:51:11.2	15.521	–	2.194	1.240	0.577	0.222	0.479	0.046	–	0.100	0.063	0.057	0.062	0.063	a4 III	1.46	4185.0
330	01:00:26.80	+60:55:08.5	15.132	–	2.253	1.357	0.589	0.237	0.563	0.038	–	0.075	0.053	0.049	0.052	0.051	a6 V	1.373	2047.0
331	01:00:27.77	+60:50:49.3	15.357	–	2.149	1.185	0.557	0.226	0.427	0.041	–	0.088	0.059	0.053	0.054	0.057	a4 III	1.377	6647.0
332	01:00:28.68	+60:58:01.1	14.903	–	2.579	1.651	0.714	0.273	0.605	0.037	–	0.078	0.052	0.047	0.048	0.049	a7 IV	1.835	2160.0
333	01:00:28.81	+60:47:45.7	12.563	2.761	2.086	1.369	0.589	0.226	0.580	0.027	0.048	0.040	0.035	0.033	0.032	0.034	f3 IV	0.761	738.0
334	01:00:28.88	+61:07:39.2	12.128	2.526	1.812	1.172	0.594	0.236	0.509	0.025	0.043	0.035	0.030	0.029	0.027	0.030	b9 V	1.814	1262.0
335	01:00:29.28	+61:14:28.4	15.041	–	2.555	1.790	0.743	0.291	0.736	0.036	–	0.093	0.053	0.049	0.049	0.046	g7 V	0.587	766.0
336	01:00:30.09	+61:21:01.7	12.179	2.768	1.983	1.167	0.551	0.221	0.464	0.027	0.046	0.037	0.033	0.031	0.030	0.038	a2 V	1.439	1409.0
337	01:00:30.23	+60:54:25.3	13.218	2.762	1.980	1.125	0.438	0.180	0.424	0.028	0.044	0.038	0.033	0.033	0.030	0.036	a2 V	0.924	2359.0
338	01:00:30.32	+60:47:54.5	15.215	–	2.265	1.583	0.740	0.326	0.636	0.048	–	0.102	0.067	0.063	0.080	0.068	g0 V	0.874	1144.0
339	01:00:31.55	+60:52:19.6	13.339	–	3.936	2.668	1.069	0.424	1.002	0.027	–	0.068	0.040	0.034	0.032	0.034	k3 III	0.653	2112.0
340	01:00:31.68	+60:59:32.8	15.075	–	2.708	1.862	0.757	0.307	0.739	0.039	–	0.091	0.053	0.051	0.052	0.050	g9 V	0.553	710.0
341	01:00:31.88	+60:50:27.7	12.626	1.662	1.188	0.726	0.356	0.141	0.311	0.025	0.042	0.036	0.031	0.031	0.028	0.032	b6 III	1.119	3011.0
342	01:00:32.20	+61:09:32.8	13.731	2.947	2.209	1.482	0.665	0.261	0.591	0.032	0.073	0.051	0.040	0.040	0.040	0.040	f2 V	1.173	774.0
343	01:00:32.48	+61:18:08.5	15.667	–	2.603	1.542	0.741	0.300	0.611	0.046	–	0.097	0.067	0.063	0.068	0.068	a3 III	2.205	3589.0
344	01:00:33.12	+61:15:48.5	13.830	2.830	2.168	1.442	0.628	0.236	0.614	0.030	0.071	0.050	0.039	0.037	0.038	0.040	f0 V	1.236	869.0
345	01:00:33.55	+60:55:09.6	12.814	4.778	3.931	2.678	1.078	0.424	0.984	0.026	0.091	0.073	0.036	0.033	0.030	0.033	k1 III	1.111	1447.0
346	01:00:33.79	+61:14:21.5	15.115	–	2.470	1.519	0.669	0.260	0.571	0.037	–	0.075	0.053	0.048	0.050	0.050	a3 V	1.872	1980.0
347	01:00:34.70	+60:50:04.0	14.764	–	2.092	1.154	0.551	0.230	0.452	0.061	–	0.102	0.076	0.091	0.081	0.099	a1 V	1.493	2986.0
348	01:00:34.72	+60:56:34.3	13.083	2.535	1.776	0.963	0.466	0.191	0.373	0.026	0.050	0.041	0.033	0.031	0.029	0.032	a0 V	1.206	1541.0
349	01:00:34.96	+61:00:50.7	11.125	2.594	2.100	1.382	0.536	0.227	0.551	0.023	0.040	0.033	0.029	0.028	0.025	0.028	g4 V	0.0	169.0
350	01:00:35.21	+61:17:23.9	12.240	2.636	2.049	1.438	0.608	0.252	0.627	0.027	0.048	0.039	0.034	0.032	0.030	0.034	f7 V	0.495	365.0
351	01:00:35.51	+60:59:17.2	15.339	–	2.354	1.382	0.635	0.260	0.478	0.064	–	0.103	0.077	0.085	0.090	0.096	a4 III	1.701	3363.0
352	01:00:36.19	+61:21:24.0	12.817	2.597	1.934	1.277	0.534	0.222	0.525	0.027	0.055	0.042	0.034	0.032	0.032	0.039	f2 V	0.628	548.0
353	01:00:37.32	+61:12:51.1	15.062	2.403	1.617	0.840	0.398	0.156	0.333	0.036	0.092	0.072	0.052	0.044	0.049	0.046	g5 V	0.691	1148.0
354	01:00:37.36	+60:49:53.9	12.890	–	2.515	1.759	0.751	0.278	0.715	0.036	–	0.087	0.054	0.050	0.050	0.045	a2 III	0.84	2093.0
355	01:00:37.63	+61:19:10.3	14.568	–	2.552	0.944	0.560	1.017	0.044	–	–	0.093	0.062	0.071	0.059	0.059	f3 IV	1.776	1342.0
356	01:00:38.48	+60:54:47.2	13.332	2.927	2.344	1.564	0.641	0.259	0.636	0.027	0.057	0.046	0.035	0.033	0.032	0.033	g4 V	0.27	496.0
357	01:00:39.47	+60:47:58.3	16.500	–	2.302	1.681	0.710	0.277	0.735	0.071	–	0.130	0.108	0.095	0.107	0.095	g7 V	0.449	1729.0
358	01:00:39.60	+60:50:11.0	15.408	–	2.591	1.851	0.784	0.329	0.651	0.079	–	0.116	0.099	0.102	0.115	0.118	g5 V	0.828	1001.0
359	01:00:40.63	+60:48:42.1	14.901	–	2.442	1.524	0.670	0.260	0.594	0.038	–	0.073	0.052	0.048	0.051	0.050	a5 III	1.785	2887.0
360	01:00:40.70	+60:55:34.8	15.694	–	1.714	0.999	0.452	0.172	0.428	0.046	–	0.098	0.067	0.059	0.060	0.068	a6 III	0.811	5521.0
361	01:00:40.87	+61:12:02.2	14.685	–	2.252	1.323	0.624	0.232	0.527	0.033	–	0.063	0.046	0.044	0.044	0.044	a4 IV	1.643	2510.0
362	01:00:40.99	+61:15:15.3	11.272	–	1.640	0.781	0.278	0.737	0.057	–	–	0.096	0.089	0.085	0.082	0.082	k3 III	0.387	727.0
363	01:00:41.54	+60:24:45.5	13.721	–	1.493	0.733	0.367	0.624	0.080	–	–	0.119	0.104	0.117	0.115	0.115	b7 V	1.697	3381.0
364	01:00:41.97	+61:14:57.5	15.823	–	1.626	0.607	0.226	0.849	0.100	–	–	0.119	0.124	0.126	0.127	0.127	g4 V	0.757	1103.0
365	01:00:42.81	+60:59:04.2	15.357	–	2.604	1.801	0.814	0.325	0.748	0.041	–	0.092	0.059	0.057	0.058	0.054	g3 IV	1.011	1369.0
366	01:00:43.68	+61:17:24.3	14.828	–	2.413	1.560	0.696	0.273	0.630	0.036	–	0.076	0.049	0.046	0.049	0.047	a7 IV	1.76	1869.0
367	01:00:43.84	+60:49:01.3	15.818	–	2.284	1.260	0.540	0.219	0.438	0.049	–	0.110	0.070	0.062	0.067	0.069	a5 V	1.223	3462.0
368	01:00:44.02	+61:14:01.5	15.708	–	2.501	1.588	0.787	0.312	0.766	0.063	–	0.111	0.077	0.083	0.098	0.098	a0 III	2.588	3973.0
369	01:00:44.27	+61:09:49.7	13.377	2.874	2.275	1.576	0.679	0.272	0.693	0.027	0.057	0.045	0.036	0.034	0.034	0.033	f8 V	0.728	523.0
370	01:00:45.02	+60:53:59.2	13.921	–	3.315	2.316	0.999	0.377	0.940	0.029	–	0.067	0.045	0.038	0.036	0.035	g8 III	1.194	4548.0
371	01:00:45.02	+61:11:09.0	14.457	2.582	1.977	1.433	0.650	0.232	0.630	0.032	0.075	0.058	0.043	0.040	0.042	0.041	f7 V	0.67	611.0
372	01:00:45.47	+61:22:04.8	15.044	–	3.098	2.039	0.726	0.371	0.825	0.038	–	0.106	0.053	0.050	0.056	0.054	k3 V	0.079	464.0
373	01:00:46.16	+60:51:46.0	15.202	–	2.057	1.135	0.468	0.187	0.419	0.042	–	0.078	0.055	0.052	0.056	0.060	a4 V	0.982	1846.0
374	01:00:46.75	+61:05:42.5	13.938	3.103	2.250	1.415	0.689	0.256	0.582	0.030	0.081	0.047	0.039	0.036	0.039	0.039	a8 V	1.656	1623.0
375	01:00:46.77	+60:53:35.9	13.743	2.763	2.101	1.411	0.611	0.239	0.592	0.030	0.060	0.046	0.039	0.036	0.038	0.039	f1 V	1.061	743.0
376	01:00:46.90	+61:19:16.5	13.585	–	1.961	0.918	0.366	0.763	0.045	–	–	0.061	0.062	0.062	0.061	0.061	g4		

No.	RA (J2000) (hh:mm:ss)	DEC (J2000) (dd:mm:ss)	V (mag)	$U - V$ (mag)	$P - V$ (mag)	$X - V$ (mag)	$Y - V$ (mag)	$Z - V$ (mag)	$V - S$ (mag)	$e(V)$ (mag)	$e(U - V)$ (mag)	$e(P - V)$ (mag)	$e(X - V)$ (mag)	$e(Y - V)$ (mag)	$e(Z - V)$ (mag)	$e(V - S)$ (mag)	Sp type	A_V (mag)	d (pc)
391	01:00:51.65	+60:52:47.7	13.830	2.682	2.019	1.352	0.578	0.221	0.568	0.030	0.064	0.044	0.040	0.037	0.038	0.039	f2 V	0.811	764.0
392	01:00:51.95	+60:50:11.9	13.638	3.023	2.080	1.151	0.517	0.201	0.469	0.031	0.071	0.050	0.038	0.038	0.037	0.041	a1 V	1.352	1518.0
393	01:00:52.07	+61:09:59.2	15.734	–	2.567	1.455	0.677	0.239	0.619	0.047	–	0.106	0.068	0.060	0.067	0.065	a3 III	1.939	3376.0
394	01:00:53.02	+60:50:56.0	15.316	–	2.205	1.393	0.610	0.228	0.600	0.043	–	0.084	0.058	0.054	0.055	0.057	a9 V	1.252	1676.0
395	01:00:54.20	+61:24:38.8	13.986	–	3.334	2.160	0.769	0.463	0.796	0.030	–	0.065	0.045	0.038	0.035	0.063	k4 V	0.029	268.0
396	01:00:54.63	+60:54:10.1	14.889	–	3.644	2.464	1.034	0.394	0.982	0.038	–	0.103	0.057	0.050	0.051	0.047	k0 III	1.094	3125.0
397	01:00:54.83	+60:58:16.2	15.552	–	1.722	0.729	0.292	0.743	0.065	–	–	0.101	0.082	0.086	0.085	0.048	a3 V	1.681	2293.0
398	01:00:55.08	+60:49:15.6	14.692	2.955	2.148	1.271	0.557	0.206	0.551	0.033	0.098	0.063	0.046	0.043	0.044	0.047	a8 III	1.107	3192.0
399	01:00:55.35	+60:59:58.5	14.399	2.039	1.532	0.950	0.483	0.201	0.385	0.031	0.072	0.057	0.043	0.038	0.040	0.041	g6 V	0.27	548.0
400	01:00:55.36	+60:58:40.7	13.318	2.906	2.409	1.659	0.656	0.261	0.708	0.033	0.093	0.061	0.046	0.041	0.042	0.043	b9 V	1.352	2579.0
401	01:00:55.83	+60:54:18.5	14.274	–	1.480	0.633	0.252	0.524	0.069	–	–	0.089	0.083	0.085	0.086	0.048	a2 V	1.044	2171.0
402	01:00:56.11	+61:20:56.7	13.594	–	2.339	1.051	0.375	0.107	0.044	–	–	0.075	0.071	0.064	0.056	0.056	k1 III	1.181	2063.0
403	01:00:56.50	+60:48:52.7	13.748	–	1.677	0.792	0.256	0.748	0.087	–	–	0.133	0.108	0.111	0.104	0.072	g7 III	1.098	3315.0
404	01:00:57.15	+61:02:05.8	12.621	2.786	1.993	1.069	0.439	0.173	0.373	0.025	0.048	0.037	0.032	0.030	0.028	0.032	a5 V	0.803	869.0
405	01:00:57.32	+60:54:11.9	15.856	–	2.613	1.736	0.801	0.312	0.718	0.060	–	0.109	0.084	0.075	0.076	0.077	a6 IV	2.259	2312.0
406	01:00:57.55	+60:58:22.2	15.401	–	2.543	1.624	0.763	0.278	0.736	0.041	–	0.101	0.060	0.054	0.058	0.054	f0 III	1.793	2645.0
407	01:00:57.58	+61:22:38.8	15.185	–	2.329	1.320	0.603	0.232	0.475	0.040	–	0.077	0.056	0.052	0.056	0.060	a4 V	1.543	1996.0
408	01:00:57.80	+60:49:39.7	14.299	–	2.375	1.316	0.605	0.177	0.502	0.058	–	0.106	0.086	0.071	0.080	0.074	a2 V	0.907	3157.0
409	01:00:57.81	+60:59:21.5	16.199	2.499	1.786	0.931	0.423	0.161	0.337	0.053	0.126	0.118	0.080	0.070	0.070	0.072	a2 V	1.664	2402.0
410	01:00:58.31	+61:15:24.1	15.309	–	2.669	1.861	0.875	0.319	0.771	0.044	–	0.095	0.060	0.058	0.055	0.055	f8 IV	1.535	2309.0
411	01:00:58.44	+60:49:47.6	11.688	2.603	1.821	0.895	0.358	0.141	0.318	0.028	0.044	0.039	0.034	0.033	0.030	0.035	a4 V	0.524	746.0
412	01:00:58.57	+60:54:09.1	14.265	–	3.278	2.270	0.956	0.370	0.911	0.032	–	0.080	0.049	0.041	0.041	0.040	g9 III	0.899	3310.0
413	01:00:58.86	+60:57:28.7	14.282	–	2.199	0.834	0.391	0.819	0.044	–	–	0.075	0.058	0.060	0.058	0.060	k4 V	0.399	342.0
414	01:00:58.99	+60:52:02.5	13.050	2.609	2.002	1.360	0.579	0.219	0.580	0.028	0.050	0.040	0.035	0.035	0.032	0.034	f4 V	0.599	511.0
415	01:00:59.12	+60:47:56.1	15.883	–	2.044	1.226	0.586	0.230	0.509	0.048	–	0.105	0.072	0.062	0.063	0.064	g1 V	0.682	847.0
416	01:00:59.13	+61:11:51.5	15.545	–	2.376	1.644	0.706	0.278	0.735	0.048	–	0.102	0.073	0.066	0.068	0.068	a6 V	1.36	2942.0
417	01:00:59.78	+60:53:21.9	16.157	–	2.592	1.155	0.451	1.129	0.052	–	–	0.079	0.069	0.069	0.070	0.070	a3 V	1.161	4060.0
418	01:01:00.48	+61:13:20.3	14.670	–	3.206	2.295	1.019	0.362	0.982	0.039	–	0.091	0.069	0.054	0.054	0.055	g3 IV	1.864	2444.0
419	01:01:02.07	+60:47:34.1	15.903	–	2.086	1.262	0.560	0.217	0.540	0.052	–	0.106	0.073	0.068	0.073	0.068	a9 V	1.044	2742.0
420	01:01:02.27	+60:52:35.7	15.576	–	2.205	1.500	0.686	0.255	0.677	0.045	–	0.093	0.064	0.060	0.061	0.057	f4 V	1.044	1736.0
421	01:01:02.29	+61:23:47.9	13.617	–	2.351	1.582	0.728	0.281	0.681	0.040	–	0.081	0.058	0.056	0.054	0.055	a8 IV	1.543	1120.0
422	01:01:02.30	+60:55:04.5	15.198	3.194	2.384	1.490	0.660	0.252	0.593	0.038	0.096	0.078	0.055	0.047	0.051	0.049	f3 V	1.319	1191.0
423	01:01:02.34	+60:48:28.8	14.935	–	2.388	1.646	0.707	0.326	0.690	0.039	–	0.082	0.055	0.050	0.054	0.052	g6 V	0.483	933.0
424	01:01:02.89	+61:10:53.4	15.658	–	2.430	0.996	0.338	0.951	0.059	–	–	0.116	0.079	0.079	0.083	0.083	b9 V	2.063	1714.0
425	01:01:02.91	+61:04:27.7	13.805	2.798	2.114	1.362	0.595	0.219	0.558	0.028	0.069	0.048	0.037	0.035	0.036	0.036	a9 V	1.19	943.0
426	01:01:02.96	+61:00:43.4	15.268	–	2.326	1.544	0.649	0.221	0.687	0.040	–	0.082	0.057	0.052	0.053	0.055	g4 V	0.304	1054.0
427	01:01:03.54	+61:19:48.0	15.293	–	2.406	1.391	0.667	0.260	0.497	0.056	–	0.091	0.072	0.073	0.077	0.091	a4 V	1.81	2216.0
428	01:01:04.13	+61:09:53.3	15.219	–	2.699	1.864	0.805	0.310	0.734	0.045	–	0.096	0.065	0.062	0.064	0.063	g6 V	0.89	740.0
429	01:01:04.96	+61:06:51.2	14.518	2.969	2.239	1.513	0.666	0.245	0.647	0.033	0.085	0.059	0.048	0.041	0.042	0.044	a8 V	1.56	1024.0
430	01:01:05.13	+60:51:59.8	15.513	–	2.200	1.294	0.603	0.234	0.503	0.043	–	0.091	0.063	0.054	0.057	0.061	a4 V	1.543	2463.0
431	01:01:05.46	+61:17:26.9	16.024	–	2.374	1.688	0.770	0.304	0.691	0.050	–	0.111	0.076	0.066	0.070	0.071	f8 IV	1.098	2248.0
432	01:01:05.99	+61:16:00.8	14.277	–	2.135	0.845	0.337	0.836	0.057	–	–	0.112	0.075	0.086	0.074	0.074	f2 III	1.086	3468.0
433	01:01:06.15	+61:01:09.0	14.663	2.984	2.350	1.619	0.713	0.284	0.673	0.033	0.105	0.067	0.046	0.043	0.044	0.044	f7 V	0.932	898.0
434	01:01:06.45	+61:14:08.7	14.820	–	2.077	1.154	0.527	0.212	0.440	0.035	–	0.066	0.048	0.046	0.047	0.047	a2 V	1.34	2313.0
435	01:01:07.35	+61:12:14.5	15.405	2.740	2.042	1.177	0.508	0.200	0.421	0.049	0.109	0.087	0.063	0.063	0.067	0.066	g0 V	1.489	406.0
436	01:01:07.35	+60:47:44.4	15.147	–	2.696	1.929	0.888	0.326	0.793	0.056	–	0.101	0.074	0.067	0.076	0.079	a6 V	1.036	2324.0
437	01:01:07.83	+61:19:36.6	14.769	–	3.358	2.240	0.991	0.420	0.895	0.034	–	0.098	0.053	0.047	0.048	0.047	g6 III	1.36	2064.0
438	01:01:08.41	+60:59:10.8	14.595	–	4.149	2.839	1.170	0.451	1.088	0.038	–	0.106	0.061	0.048	0.050	0.048	k3 III	1.073	1560.0
439	01:01:08.49	+60:48:27.8	14.659	2.367	1.650	0.870	0.412	0.197	0.383	0.042	0.088	0.064	0.054	0.054	0.059	0.063	a0 IV	1.003	3647.0
440	01:01:08.95	+61:05:42.7	14.880	–	2.492	1.694	0.760	0.301	0.694	0.041	–	0.084	0.054	0.052	0.055	0.050	g3 V	0.811	741.0
441	01:01:09.89	+61:08:52.3	14.157	3.429	2.511	1.437	0.672	0.248	0.558	0.032	0.095	0.057	0.042	0.039	0.041	0.042	a2 IV	1.959	1613.0
44																			

No.	RA (J2000) (hh:mm:ss)	DEC (J2000) (dd:mm:ss)	<i>V</i>	<i>U</i> – <i>V</i>	<i>P</i> – <i>V</i>	<i>X</i> – <i>V</i>	<i>Y</i> – <i>V</i>	<i>Z</i> – <i>V</i>	<i>V</i> – <i>S</i>	<i>e</i> (<i>V</i>)	<i>e</i> (<i>U</i> – <i>V</i>)	<i>e</i> (<i>P</i> – <i>V</i>)	<i>e</i> (<i>X</i> – <i>V</i>)	<i>e</i> (<i>Y</i> – <i>V</i>)	<i>e</i> (<i>Z</i> – <i>V</i>)	<i>e</i> (<i>V</i> – <i>S</i>)	Sp type	<i>A_V</i> (mag)	d (pc)
456	01:01:15.74	+61:01:05.2	13.928	3.290	2.346	1.365	0.646	0.245	0.570	0.028	0.084	0.057	0.042	0.033	0.036	0.034	a2 V	1.835	1641.0
457	01:01:15.83	+60:53:57.6	13.991	2.611	1.965	1.226	0.533	0.197	0.527	0.030	0.070	0.049	0.039	0.038	0.038	0.039	a3 V	1.007	1046.0
458	01:01:16.33	+61:10:28.2	14.920	–	2.080	1.218	0.592	0.242	0.498	0.037	–	0.068	0.049	0.046	0.048	0.051	a0 V	1.731	2991.0
459	01:01:16.68	+60:56:28.0	15.601	–	–	1.414	0.566	0.160	0.665	0.072	–	–	0.099	0.096	0.104	0.089	g8 V	0.37	1026.0
460	01:01:16.83	+60:48:01.5	16.451	–	2.155	1.228	0.503	0.176	0.450	0.065	–	0.128	0.086	0.083	0.114	0.083	a2 V	1.24	3619.0
461	01:01:16.88	+61:24:16.3	15.725	–	–	1.333	0.635	0.211	0.546	0.046	–	–	0.072	0.062	0.064	0.068	a0 V	2.092	2865.0
462	01:01:17.23	+60:51:04.4	14.719	–	–	2.467	0.886	0.599	0.959	0.047	–	–	0.079	0.063	0.074	0.060	f0 IV	1.652	1414.0
463	01:01:18.19	+60:52:24.7	14.332	2.796	2.205	1.501	0.650	0.235	0.646	0.033	0.086	0.055	0.044	0.042	0.042	0.042	f7 V	0.67	927.0
464	01:01:18.21	+61:00:28.3	11.158	2.843	1.999	1.085	0.450	0.179	0.419	0.024	0.040	0.033	0.029	0.028	0.025	0.028	a6 III	0.803	767.0
465	01:01:18.29	+60:55:24.4	12.525	2.813	2.024	1.228	0.531	0.197	0.520	0.025	0.051	0.037	0.031	0.030	0.027	0.030	f1 III	0.736	1004.0
466	01:01:19.05	+60:54:58.2	15.624	–	–	1.753	0.811	0.327	0.813	0.061	–	–	0.096	0.078	0.082	0.081	f3 V	1.032	2286.0
467	01:01:19.17	+61:00:07.0	13.846	–	4.243	2.950	1.209	0.476	1.104	0.035	–	0.099	0.056	0.043	0.044	0.043	k1 III	1.656	2351.0
468	01:01:19.49	+61:02:13.3	13.761	2.812	2.072	1.233	0.518	0.192	0.495	0.030	0.067	0.050	0.038	0.037	0.035	0.038	a5 V	1.132	1041.0
469	01:01:19.64	+61:17:14.1	14.845	–	–	1.346	0.522	0.154	0.732	0.100	–	–	0.129	0.124	0.117	0.119	f9 V	0.591	1156.0
470	01:01:19.90	+61:10:46.6	13.373	2.780	2.099	1.354	0.584	0.229	0.565	0.028	0.061	0.040	0.034	0.033	0.033	0.036	a8 V	1.219	708.0
471	01:01:21.12	+61:03:49.1	15.261	–	3.099	2.158	1.031	0.412	0.901	0.072	–	0.111	0.114	0.111	0.108	0.091	f5 III	2.429	1852.0
472	01:01:21.93	+61:02:52.9	15.171	–	2.240	1.307	0.641	0.231	0.525	0.042	–	0.077	0.058	0.055	0.058	0.078	a1 V	1.868	6213.0
473	01:01:22.44	+60:59:37.8	13.864	–	–	1.531	0.725	0.262	0.781	0.092	–	–	0.122	0.111	0.110	0.114	g9 IV	0.229	775.0
474	01:01:22.51	+60:48:40.9	14.357	4.174	3.428	2.332	0.938	0.356	0.905	0.030	0.071	0.056	0.042	0.038	0.040	0.040	a4 V	1.136	1557.0
475	01:01:22.52	+61:12:04.6	12.038	–	–	1.434	0.673	0.271	0.666	0.062	–	–	0.084	0.078	0.089	0.091	k0 III	0.695	1128.0
476	01:01:22.72	+61:06:19.5	15.218	–	–	2.434	1.062	0.429	0.996	0.048	–	–	0.080	0.070	0.073	0.067	f8 IV	1.298	1480.0
477	01:01:23.21	+60:59:05.2	15.206	–	2.657	1.877	0.820	0.303	0.780	0.064	–	0.098	0.092	0.084	0.082	0.087	f9 IV	1.726	1834.0
478	01:01:23.36	+60:50:34.4	15.824	–	2.739	1.996	0.935	0.354	0.784	0.058	–	0.115	0.084	0.074	0.070	0.076	g5 V	0.978	1111.0
479	01:01:23.57	+61:08:37.6	11.952	–	2.847	1.868	0.719	0.333	0.758	0.043	–	0.096	0.060	0.052	0.051	0.053	k6 III	0.179	1014.0
480	01:01:23.70	+61:11:46.4	14.980	–	–	2.470	1.239	0.517	1.054	0.064	–	–	0.111	0.101	0.098	0.090	k1 V	0.279	575.0
481	01:01:24.26	+61:08:08.6	15.463	–	2.789	2.043	0.915	0.377	0.827	0.042	–	0.102	0.073	0.055	0.056	0.054	g7 IV	1.194	1479.0
482	01:01:24.34	+60:57:49.6	15.147	–	2.123	1.173	0.553	0.240	0.444	0.044	–	0.082	0.055	0.053	0.057	0.057	a6 III	1.231	3767.0
483	01:01:24.75	+60:47:52.3	14.601	–	–	1.669	0.802	0.313	0.591	0.091	–	–	0.106	0.105	0.101	0.109	b9 IV	1.215	4796.0
484	01:01:24.76	+60:59:14.7	12.942	3.086	2.062	1.115	0.573	0.214	0.427	0.045	0.070	0.072	0.056	0.057	0.062	0.058	a0 III	1.697	2925.0
485	01:01:26.25	+60:50:00.0	14.899	–	2.436	1.658	0.738	0.310	0.739	0.038	–	0.076	0.051	0.050	0.051	0.049	g3 IV	0.695	1204.0
486	01:01:26.57	+60:51:23.8	15.916	–	2.343	1.691	0.767	0.259	0.755	0.052	–	0.114	0.078	0.072	0.073	0.067	f9 V	1.04	1907.0
487	01:01:26.69	+60:54:50.2	15.630	–	2.240	1.390	0.569	0.236	0.648	0.059	–	0.095	0.074	0.074	0.070	0.068	a6 IV	1.294	2418.0

Table 4. Polarization and extinction measurements towards IC 59 and IC 63

No.	RA (J2000) (hh:mm:ss)	DEC (J2000) (dd:mm:ss)	$P \pm \sigma_P$ (%)	$\theta_{pos} \pm \sigma_{\theta_{pos}}$ ($^{\circ}$)	V_{mag} (mag)	A_V (mag)	d (pc)	P/A_V (%/mag)
IC59								
1	00:56:38.76	+61:12:48.3	1.848 \pm 0.526	94.686 \pm 7.840	15.831	2.205	2170	0.838
2	00:56:46.94	+61:10:13.2	2.544 \pm 0.232	100.928 \pm 2.535	13.316	1.023	1056	2.487
3	00:56:47.02	+61:07:52.1	3.056 \pm 0.398	65.293 \pm 3.649	14.418	1.439	2988	2.124
4	00:56:47.65	+61:12:25.0	1.148 \pm 0.159	49.301 \pm 3.723	14.963	1.747	3160	0.657
5	00:56:54.04	+61:09:04.2	5.722 \pm 1.151	90.927 \pm 5.863	17.671	3.041	3203	1.882
6	00:56:56.85	+61:06:41.4	1.653 \pm 0.578	58.167 \pm 9.562	16.817	2.026	3523	0.816
7	00:56:57.76	+61:14:25.7	1.863 \pm 0.761	94.518 \pm 11.255	15.955	0.379	1012	4.916
8	00:56:59.27	+61:09:10.9	2.121 \pm 0.308	103.422 \pm 4.012	13.558	1.069	834	1.984
9	00:57:02.71	+61:06:37.1	2.331 \pm 0.111	86.456 \pm 1.307	12.692	0.882	1013	2.643
10	00:57:04.70	+61:06:35.9	1.168 \pm 0.175	72.787 \pm 4.012	14.182	2.800	3944	0.417
11	00:57:05.20	+61:12:50.7	1.193 \pm 0.115	90.791 \pm 2.586	14.063	0.520	738	2.294
12	00:57:06.74	+61:06:19.5	1.582 \pm 0.094	86.517 \pm 1.622	12.733	0.616	771	2.568
13	00:57:07.01	+61:10:24.1	2.094 \pm 0.137	99.847 \pm 1.809	15.242	2.704	2693	0.774
14	00:57:07.11	+61:14:39.6	2.862 \pm 0.124	91.215 \pm 1.202	14.122	2.184	2338	1.310
15	00:57:07.71	+61:12:34.9	2.162 \pm 0.366	95.468 \pm 4.670	16.820	1.939	2648	1.115
16	00:57:08.89	+61:14:29.9	2.552 \pm 0.315	88.007 \pm 3.428	16.169	2.126	2974	1.200
17	00:57:09.45	+61:09:04.3	2.138 \pm 0.503	108.411 \pm 6.491	17.060	2.658	1348	0.804
18	00:57:10.54	+61:14:38.2	3.557 \pm 0.285	92.992 \pm 2.247	15.127	1.914	1503	1.858
19	00:57:11.03	+61:04:58.5	2.139 \pm 0.767	121.211 \pm 9.915	16.972	2.459	2345	0.870
20	00:57:12.35	+61:11:58.8	1.997 \pm 0.300	89.814 \pm 4.136	16.254	0.803	949	2.487
21	00:57:12.93	+61:14:04.5	2.336 \pm 0.230	97.939 \pm 2.736	15.730	2.300	1471	1.016
22	00:57:14.96	+61:09:32.2	2.503 \pm 0.415	89.062 \pm 4.600	15.323	1.107	1028	2.261
23	00:57:17.96	+61:11:31.9	0.828 \pm 0.125	79.834 \pm 3.958	14.460	2.292	1580	0.361
24	00:57:18.88	+61:08:08.9	3.502 \pm 0.796	80.212 \pm 6.458	16.440	3.041	2500	1.152
25	00:57:23.69	+61:11:33.5	1.527 \pm 0.308	79.678 \pm 5.516	14.751	0.957	876	1.596
26	00:57:25.66	+61:12:23.8	2.370 \pm 0.127	90.876 \pm 1.485	15.110	1.731	2675	1.369
27	00:57:27.73	+61:10:06.6	1.712 \pm 0.341	91.326 \pm 5.456	15.259	0.990	887	1.729
28	00:57:27.82	+61:12:40.5	1.821 \pm 0.258	92.756 \pm 3.881	15.473	0.853	1072	2.135
29	00:57:28.33	+61:07:26.5	2.044 \pm 0.352	108.154 \pm 4.743	15.431	0.820	735	2.493
30	00:57:28.37	+61:09:55.1	2.258 \pm 0.302	89.787 \pm 3.689	15.715	0.915	1121	2.468
31	00:57:28.42	+61:08:19.1	3.279 \pm 0.887	98.010 \pm 7.558	17.133	2.271	3862	1.444
32	00:57:30.04	+61:05:01.2	2.080 \pm 0.157	83.626 \pm 2.078	13.264	1.127	1037	1.846
33	00:57:30.66	+61:11:45.5	1.472 \pm 0.272	104.305 \pm 5.018	16.059	1.065	718	1.382
34	00:57:32.10	+61:03:14.5	1.202 \pm 0.544	86.038 \pm 12.259	16.737	1.090	333	1.103
35	00:57:32.74	+61:13:04.9	0.660 \pm 0.185	136.687 \pm 6.887	12.747	0.291	199	2.268
36	00:57:36.04	+61:08:51.8	2.193 \pm 0.418	98.633 \pm 5.271	15.511	1.048	833	2.093
37	00:57:36.61	+61:03:38.2	3.023 \pm 0.424	89.812 \pm 3.912	15.763	0.828	989	3.651
38	00:57:39.63	+61:03:45.8	3.941 \pm 0.853	89.027 \pm 6.082	17.327	2.192	2144	1.798
39	00:57:40.09	+61:07:45.2	1.990 \pm 0.334	109.271 \pm 4.617	14.780	1.240	682	1.605
40	00:57:40.36	+61:13:33.0	2.036 \pm 0.431	86.359 \pm 5.853	16.358	0.807	909	2.523
41	00:57:41.12	+61:04:29.6	3.928 \pm 0.432	91.308 \pm 3.092	15.937	1.997	1736	1.967
42	00:57:43.20	+61:12:40.2	3.259 \pm 0.624	96.742 \pm 5.540	16.523	1.597	2592	2.041
43	00:57:47.29	+61:04:46.9	2.405 \pm 0.691	84.773 \pm 7.809	16.388	1.756	4087	1.370
44	00:57:47.86	+61:14:12.4	1.817 \pm 0.343	97.067 \pm 5.351	14.050	0.790	910	2.300
45	00:57:49.65	+61:05:58.2	2.510 \pm 1.049	85.049 \pm 11.645	17.149	1.764	2417	1.423
46	00:57:49.60	+61:12:09.3	1.658 \pm 0.605	85.945 \pm 10.674	14.927	2.088	3916	0.794
47	00:57:50.56	+61:11:08.9	1.122 \pm 0.223	89.669 \pm 5.570	14.468	0.624	481	1.798
48	00:57:54.82	+61:11:16.3	3.217 \pm 0.511	82.089 \pm 4.720	15.168	2.088	1280	1.541
49	00:57:56.72	+61:05:16.4	4.283 \pm 1.304	77.353 \pm 8.601	17.414	1.718	3290	2.493
50	00:57:57.34	+61:12:22.2	4.317 \pm 1.765	121.027 \pm 10.697	17.059	1.468	2698	2.941

No.	RA (J2000) (hh:mm:ss)	DEC (J2000) (dd:mm:ss)	$P \pm \sigma_P$ (%)	$\theta_{pos} \pm \sigma_{\theta_{pos}}$ ($^{\circ}$)	V_{mag} (mag)	A_V (mag)	d (pc)	P/A_V (%/mag)
51	00:57:57.43	+61:07:36.7	1.685 \pm 0.651	91.162 \pm 10.653	15.876	0.549	913	3.069
52	00:57:58.76	+61:11:14.8	3.133 \pm 0.091	85.642 \pm 0.857	12.325	1.756	2331	1.784
53	00:58:01.12	+61:12:20.0	2.278 \pm 0.550	86.667 \pm 7.094	15.704	1.772	3848	1.286
54	00:58:03.45	+61:05:57.6	2.725 \pm 1.217	115.314 \pm 12.254	17.582	1.302	4231	2.093
55	00:58:06.96	+61:10:52.7	2.412 \pm 0.306	87.118 \pm 3.724	15.030	1.805	3326	1.336
56	00:58:08.18	+61:11:23.6	3.171 \pm 0.132	89.364 \pm 1.210	13.724	1.880	1918	1.687
57	00:58:09.16	+61:11:02.9	3.595 \pm 0.215	84.604 \pm 1.759	14.009	1.448	2419	2.483
58	00:58:12.66	+61:10:34.6	2.318 \pm 0.227	88.378 \pm 2.853	14.514	0.616	825	3.763
59	00:56:19.17	+61:06:30.2	0.873 \pm 0.131	101.670 \pm 3.936	13.715	0.636	908	1.373
60	00:56:25.92	+61:07:08.3	0.692 \pm 0.088	63.898 \pm 3.256	11.934	0.620	398	1.116
61	00:56:27.43	+61:06:50.4	1.583 \pm 0.282	71.352 \pm 4.878	14.702	1.635	2198	0.968
62	00:56:30.02	+61:10:38.0	0.998 \pm 0.448	90.258 \pm 11.973	14.272	0.508	662	1.965
63	00:56:32.96	+61:08:45.7	1.222 \pm 0.178	87.730 \pm 3.949	12.740	0.316	411	3.867
64	00:56:35.59	+61:05:22.5	1.851 \pm 0.312	85.628 \pm 4.649	15.195	0.728	919	2.543
65	00:56:52.05	+61:17:11.1	2.336 \pm 0.821	98.123 \pm 9.709	15.507	0.566	752	4.127
66	00:56:52.43	+61:16:05.1	1.555 \pm 0.645	116.492 \pm 11.222	15.007	2.542	4963	0.612
67	00:56:56.95	+61:17:46.6	0.540 \pm 0.138	88.971 \pm 6.332	13.851	0.491	428	1.010
68	00:56:59.40	+61:12:43.4	1.377 \pm 0.485	92.845 \pm 9.567	15.218	1.951	1949	0.706
69	00:57:33.71	+61:15:27.0	1.423 \pm 0.295	103.902 \pm 5.628	14.927	0.508	1054	2.801
70	00:57:41.12	+61:02:29.6	1.442 \pm 0.533	82.360 \pm 10.152	15.628	0.574	1125	2.512
71	00:57:43.50	+61:16:01.2	3.757 \pm 0.447	109.991 \pm 3.280	15.966	2.675	3342	1.404
72	00:57:43.90	+61:10:48.6	3.326 \pm 0.063	90.422 \pm 0.552	12.828	2.887	1377	1.152
73	00:57:47.79	+61:15:35.6	3.550 \pm 0.131	95.825 \pm 1.039	13.583	1.897	2649	1.871
74	00:57:49.60	+61:14:51.5	1.992 \pm 0.513	102.537 \pm 7.171	15.213	0.670	1042	2.973
75	00:57:53.16	+61:15:46.7	3.572 \pm 0.802	92.577 \pm 6.638	15.500	1.905	3981	1.875
76	00:57:58.44	+61:15:18.3	0.930 \pm 0.322	111.760 \pm 8.952	14.323	0.495	553	1.879
77	00:58:05.05	+61:16:15.3	3.738 \pm 0.223	96.867 \pm 1.719	14.542	1.880	1919	1.988
78	00:58:11.94	+60:50:39.6	1.022 \pm 0.416	107.767 \pm 10.727	14.473	0.212	1003	4.821
IC63								
1	00:58:40.22	+60:52:19.8	3.545 \pm 0.323	88.268 \pm 2.660	14.451	1.847	1265	1.919
2	00:58:41.25	+60:51:00.1	3.334 \pm 0.412	87.728 \pm 3.571	15.884	1.568	5994	2.126
3	00:58:41.50	+60:54:37.9	3.210 \pm 0.765	87.937 \pm 6.559	16.802	1.772	2533	1.812
4	00:58:41.88	+60:52:41.7	2.547 \pm 0.237	88.994 \pm 2.679	13.558	1.123	1118	2.268
5	00:58:46.39	+60:52:12.0	4.526 \pm 0.213	89.716 \pm 1.324	14.143	1.772	1329	2.554
6	00:58:48.35	+60:56:00.2	1.536 \pm 0.147	87.646 \pm 2.605	13.458	0.412	561	3.728
7	00:58:50.13	+60:52:14.2	3.947 \pm 0.307	88.258 \pm 2.180	15.093	1.826	1840	2.162
8	00:58:51.81	+61:01:02.6	2.143 \pm 0.098	87.787 \pm 1.262	11.541	0.524	922	4.090
9	00:58:52.86	+60:51:55.8	2.265 \pm 0.443	80.266 \pm 5.431	16.546	1.327	3899	1.707
10	00:58:52.96	+60:55:34.4	1.111 \pm 0.290	87.062 \pm 6.957	15.050	0.620	727	1.792
11	00:58:53.33	+61:00:12.2	3.342 \pm 0.816	68.122 \pm 6.816	16.488	2.167	4402	1.542
12	00:58:54.96	+60:51:58.0	3.643 \pm 0.462	92.876 \pm 3.560	16.107	1.302	1777	2.798
13	00:58:55.05	+60:52:31.9	2.205 \pm 0.114	89.438 \pm 1.431	13.046	0.703	747	3.137
14	00:58:55.67	+60:59:53.3	3.058 \pm 0.596	88.485 \pm 5.437	16.302	1.265	4006	2.417
15	00:58:55.66	+60:52:11.2	3.722 \pm 0.153	91.288 \pm 1.149	14.183	1.797	2818	2.071
16	00:58:55.75	+61:00:11.4	1.406 \pm 0.064	87.251 \pm 1.229	11.311	0.678	574	2.074
17	00:58:57.22	+60:53:16.8	2.182 \pm 0.487	87.184 \pm 6.108	15.518	0.795	905	2.745
18	00:59:00.19	+60:55:04.9	1.569 \pm 0.470	63.125 \pm 8.169	16.261	1.980	3147	0.792
19	00:59:02.80	+60:55:18.1	2.550 \pm 0.374	68.499 \pm 4.061	15.433	2.167	3730	1.177
20	00:59:04.21	+60:51:27.9	2.485 \pm 0.592	94.355 \pm 6.622	15.916	1.518	3915	1.637
21	00:59:04.58	+60:50:59.7	4.171 \pm 0.393	100.785 \pm 2.664	16.578	1.277	1413	3.266
22	00:59:05.49	+60:59:50.9	3.712 \pm 0.426	111.196 \pm 3.217	15.591	1.444	3163	2.571
23	00:59:05.68	+60:55:00.0	1.375 \pm 0.562	90.84 \pm 11.048	15.635	0.653	941	2.106
24	00:59:05.91	+60:58:52.0	1.337 \pm 0.134	84.027 \pm 2.722	13.030	0.516	563	2.591
25	00:59:06.09	+60:52:08.9	4.572 \pm 0.819	88.539 \pm 5.036	16.594	1.739	4926	2.629

No.	RA (J2000) (hh:mm:ss)	DEC (J2000) (dd:mm:ss)	$P \pm \sigma_P$ (%)	$\theta_{pos} \pm \sigma_{\theta_{pos}}$ ($^{\circ}$)	V_{mag} (mag)	A_V (mag)	d (pc)	P/A_V (%/mag)
26	00:59:09.71	+60:51:14.3	3.822 \pm 0.486	94.481 \pm 3.573	16.760	1.676	4970	2.280
27	00:59:10.24	+60:57:07.1	2.119 \pm 0.167	89.030 \pm 2.176	13.733	0.703	947	3.014
28	00:59:10.34	+60:55:26.7	3.448 \pm 0.504	90.528 \pm 4.070	16.199	1.514	2292	2.277
29	00:59:11.15	+60:51:48.2	2.774 \pm 0.735	90.734 \pm 7.378	16.422	1.489	1007	1.863
30	00:59:13.57	+61:00:33.1	2.213 \pm 0.146	76.950 \pm 1.825	14.266	2.820	1670	0.785
31	00:59:15.41	+60:51:41.5	4.946 \pm 0.958	95.312 \pm 5.442	16.870	1.298	2232	3.810
32	00:59:16.98	+60:57:39.3	3.882 \pm 0.639	66.999 \pm 4.609	17.100	1.860	1838	2.087
33	00:59:17.61	+60:52:02.6	2.635 \pm 0.315	85.077 \pm 3.322	15.254	0.786	1027	3.352
34	00:59:18.12	+60:58:30.6	1.276 \pm 0.128	86.726 \pm 2.707	12.585	0.620	615	2.058
35	00:59:18.52	+60:55:34.4	1.536 \pm 0.161	61.012 \pm 2.860	13.966	0.973	291	1.579
36	00:59:19.44	+60:57:57.5	3.918 \pm 0.290	95.696 \pm 2.082	15.394	1.468	2241	2.669
37	00:59:20.03	+60:59:09.1	2.485 \pm 0.101	89.294 \pm 1.125	12.302	1.036	947	2.399
38	00:59:22.61	+60:56:48.2	2.336 \pm 0.184	87.893 \pm 2.180	14.831	2.209	3682	1.057
39	00:59:25.53	+60:58:55.5	2.534 \pm 0.368	92.686 \pm 4.044	15.340	0.894	1119	2.834
40	00:59:25.54	+60:55:18.7	2.874 \pm 0.676	101.108 \pm 6.577	16.844	2.471	2929	1.163
41	00:59:28.96	+60:54:43.0	3.655 \pm 0.225	81.605 \pm 1.719	15.316	2.205	2699	1.658
42	00:59:28.96	+61:00:03.4	2.470 \pm 0.067	92.143 \pm 0.759	11.479	1.543	1086	1.601
43	00:59:30.70	+61:00:18.1	3.195 \pm 0.114	86.815 \pm 0.998	13.377	2.109	2374	1.515
44	00:59:31.23	+60:59:50.5	2.613 \pm 0.771	59.021 \pm 8.202	16.674	1.980	2034	1.320
45	00:59:32.97	+60:54:56.9	3.928 \pm 0.411	84.442 \pm 2.925	15.422	2.438	2415	1.611
46	00:59:33.06	+60:58:50.6	3.682 \pm 0.756	118.725 \pm 5.814	16.806	1.643	3936	2.241
47	00:59:34.51	+61:00:03.0	2.939 \pm 0.711	91.207 \pm 6.766	16.016	1.810	2211	1.624
48	00:59:36.12	+60:54:26.0	2.178 \pm 0.692	102.096 \pm 8.783	16.795	2.188	3199	0.995
49	00:59:36.82	+60:54:16.1	5.511 \pm 0.770	102.210 \pm 3.953	17.227	1.606	2514	3.432
50	00:59:37.24	+60:52:55.4	3.141 \pm 0.458	92.239 \pm 4.078	15.775	2.059	2251	1.525
51	00:59:37.43	+60:51:03.5	3.286 \pm 0.518	96.491 \pm 4.399	15.976	1.493	1730	2.201
52	00:59:39.54	+60:49:54.1	1.909 \pm 0.245	96.840 \pm 3.484	14.191	0.836	1058	2.283
53	00:59:40.78	+60:52:10.7	4.198 \pm 0.684	76.369 \pm 4.573	16.646	1.918	3685	2.189
54	00:59:41.16	+60:55:00.6	3.356 \pm 0.338	102.655 \pm 2.811	15.677	2.592	2963	1.295
55	00:59:41.23	+60:59:29.8	4.356 \pm 0.434	87.787 \pm 2.808	15.870	1.697	4428	2.567
56	00:59:46.19	+60:50:31.1	1.798 \pm 0.362	88.516 \pm 5.520	15.186	1.477	474	1.217
57	00:59:46.46	+60:51:43.3	5.929 \pm 1.082	78.698 \pm 5.124	16.811	1.606	4324	3.692
58	00:59:46.54	+60:54:45.2	2.357 \pm 0.197	84.220 \pm 2.314	14.001	0.907	874	2.599
59	00:59:47.06	+60:53:11.7	2.765 \pm 0.425	103.085 \pm 4.276	15.840	1.194	2095	2.316
60	00:59:50.58	+60:52:16.8	2.911 \pm 0.194	95.544 \pm 1.858	14.464	1.681	2378	1.732
61	00:59:50.79	+60:50:52.1	2.263 \pm 0.199	94.562 \pm 2.426	13.845	1.344	2672	1.684
62	00:59:52.23	+60:51:30.6	2.049 \pm 0.278	99.130 \pm 3.736	14.544	1.215	2722	1.686
63	00:59:54.68	+60:55:39.2	2.844 \pm 0.796	83.939 \pm 7.671	16.288	1.776	4421	1.601
64	00:59:55.26	+60:59:57.8	4.328 \pm 1.149	90.962 \pm 6.089	16.475	0.724	1021	5.978
65	00:59:56.20	+60:54:31.7	3.081 \pm 0.446	92.155 \pm 3.995	15.556	1.614	2523	1.909
66	00:59:56.45	+61:00:21.1	4.145 \pm 2.015	93.549 \pm 11.268	16.425	1.581	4570	2.623
67	00:59:57.51	+60:56:07.0	2.958 \pm 0.290	83.536 \pm 2.715	14.584	1.697	2662	1.743
68	00:59:57.65	+60:55:32.4	4.712 \pm 0.457	83.722 \pm 2.712	15.857	1.427	2275	3.302
69	00:59:58.13	+60:54:28.7	2.835 \pm 0.350	92.243 \pm 3.419	15.192	1.660	3526	1.708
70	01:00:00.29	+60:58:44.0	2.469 \pm 0.561	89.902 \pm 5.267	16.244	1.939	1444	1.273
71	01:00:00.89	+60:54:44.9	3.309 \pm 0.423	90.908 \pm 3.547	15.625	1.947	2211	1.700
72	01:00:02.44	+60:50:54.1	2.802 \pm 0.420	98.487 \pm 4.174	15.478	1.564	2281	1.792
73	01:00:02.58	+60:55:28.5	3.757 \pm 0.401	80.216 \pm 2.971	15.334	1.552	2532	2.421
74	01:00:06.20	+60:49:54.4	2.961 \pm 0.634	95.566 \pm 5.931	16.155	1.602	2773	1.848
75	01:00:06.35	+60:52:08.5	2.207 \pm 0.156	87.631 \pm 1.948	13.427	0.986	1070	2.238
76	01:00:09.81	+60:56:46.0	2.676 \pm 0.230	92.090 \pm 2.374	14.183	1.614	4209	1.658
77	01:00:13.34	+60:53:24.2	1.645 \pm 0.237	78.769 \pm 3.900	14.232	0.616	684	2.670
78	01:00:13.37	+60:59:55.1	1.648 \pm 0.273	91.158 \pm 4.516	15.906	0.691	389	2.385

No.	RA (J2000) (hh:mm:ss)	DEC (J2000) (dd:mm:ss)	$P \pm \sigma_P$ (%)	$\theta_{pos} \pm \sigma_{\theta_{pos}}$ ($^{\circ}$)	V_{mag} (mag)	A_V (mag)	d (pc)	P/A_V (%/mag)
79	01:00:13.98	+60:51:47.3	2.367 \pm 0.684	105.824 \pm 8.013	16.362	1.082	1650	2.188
80	01:00:14.21	+60:56:05.5	2.451 \pm 0.222	88.042 \pm 2.506	15.047	1.331	3868	1.841
81	01:00:14.22	+60:59:43.0	2.647 \pm 0.340	80.729 \pm 3.555	16.368	1.090	1935	2.428
82	01:00:14.26	+60:58:43.7	4.000 \pm 0.407	91.987 \pm 2.866	16.713	1.884	2022	2.123
83	01:00:14.60	+60:53:58.0	3.268 \pm 0.268	90.165 \pm 2.275	14.348	1.360	1637	2.403
84	01:00:15.37	+60:51:29.9	2.595 \pm 0.672	91.743 \pm 7.104	16.781	0.961	755	2.700
85	01:00:17.32	+60:59:36.0	4.788 \pm 0.330	94.843 \pm 1.735	14.786	1.302	3137	3.677
86	01:00:18.75	+60:52:27.1	2.156 \pm 0.135	87.699 \pm 1.723	13.013	0.998	908	2.160
87	01:00:19.45	+60:59:51.0	2.917 \pm 0.862	89.099 \pm 6.795	15.242	1.419	2682	2.056
88	00:58:14.86	+60:51:49.5	2.040 \pm 0.121	87.233 \pm 1.692	11.699	0.657	957	3.105
89	00:58:17.68	+60:48:39.4	3.041 \pm 0.258	104.245 \pm 2.378	13.885	1.810	3494	1.680
90	00:58:20.28	+60:48:47.9	1.998 \pm 0.654	102.848 \pm 9.080	15.819	0.853	2279	2.342
91	00:58:21.13	+60:52:14.8	1.306 \pm 0.380	87.450 \pm 8.239	14.923	0.869	656	1.503
92	00:58:34.36	+60:52:58.8	1.847 \pm 0.227	92.128 \pm 3.490	13.815	1.073	916	1.721
93	00:58:34.40	+60:51:05.5	1.941 \pm 0.115	89.602 \pm 1.686	12.278	0.628	988	3.091
94	00:58:35.05	+60:49:51.9	3.395 \pm 0.475	90.982 \pm 4.043	15.146	1.889	1765	1.797
95	00:59:04.01	+61:02:42.3	2.763 \pm 0.139	93.770 \pm 1.402	13.030	0.803	1012	3.441
96	00:59:13.40	+61:03:28.4	2.404 \pm 0.298	89.894 \pm 3.440	14.605	1.826	2065	1.317
97	00:59:26.12	+61:02:43.8	3.433 \pm 0.454	75.750 \pm 3.706	15.398	1.718	2317	1.100
98	00:59:31.44	+61:02:10.0	2.142 \pm 0.590	87.491 \pm 7.598	15.629	0.711	720	3.013
99	00:59:34.51	+61:01:02.2	2.620 \pm 0.502	95.467 \pm 5.354	15.726	1.797	3268	1.458
100	00:59:41.51	+61:02:12.0	3.597 \pm 0.262	88.405 \pm 2.045	14.254	1.743	3088	2.064
101	00:59:42.79	+61:02:59.5	3.948 \pm 0.179	87.465 \pm 1.279	13.671	1.468	2557	2.689
102	00:59:50.41	+61:02:04.6	1.813 \pm 0.307	86.122 \pm 3.919	14.575	0.957	891	1.894
103	00:59:56.07	+61:02:44.6	2.811 \pm 0.627	95.552 \pm 5.500	14.106	2.267	1956	1.240
104	00:59:57.48	+60:50:17.7	2.798 \pm 0.139	91.732 \pm 1.379	12.993	1.423	232	1.966
105	01:00:01.79	+61:02:22.7	2.551 \pm 0.393	87.924 \pm 3.624	14.653	0.778	1014	3.279
106	01:00:04.33	+60:55:13.8	2.091 \pm 0.084	86.651 \pm 1.110	12.021	1.065	1884	1.963
107	01:00:11.44	+61:02:44.4	3.000 \pm 0.386	89.279 \pm 3.065	13.566	2.163	3135	1.387
108	01:00:15.81	+61:03:19.9	3.496 \pm 0.601	88.264 \pm 4.025	13.764	2.163	3113	1.616
109	01:00:18.82	+61:03:59.1	4.798 \pm 1.115	97.847 \pm 5.838	15.553	0.670	758	7.161
110	01:00:20.57	+60:59:04.8	3.782 \pm 0.758	93.701 \pm 5.588	16.040	0.978	7654	3.867
111	01:00:26.80	+60:55:08.5	3.527 \pm 0.554	90.979 \pm 4.398	15.132	1.373	2047	2.569
112	01:00:28.68	+60:58:01.1	2.987 \pm 0.321	86.084 \pm 2.993	14.903	1.835	2160	1.628
113	01:00:30.23	+60:54:25.3	3.422 \pm 0.191	89.823 \pm 1.547	13.218	0.924	2359	3.703
114	01:00:31.68	+60:59:32.8	5.220 \pm 0.596	94.779 \pm 2.816	15.075	0.553	710	9.439
115	01:00:34.72	+60:56:34.3	2.752 \pm 0.199	85.776 \pm 2.005	13.083	1.206	1541	2.282
116	01:00:38.48	+60:54:47.2	1.340 \pm 0.106	81.381 \pm 2.138	13.332	0.270	496	4.963
117	01:00:40.70	+60:55:34.8	3.271 \pm 0.897	86.175 \pm 7.674	15.694	0.811	5521	4.033
118	01:00:41.54	+61:00:24.5	3.483 \pm 0.219	96.287 \pm 1.602	13.721	1.697	3381	2.052
119	01:00:42.81	+60:59:04.2	2.302 \pm 0.202	94.634 \pm 2.431	15.357	1.011	1369	2.277
120	01:00:49.06	+60:56:37.4	3.210 \pm 0.779	95.649 \pm 6.757	15.845	1.847	2262	1.738
121	01:00:54.83	+60:58:16.2	1.910 \pm 0.243	90.776 \pm 3.49	15.552	1.681	2293	1.136
122	01:00:55.36	+60:58:40.7	2.308 \pm 0.235	95.924 \pm 2.804	13.318	1.352	2579	1.707
123	01:00:55.35	+60:59:58.5	1.549 \pm 0.201	85.505 \pm 3.513	14.399	0.270	548	5.737
124	01:00:57.55	+60:58:22.2	2.223 \pm 0.210	90.538 \pm 2.608	15.401	1.793	2645	1.240
125	01:00:57.81	+60:59:21.5	2.085 \pm 0.885	104.854 \pm 11.705	16.199	1.664	2402	1.253
126	01:00:58.86	+60:57:28.7	0.953 \pm 0.111	86.954 \pm 3.087	14.282	0.399	342	2.388